

Progressive Collapse in Long-Span Cable-Supported Bridges

Vom Promotionsausschuss der
Technischen Universität Hamburg
zur Erlangung des akademischen Grades

Doktor-Ingenieur (Dr.-Ing.)

genehmigte Dissertation

von

Mohammad Shoghijavan

aus

Mashhad, Iran

2020

1. Gutachter: Prof. Dr.-Ing. Uwe Starossek

2. Gutachter: Prof. Dr.-Ing. habil. Marcus Rutner

Tag der mündlichen Prüfung: 15.09.2020

This dissertation is dedicated to my parents,
for their endless love, support, and encouragement.

Acknowledgements

The presented work has been carried out during the years 2013-2020 at the Structural Analysis Institute at Hamburg University of Technology. This study is funded by the German Academic Exchange Service (DAAD), which is gratefully acknowledged.

I want to express my gratitude to Professor Dr.-Ing. Uwe Starossek for supervising my Ph.D. dissertation and for his insightful suggestions as well as all of his supports during my studies in his Institute. I learned from his insight a lot.

In addition, I thank my colleagues for the pleasant working atmosphere and the associated short time during and after working hours. I want to thank Dr.-Ing. Priebe for his technical supports. I especially want to thank Mrs. Spahn and Mr. Seils for their kindness and supports during my studies at the Hamburg University of Technology.

Finally and foremost, I have to thank my parents for their love and support throughout my life. My sister and my brother deserve my wholehearted thanks as well.

Hamburg, March 2020

Mohammad Shoghijavan

Abstract

Parallel load-bearing systems are structural systems with load-bearing members that are similar in type and function and constitute alternative load paths. Cable-supported bridges are good examples of such a structural system. In the case of the failure of one of the parallel load-bearing elements (cables), the load carried by the failed member must be redistributed to the remaining structure. In this situation, the member adjacent to the failed member receives most of the redistributed load and becomes the critical member. If this member cannot tolerate the redistributed load, the collapse can progress to the subsequent members and, possibly, the entire structure. Hence, because of the vital role of the critical member in the robustness of the structural system, the focus of this study is mostly on this member.

In this study, a parallel-load bearing system is considered as a conceptual model of long-span cable-supported bridges. The target is to calculate the “stress increase ratio” of the critical cable in a cable-loss scenario. The structural characteristics of the system, including the bending stiffness of the girder and a unique axial stiffness in each cable, have been taken into account. The failure of several cables has also been considered. An analytical approach based on differential equations of the system has been used, and an approximation function for the calculation of the stress increase ratio of the critical cable in a cable-loss scenario has been derived. The least squares method has been applied to minimize the error of the approximation function. The results show that by increasing the ratio of the bending stiffness of the girder to the axial stiffness of the cables (β -value), the stress increase ratio of the critical cable decreases. The acceptable accuracy of the presented approximation function has been proved by the comparison of the exact stress increase ratio values, and the one calculated from the proposed approximation function. Except for small β -values, the error of the proposed approximation function is less than 5% in the investigated systems. The developed approximation function has been used to derive a reserve-based robustness index. Besides, the structural robustness of a system segmented by zipper-stoppers has been investigated, and the stress increase ratio of the zipper-stopper in a cable-loss scenario has been examined.

In addition, a similar approach for the calculation of the increase of maximum bending moment on the girder due to cable failure has been performed. The results show that by increasing the β -value, cable failure produces a larger bending moment on the girder. This means that for systems with smaller β -values, bending moments are smaller.

Finally, a practical method for the optimization of cable distance in cable-supported bridges has been developed, and the optimum design of cable-supported bridges considering the failure of several cables has been investigated. The method minimizes the cost of bridge construction and guarantees a certain level of robustness.

Kurzfassung

Parallele Tragsysteme sind strukturelle Systeme mit tragenden Elementen, die in Art und Funktion ähnlich sind und alternative Lastpfade darstellen. Seilunterstützte Brücken sind gute Beispiele für ein solches Tragwerkssystem. Im Falle des Versagens eines der parallelen tragenden Elemente (Kabel) muss die Last, die von dem versagenden Element getragen wird, auf die verbleibende Struktur neu verteilt werden. In dieser Situation erhält das an das ausgefallene Element angrenzende Element den größten Teil der umverteilten Last und wird zum kritischen Element. Wenn dieses Element die umverteilte Last nicht ertragen kann, kann der Zusammenbruch auf die nachfolgenden Elemente und möglicherweise auf die gesamte Struktur übergreifen. Aufgrund der entscheidenden Rolle des kritischen Elements für die Robustheit des Tragwerkssystems liegt der Schwerpunkt dieser Studie daher hauptsächlich auf diesem Element.

In dieser Studie wird ein paralleles Tragsystem als ein konzeptionelles Modell für seilunterstützte Brücken mit großer Spannweite betrachtet. Das Ziel ist die Berechnung des "Spannungszunahmeverhältnisses" des kritischen Kabels in einem Kabelverlust-Szenario. Die strukturellen Eigenschaften des Systems, einschließlich der Biegesteifigkeit des Trägers und einer einzigartigen axialen Steifigkeit in jedem Kabel, wurden berücksichtigt. Das Versagen mehrerer Kabel wurde ebenfalls berücksichtigt. Ein analytischer Ansatz auf der Grundlage von Differentialgleichungen des Systems wurde verwendet, und es wurde eine Approximationsfunktion für die Berechnung des Spannungszunahmeverhältnisses des kritischen Kabels in einem Kabelverlustszenario abgeleitet. Die Methode der kleinsten Quadrate wurde angewandt, um den Fehler der Näherungsfunktion zu minimieren. Die Ergebnisse zeigen, dass durch Erhöhen des Verhältnisses der Biegesteifigkeit des Trägers zur axialen Steifigkeit der Kabel (β -Wert) das Spannungszunahmeverhältnis des kritischen Kabels abnimmt. Die akzeptable Genauigkeit der vorgestellten Approximationsfunktion wurde durch den Vergleich der genauen Werte des Spannungszunahmeverhältnisses mit dem aus der vorgeschlagenen Näherungsfunktion berechneten Wert nachgewiesen. Abgesehen von kleinen β -Werten beträgt der Fehler der vorgeschlagenen Näherungsfunktion in den untersuchten Systemen weniger als 5%. Die entwickelte Approximationsfunktion wurde verwendet, um einen reservebasierten Robustheitsindex abzuleiten. Außerdem wurde die strukturelle Robustheit eines durch Zipper-Stopper segmentierten Systems untersucht und das Spannungszunahmeverhältnis des Zipper-Stoppers in einem Kabelverlust-Szenario untersucht.

Darüber hinaus wurde ein ähnlicher Ansatz für die Berechnung der Erhöhung des maximalen Biegemoments auf den Träger aufgrund von Kabelversagen durchgeführt. Die Ergebnisse zeigen, dass ein Kabelversagen durch Erhöhung des β -Wertes ein größeres Biegemoment auf den Träger erzeugt. Dies bedeutet, dass bei Systemen mit kleineren β -Werten die Biegemomente kleiner sind.

Schließlich wurde eine praktische Methode zur Optimierung des Kabelabstands in seilunterstützten Brücken entwickelt, und es wurde die optimale Auslegung von seilunterstützten Brücken unter Berücksichtigung des Versagens mehrerer Kabel untersucht. Die Methode minimiert die Kosten der Brückenkonstruktion und garantiert eine gewisse Robustheit.

Table of Contents

1. Introduction	1
1.1 Defining the problem	1
1.2 Thesis objectives	2
1.3 Structure of the thesis	2
2. Literature Review	4
2.1 Introduction	4
2.2 History of progressive collapse in engineering structures	4
2.3 Definition of progressive collapse	5
2.4 Classification of different types of progressive collapse	8
2.5 Actual examples of progressive collapse in parallel load-bearing systems	8
2.5.1 Hyatt Regency walkway collapse	8
2.5.2 The collapse of the Tacoma Narrows Bridge	9
2.5.2.1 Structural failure	12
2.5.2.2 External resonance	12
2.5.2.3 Vortices	12
2.5.2.4 Aerodynamic Instability (flutter theory)	13
2.6 Progressive collapse in cable-supported bridges	13
2.6.1 Determination of dynamic amplification factor (DAF)	18
2.6.2 Cable breakage duration	22
2.7 Mathematical models for the analysis of suspension bridges	24
2.7.1 Conceptual models of suspension bridges	28
2.7.2 Considering the cable failure in the mathematical models of cable supported bridges	33
3. Developing an Analytical Method for the Investigation of Cable Failure in Long-Span Cable-Supported Bridges	36
3.1 Introduction	36
3.2 Conceptual model	37
3.3 Analytical approach for the determination of the stress increase ratio of the critical cable due to cable loss	38
3.4 Determination of the stress increase ratio of the critical cable due to the failure of several cables	56

3.5 Developing a reserve-based robustness index.....	67
3.5.1 Definition of robustness	67
3.5.2 Assessment of structural robustness.....	67
3.6 Structural robustness of long-span cable-supported bridges segmented by zipper-stoppers to prevent progressive collapse	72
3.7 Modifying the approximation function for a more detailed conceptual model	81
4. Bending Moment Acting on the Girder of a Long-Span Cable-Supported Bridge Suffering from Cable Failure.....	85
4.1 Introduction.....	85
4.2 An analytical approach for the determination of the increase of the maximum bending moment of the girder due to the cable loss	86
5. Investigation of the Optimum Design of Long-Span Cable-Supported Bridges Considering Cable-Loss Scenarios.....	97
5.1 Introduction.....	97
5.2 Structural specifications and loading conditions	100
5.3 Estimation of the construction cost.....	102
5.4 Finding the optimum cable distance.....	103
5.5 Summary and discussion	108
6. Conclusions and Recommendations	110
References.....	114
Lebenslauf	125

Chapter 1

Introduction

1.1 Defining the problem

All types of structural systems may experience abnormal loads in their lifetime. Abnormal loads are loads other than conventional design loads (dead, live, wind, seismic, etc.). In other words, abnormal loads can be defined as low-probability loads, which might have high consequences. Such extreme loads usually cause local damage. If a large part of the structure collapse because of local damage, the term progressive collapse comes in mind. According to ASCE (2002), “progressive collapse is defined as the spread of an initial local failure from element to element, eventually resulting in the collapse of an entire structure or a disproportionately large part of it.”

Studies about the progressive collapse of structures have been initiated after the collapse of the Ronan Point apartment in London (1968). However, it was mostly after the collapse of the World Trade Center in New York (2001) that the devastating consequences of progressive collapse in the engineering structures were clearly understood. The issue of progressive collapse has been mainly studied in buildings. Most of the guidelines that address progressive collapse are exclusively designed for buildings. Standards addressing progressive collapse and cable-loss scenarios in bridges are few and widely scattered. However, bridges suffer a higher level of vulnerability against progressive collapse. Hence, the issue of progressive collapse in bridges deserves more attention.

Parallel load-bearing systems are structural systems with load-bearing members that are similar in type and function. These systems are distinguished by their ability to constitute alternative load paths. Cable-supported bridges, including suspension bridges and cable-stayed bridges, are good examples of such a structural system. In suspension bridges and cable-stayed bridges, hangers and stay cables are parallel load-bearing elements, respectively.

There are two main approaches to preventing progressive collapse. First, ensure a high level of safety against local failure by using structural or non-structural strategies. Second, prevent failure from spreading by designing a robust structure that allows local failure. In the case of the failure of one of the parallel load-bearing elements (cables), the load carried by the failed member must be redistributed to the remaining structure. In this situation, the member adjacent to the failed member receives most of the redistributed load and becomes the critical member. If this member cannot tolerate the redistributed load, the collapse will progress to the

Chapter 1. Introduction

subsequent members and, possibly, the entire structure. Hence, because of the vital role of the critical member in the robustness of the structural system, the focus of this study is mainly on this member.

1.2 Thesis objective

In this study, a parallel-load bearing system is considered as a conceptual model of long-span cable-supported bridges. The target is to investigate the structural robustness of long-span cable-supported bridges in a cable-loss scenario. The conceptual model consists of a beam suspended from cables (tension elements). A simplified model is intentionally selected to make the analytical approach easier. Hence, some differences between an accurate bridge model and the simplified model used here are unavoidable. If examining the simplified model shows a certain phenomenon, a similar phenomenon in more sophisticated models can also be expected. One of the main targets of this study is to develop an analytical method that increases our understanding of the behavior of long-span cable-supported bridges in the case of the failure of one or several cables, which could be useful for academic research. The proposed method is expected to set the basis for further developments of practical methods for more complex structures. Immediate practical applications are not intended.

1.3 Structure of the Thesis

This study is intended to achieve a better understanding of the structural robustness of long-span cable-supported bridges in a cable-loss scenario. This dissertation consists of six chapters. In the following, the framework of each chapter is presented.

Chapter 1- Introduction:

This chapter provides an overview of the thesis, its objectives, and the structure of the research.

Chapter 2- Literature review:

This chapter comprises a brief overview of the existing research on the progressive collapse of cable-supported bridges. The review of mathematical models for the analysis of suspension bridges is also presented here.

Chapter 3- Developing an analytical method for the investigation of cable failure in long-span cable-supported bridges:

Chapter 1. Introduction

In this chapter, the structural response of long-span cable-supported bridges after the sudden rupture of some of its cables is investigated. The main focus is on the stress increase ratio of the critical cable due to cable failure and the development of a robustness index.

Chapter 4- Bending moment acting on the girder of a long-span cable-supported bridge suffering from cable failure:

The focus of this chapter is to find the increase of maximum bending moment on the girder due to cable failure.

Chapter 5- Investigation of the optimum design of long-span cable-supported bridges using the developed robustness index:

The target of this chapter is to use a practical method for the optimization of cable distance in cable-supported bridges using the robustness index. The proposed optimization method minimizes the cost of bridge construction and guarantees a certain level of robustness.

Chapter 6- Conclusions and Recommendations:

In this chapter, conclusions made from this study are provided, and some recommendations for future research are given.

Chapter 2

Literature Review

2.1 Introduction

This section presents a brief literature review about the issue of progressive collapse in cable-supported bridges. First, the term progressive collapse will be defined, and different types of progressive collapse will be introduced. Then, two actual examples of progressive collapse in parallel load-bearing systems will be investigated, and related studies about the reasons for their collapse will be reviewed. Then, associated studies about cable failure in cable-supported bridges will be reviewed. Finally, the structural behavior of cable-supported bridges in a cable-loss scenario will be explained, and a brief review of the available conceptual models for the analysis of suspension bridges will be presented.

2.2 History of progressive collapse in engineering structures

Studies about the progressive collapse of structures have been initiated after the collapse of the Ronan Point apartment in London (1968). Ronan Point was a 22-story tower that partly collapsed due to a gas explosion. Consequently, the entire corner of the tower collapsed because some load-bearing walls blew out. This accident killed four people and injured 17. Investigations showed that the main reason for this collapse was poor design and construction of the tower. Accordingly, UK building guidelines have been changed. The second event that highlighted the risk of progressive collapse in structures was the collapse of the Murrah Federal Building in Oklahoma (1995). The detonation of a truck bomb caused the collapse of half of the building and killed 168 people. However, it was mostly after the collapse of the World Trade Center in New York (2001) that the importance of progressive collapse in the engineering structures and its devastating consequences became clear to the stakeholders (e.g., building officials, owners, lenders, insurers, government agencies, and emergency planners) and the need for new standards and guidelines was deeply felt. Hence, the scientific community accelerated its effort in studying this field to provide the required standards and recommendations.

In Fig. 2.1, the dramatic increase of the published papers regarding the progressive collapse of structures after the collapse of the World Trade Center is highlighted.

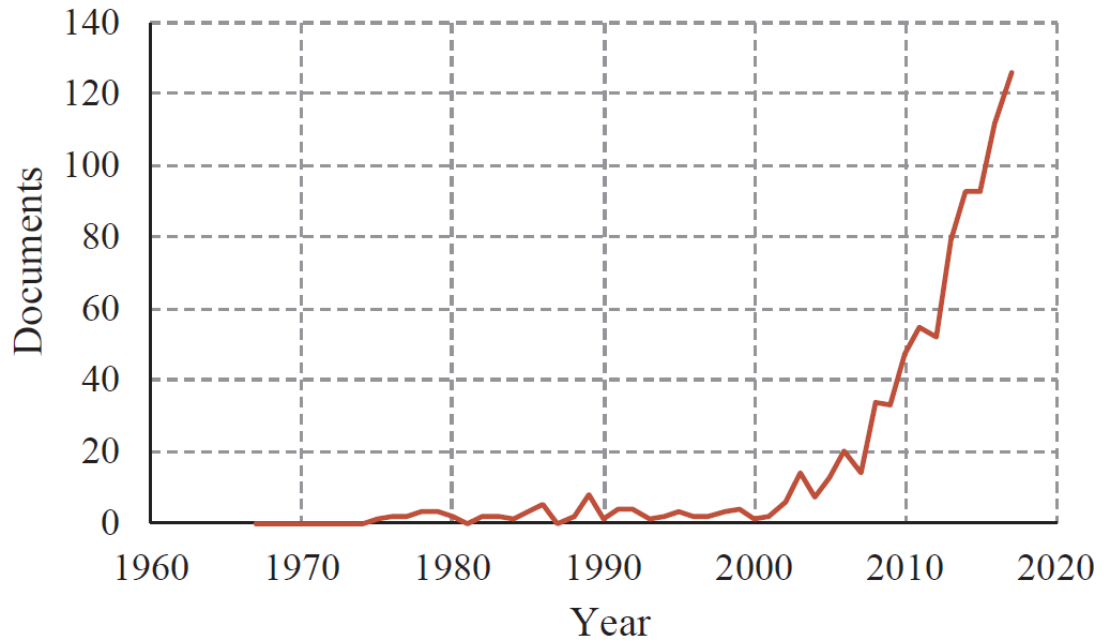


Fig. 2.1 Evolution of the number of papers published yearly in Scopus-indexed journals concerning the progressive collapse of structures (Adam et al.2018)

Some of the most important progressive collapse incidents with regard to the extent of the damage, the numbers of casualties and the social impact of the collapse include Capitan Arenas (Barcelona, 1972), Kansas City Hyatt Regency Hotel (Kansas City,1981), the U.S. Marine Barracks (Beirut, 1983), the Sampoong Department Store (Seoul, 1995), and the Achimota Melcom Shopping Centre (Acra, 2012).

2.3 Definition of progressive collapse

All types of structural systems may experience abnormal loads in their lifetime. The General Services Administration guidelines (GSA 2003) defines abnormal loads as the “loads other than conventional design loads (dead, live, wind, seismic, etc.) for structures such as air blast pressure generated by an explosion or impact by vehicles, etc.” Such extreme loads usually cause local damage. If a large part of the structure collapses because of local damage, the term progressive collapse comes in mind. The probability of the occurrence of abnormal loads is lower than that of their normal counterparts. Abnormal loads can be defined as low-probability loads, which might have high consequences.

Extreme events that cause abnormal loads can be classified as follows:

- extreme natural events, such as windstorms and megathrust earthquakes
- extreme accidental events, such as explosions, impacts, and fire
- human errors in design, construction, usage or maintenance
- malicious actions

Although studies about progressive collapse began in the late 1960s after the collapse of the Ronan Point Apartment (1968) and there are a lot of related studies, there is no consensus on the terminology of progressive collapse. There are different definitions in the literature for several terms, such as progressive collapse, disproportionate collapse, and robustness.

Two terms “disproportionate collapse” and “progressive collapse” have very similar definitions and are sometimes used in the literature interchangeably. However, there is a difference in their descriptions, which should be noticed. The main characteristic of disproportionate collapse is a prominent disproportion in size between a relatively small triggering event and the final state of collapse, which includes a large part or even the whole of the structure. It means that the term disproportionate collapse only describes that the final size of the damage is disproportionate to the triggering event and does not provide any description of the structural behavior. On the other hand, the main characteristic of progressive collapse is the propagation of failure within the structure.

The term progressive collapse describes the response of the structural system to the initial damage. Progressive collapse is usually disproportionate. However, a proportionate progressive collapse might happen.

For a better understanding, Adam et al. (2018) provided two sets of examples. According to their definition, a progressive collapse may be proportionate in size, for instance, if failure propagation is arrested by some elements, without spreading over a major portion of the structure. Vice versa, a collapse may be disproportionate in size, even without failure propagation. For example, in case the collapse of a statically determinate structure is originated from the failure of a single member. Considering the mentioned definitions, the term progressive collapse is more appropriate when the mechanism of collapse is of concern, and the term disproportionate collapse is preferred when the design and the performance of a structure are of concern.

As mentioned, there are several definitions for progressive collapse. In this study, progressive collapse is defined as the spread of an initial local failure from element to element, eventually resulting in the collapse of an entire structure or a disproportionately large part of it (ASCE 2002). It is characterized by a distinct disproportion between the triggering event and the resulting widespread collapse (Starossek 2006). A summary of different definitions of progressive collapse is presented in Table 2.1.

Table 2.1. Different definitions of progressive collapse in the literature

	Definition of progressive collapse
Starossek (2018)	"If there is a pronounced disproportion between a comparatively minor event and the ensuing collapse of a major portion or even the whole of a structure, then this is a disproportionate collapse. When the collapse is initiated by the failure of one or a few structural components and then progresses over successive other components, a fitting label would be progressive collapse."
Adam et al. (2018)	"Progressive collapse is a collapse that begins with localized damage to a single or a few structural components and develops throughout the structural system, affecting other components."
Parisi and Augenti (2012)	"Progressive collapse [...] is a chain reaction mechanism resulting in a pronounced disproportion in size between a relatively minor triggering event and resulting collapse, that is, between the initial amount of directly damaged elements and the final amount of failed elements."
Kokot and Solomos (2012)	"Progressive collapse of a building can be regarded as the situation where local failure of a primary structural component leads to the collapse of adjoining members and to an overall damage which is disproportionate to the initial cause."
Agarwal and England (2008)	"Progressive collapse is the spread of damage through a chain reaction, for example through neighboring members or storey by storey."
Krauthammer (2008)	"Progressive collapse is a failure sequence that relates local damage to large scale collapse in a structure."
Ellingwood (2006)	"A progressive collapse initiates as a result of local structural damage and develops, in a chain reaction mechanism, into a failure that is disproportionate to the initiating local damage."
Canisius et al. (2007)	"Progressive collapse, where the initial failure of one or more components results in a series of subsequent failures of components not directly affected by the original action is a mode of failure that can give rise to disproportionate failure."
NISTIR 7396 (2007)	"The spread of local damage, from an initiating event, from element to element, resulting, eventually, in the collapse of an entire structure or a disproportionately large part of it."
GSA (2003)	"A progressive collapse is a situation where local failure of a primary structural component leads to the collapse of adjoining members which, in turn, leads to additional collapse. Hence, the total collapse is disproportionate to the original cause."
UFC 4-010-01 (2003)	"Progressive collapse is a chain reaction failure of building members to an extent disproportionate to the original localized damage."
ASCE (2002)	"Progressive collapse is defined as the spread of an initial local failure from element to element resulting, eventually, in the collapse of an entire structure or a disproportionate large part of it."
Gross and McGuire (1983)	"A progressive collapse is characterized by the loss of load-carrying capacity of a relatively small portion of a structure due to an abnormal load which, in turn, triggers a cascade of failure affecting a major portion of the structure."
Allen and Schriever (1972)	"Progressive collapse [...] can be defined as the phenomenon in which local failure is followed by collapse of adjoining members which in turn is followed by further collapse and so on, so that widespread collapse occurs as a result of local failure."

2.4 Classification of different types of progressive collapse

As mentioned, the main feature of progressive collapse is a profound disproportion between a small triggering event and the resulting collapse of a large part or even the entire structure. However, there are different types of progressive collapse with regard to the mechanism of collapse propagation. In other words, different kinds of structures respond differently to local damages and are susceptible to a different mechanism of collapse. Hence, the mechanism of the collapse propagation within the structural system is different. The mechanism of progressive collapse depends mainly on the kind, form, and orientation of the structure in space. As each type of collapse needs an exclusive theoretical treatment as well as proper countermeasures, the classification of different types of collapse helps researchers and design engineers to find the best approach to mitigate the risk of progressive collapse.

Starossek (2018) used the characteristic features and the propagating actions of different types of collapse and identified six types of progressive collapse, namely, pancake-type, zipper-type, domino-type, section-type, instability-type, and mixed-type collapses.

For instance, the characteristic features of zipper-type collapse are the redistribution of forces of failed elements into alternative load paths, impulsive loading due to the sudden failure of structural elements, and static and dynamic force concentration in the load-bearing elements adjacent to the failed elements.

The zipper-type collapse can occur in parallel load-bearing systems such as cable-supported bridges or anchored retaining walls. One of the targets of this study is the investigation of progressive collapse in parallel load-bearing systems. Hence, in the following section, two actual examples of progressive collapse in parallel load-bearing systems will be investigated, and the related studies concerning the reasons for their collapse will be reviewed.

2.5 Actual examples of progressive collapse in parallel load-bearing systems

2.5.1 Hyatt Regency walkway collapse

The Hyatt Regency Hotel in Kansas City opened in 1980 for the public. It has a multistory atrium with three suspended walkways. In 1981, the second and the fourth walkways, one directly above the other, collapsed due to the weight of the people. Approximately 1600 people gathered in the hotel's lobby under the walkways. Killing 114 people and injuring 200 people made this accident one of the most catastrophic structural failures in the history of the U.S. in terms of lives lost.

In Fig. 2.2, the schematic view of the walkways and construction details are shown. Several researchers, including Marshall (1982), Wilkinson (1983), Moncarz and Taylor (2000), Pfatteicher (2000), Luth (2000), Morin and Fischer (2006), Teipelke (2010), Christianson et al. (2011), and Shulman (2017), have investigated this accident. Morin and Fischer (2006) reviewed the facts and circumstances causing structural failure. According to the ASCE report, the collapse was due to “the failure of the connections between the fourth-story box beams and the hanger rods supporting the second-story and fourth-story walkways.” Further investigations revealed major errors in the design process of the walkways. The original design of the walkways consisted of three pairs of hanger rods running from the second floor to the ceiling. The final design was a double-rod system. Even the original design of the walkways could tolerate only 60 percent of the minimum load required for this structure. However, the change of the original design of the walkways was the primary cause of the failure. In addition, in the original design, the beams of the fourth walkways had to tolerate only the weight of the fourth floor walkways. However, in the final design, the weight of the second floor walkways was also added to fourth floor beams. These beams were not strong enough. They only could tolerate 30 percent of the applied load. This accident also highlighted the importance of good communication among the project participants. In fact, any engineer could have realized the impact of the applied changes on the safety of the structure by a simple design review, but each engineer had assumed that others had checked the design. The top construction engineer of the project was recognized as the main responsible for the accident because of the apparent deficiency in the design of the structure.

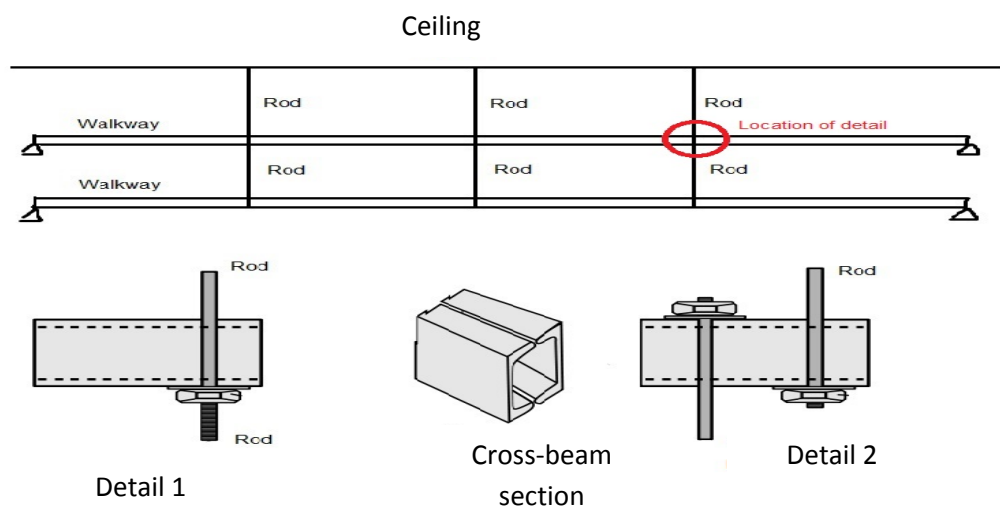


Fig. 2.2 The schematic view of the walkways and construction details (Shulman 2017)

2.5.2 The collapse of the Tacoma Narrows Bridge

The collapse of the Tacoma Narrows Bridge on November 7, 1940, due to wind-induced vibrations, is one of the most important structural failures of all time, which provoked several

studies investigating the reason for the collapse. The initial vibration of the bridge occurred due to 56 km/h winds. The amplitude of the vibration was 0.45 m. After three hours of vertical vibration, the wind increased to 67 km/h. At this point, one of the hangers at the main span snapped, causing an unbalanced loading condition. Accordingly, torsional oscillations appeared with a maximum amplitude of 8.5 m.

The torsional mode divided the bridge into two halves; one half was rotating clockwise, while the other half was rotating counter-clockwise. Finally, the bridge collapsed because of the large torsional oscillations. The bridge had been designed to withstand 161 km/h winds and vertical vibrations of the deck of the bridge during windy conditions had appeared several times. However, the torsional oscillations of the deck had happened only one time, which resulted in the collapse of the bridge. In Fig. 2.3, the torsional oscillations and the collapse of the bridge are demonstrated.

Several studies have been carried out investigating the reasons for this collapse (see Steinman and Watson (1958), Hilton (1977), Wyatt (1992), Kawada (2000), Slogoff and Berner (2000), Larsen (2000), Matsumoto (2003), Middleton (2003), Irwin et al. (2005), Green and Unruh (2006), Delatte (2009), Olson et al. (2015), and Gazzola (2015)).

Ammann et al. (1941) investigated the collapse and prepared an official report of the accident. They pointed out that the torsional oscillations, which are considered as the main reason for the collapse, had never observed before even during stronger winds. They considered the sudden change of the oscillation mode from vertical oscillations to torsional oscillations as the crucial event of the collapse. Nine years later, Andrew (1952) published a detailed report of the accident.

Plaut (2008) investigated the effects of snap loads on the hangers. He developed a continuum model of the central span, including the deck, cables, and hangers, and considered the longitudinal and torsional motions of the bridge.

Malik, J. (2013) studied the collapse of the Tacoma Narrows Bridge and proposed a continuous model of the bridge that described the collapse and revealed some of the possible reasons for the collapse. His model considered the mutual interaction of the main cables, hangers, and the deck.

Although they are different theories explaining the reasons for the collapse, all theories agree that the extreme flexibility, slenderness, and lightness of the bridge were the primary reasons for the collapse, which allowed the torsional oscillations to grow and eventually to destroy the bridge.

The existence of a structural problem within the bridge and external resonance are two main reasons outlined in the literature. The formation of vortices, due to the special shape of the bridge and the angle and the velocity of the wind, is another explanation. Several engineer mathematicians tried to develop a mathematical model explaining this collapse. A summary of these mathematical models is presented in the last section of this chapter.

Arioli and Gazzola (2013) discussed all of these explanations and stated that all of the presented theories about the collapse of the Tacoma Narrows Bridge fail to answer the question about the reason for the sudden appearance of torsional oscillations within the bridge. They mentioned that: "It is unlikely for an irregular wind to generate regular torsional oscillations or resonances which would require the matching of its frequency with an internal frequency of the bridge. Hence, the answer should not be sought in the behavior of the wind; one should instead study very carefully what happens inside the bridge."

They used a discretized model of a suspension bridge and presented a theory based on the flutter energy and the self-oscillations of the bridge due to the flutter speed of the wind. They showed that torsional vibrations could happen even in isolated systems subjected to the vertical loads. Their mathematical model will be briefly explained in the next section.

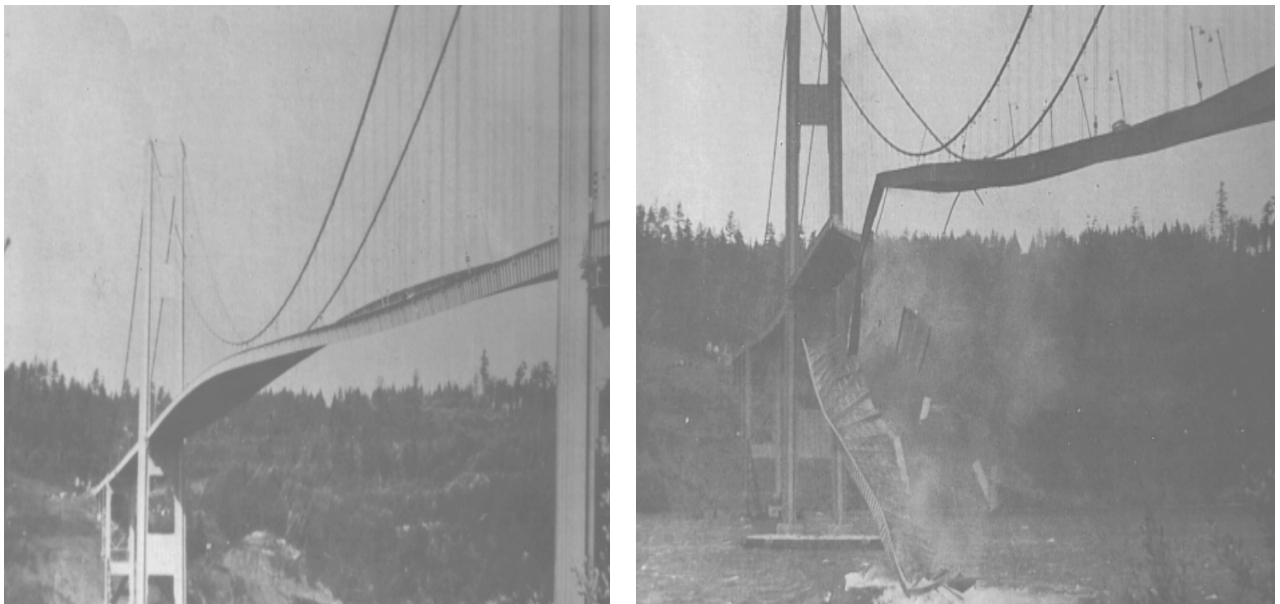


Fig. 2.3 Torsional vibrations of the Tacoma Narrows Bridge and its collapse (Hilton 1977)

As mentioned, there are different theories explaining the reason for this collapse. In the following, some of the main explanations of the Tacoma Narrows Bridge collapse will be discussed briefly.

2.5.2.1 Structural failure

The first explanation of the collapse was a mistake in the design and construction of the bridge. The chief engineer of the Tacoma Narrows Bridge claims that "the collapse probably was due to the fact that flat, solid girders were used along one side of the span. These girders caught the wind like a kite and caused the bridge to sway." However, further studies have not approved his statements.

Steinman and Watson (1958) stated that the entire profession has to be blamed because of not combining the knowledge of aerodynamics and dynamic vibrations with the rapidly advancing knowledge of structural design. In another study, Delatte (2009) justified the collapse with a structural failure due to metal fatigue.

2.5.2.2 External resonance

A federal report has mentioned the resonance with alternating periodic eddies as a possible reason for the large amplitude oscillations. However, some mathematicians have doubts about it. Lazer and McKenna (1990) stated that the phenomenon of linear resonance is very precise. The wind must generate a periodic force tuned to the natural frequency of the bridge. Therefore, the possibility of such precise conditions in the middle of the Tacoma Narrows is extremely low.

It is known that marching over the bridge could cause mechanical resonance. The collapse of the Broughton Suspension Bridge in 1831 was due to resonance induced by troops marching over the bridge. Arioli and Gazzola (2013) stated that "the probability that the step frequency of a troop coincides exactly with a natural frequency of a bridge is zero, but if these frequencies almost coincide then, unconsciously, the step of the humans tends to approach a natural frequency of the structure. However, this phenomenon cannot happen in winds. Hence, an external resonance, intended as a perfect matching between the exterior wind and the parameters of the bridge, is not the culprit for the TNB collapse."

2.5.2.3 Vortices

Karman and Edson (1967) were convinced that vortices were responsible for the large amplitude bridge oscillations. Vortex shedding is an oscillating airflow that occurs when the wind past a complex structure and produces low-pressure zones on the downwind side of the structure. Consequently, the structure moves towards the low-pressure zones in a periodic pattern.

In Fig. 2.4, a diagram of vortex shedding around a spherical body is demonstrated. As mentioned, the velocity of the wind that caused the collapse was around 67 km/h. The calculated frequency of a vortex shedding at this speed is 1 Hz. However, the torsional frequency of the bridge was around 0.2 Hz. Green and Unruh (2006) claimed that vortices produced limited torsion oscillations, but they are not responsible for the catastrophic oscillations of the bridge. Hence, this explanation is not popular in the scientific community.

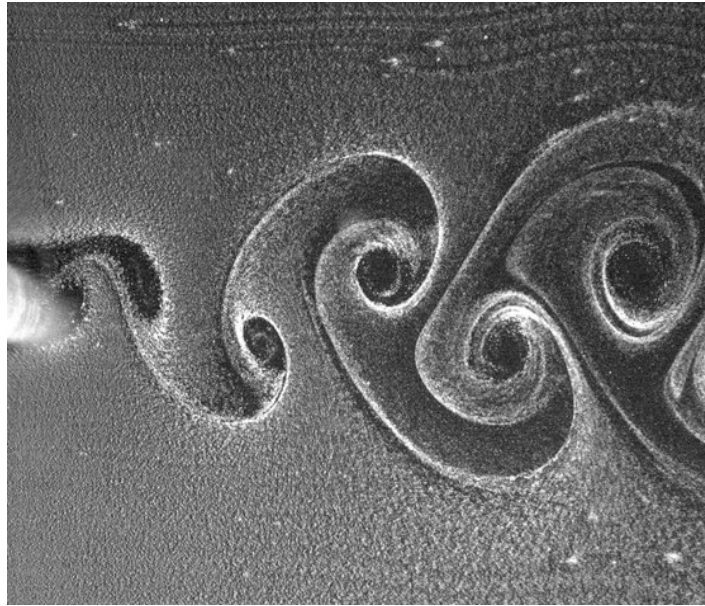


Fig. 2.4 A diagram of vortex shedding around a spherical body (Karman and Edson 1967)

2.5.2.4 Aerodynamic Instability (flutter theory)

Flutter is a self-feeding vibration that occurs when there is a positive feedback between the natural vibration mode of the structure and the aerodynamic forces. In other words, if the introduced energy in the structural system by the aerodynamic excitations is larger than the damped energy, the amplitude of vibration increases. Accordingly, self-exciting oscillations occur. This phenomenon is also called aerodynamic instability. Rocard (1957) proposed a method for the calculation of the flutter speed for suspension bridges.

Arioli and Gazzola (2013) used this method and calculated the flutter speed of the wind for the Tacoma Narrows Bridge. They claimed that the calculated flutter speed of the wind for the Tacoma Narrows Bridge was close to the wind velocity on the day of the accident. It should be noted that an unstable aerodynamic oscillation is not a resonant oscillation.

2.6 Progressive collapse in cable-supported bridges

This section provides a brief review of recent studies concerning the issue of cable failure and progressive collapse in cable-supported bridges. Some examples of progressive collapse in

cable-supported bridges are the collapse of Kutai Kartanegara suspension bridge in Indonesia (2011), Chhinchu suspension bridge in China (2007), Krong Bong suspension bridge in Vietnam (2013), Mahakam II Bridge in Indonesia (2011), and Yibin Southgate Bridge in China (2001). Fig. 2.5 demonstrates the collapse of Mahakam II Bridge in Indonesia.

As mentioned, progressive collapse is mainly studied in buildings. The two most important guidelines that address progressive collapse, the General Services Administration guidelines (GSA 2003) and the Unified Facilities Criteria (UFC 2013), are exclusively designed for buildings. Standards addressing progressive collapse and cable-loss scenarios in bridges are few. However, bridges are more vulnerable to progressive collapse, because of their unusual utilization, the low redundancy of their elements, and their placement in rough conditions (Fatollahzadeh et al. 2016). For instance, in Chinese codes, the safety factor of the hanger is 3.0 during service and it is 1.8 during the replacement of the hangers. There are no specifications provided for the sudden loss of the hangers.

According to Post-Tensioning Institute (PTI 2012), the sudden loss of any one cable must not lead to the rupture of the entire structure. For this regard, load case scenarios, including cable-loss situations, must be considered in the design process. In addition, in the case of the simplified design method (i.e., linear static analysis), a dynamic amplification factor (DAF) of two must be applied. Both of these suggestions have been further discussed in the literature.

In modern bridges, the distance between two adjacent cables is much shorter than in older bridges. Therefore, in the case of car accidents or explosions on new bridges, the rupture of more than one cable is more likely to happen. Accordingly, O'Donovan et al. (2003) suggested that the rupture of all cables within a 10 m range must be considered in the design of bridges. Several studies for the determination of the DAF in bridges have been conducted. These studies show that a DAF equal to two is not safe in all cases. While recent research proves that the suggested DAF is safe for the design of cables, it is not safe for the design of pylons, as well as the girders with negative moments (Tasai (2010), Mozos and Aparicio (2010b), Wolf and Starossek (2008), and Khuyen and Iwasaki (2016)). Studies related to the determination of DAF due to cable failure will be briefly explained in the next section.

Recently, the issue of progressive collapse in cable-supported bridges has been studied in some research (Fatollahzadeh et al. (2016), Das et al. (2016a, b) Miao and Ghosn (2016), Bi et al. (2015), Khuyen and Iwasaki (2016), Starossek (2009), and Mozos and Aparicio (2010a, b, 2006)).



Fig. 2.5 Mahakam II Bridge in Indonesia before and after the collapse (Qiu et al. 2014)

Zhou and Chen (2014) studied the behavior of cable-stayed bridges during an abrupt cable breakage event and proposed a “time-progressive nonlinear dynamic analysis methodology” for investigating the performance of cable-stayed bridges in such situations. To simulate the cable failure event in a more realistic manner, they incorporated stochastic traffic loads and dynamic bridge-vehicle interactions. By doing so, they obtained the initial dynamic states of the abrupt cable breakage event.

In order to model the cable failure, they considered two approaches. In Fig. 2.6, the demonstration of different approaches for the modeling of the cable failure is presented. In the first approach, they applied a pair of time-varying tension forces at the two ends of the cable considered to be failed. These forces had the same magnitudes but in opposite directions and counteracted the failed cable tension forces. Consequently, the failed cable remained on the numerical model, but it had zero effective axial force acting on the bridge.

In the second approach, they eliminated the failed cable from the model. They calculated the axial load of the failed cable before cable failure. Then, they applied a pair of time-varying tension forces at the two ends of this cable. For simulating the cable failure event, they removed the originally applied tension forces. They compared these approaches and showed that each of these approaches has its own advantages and limitations. They concluded that the second procedure provides more reasonable predictions of the bridge response in a cable-loss scenario.

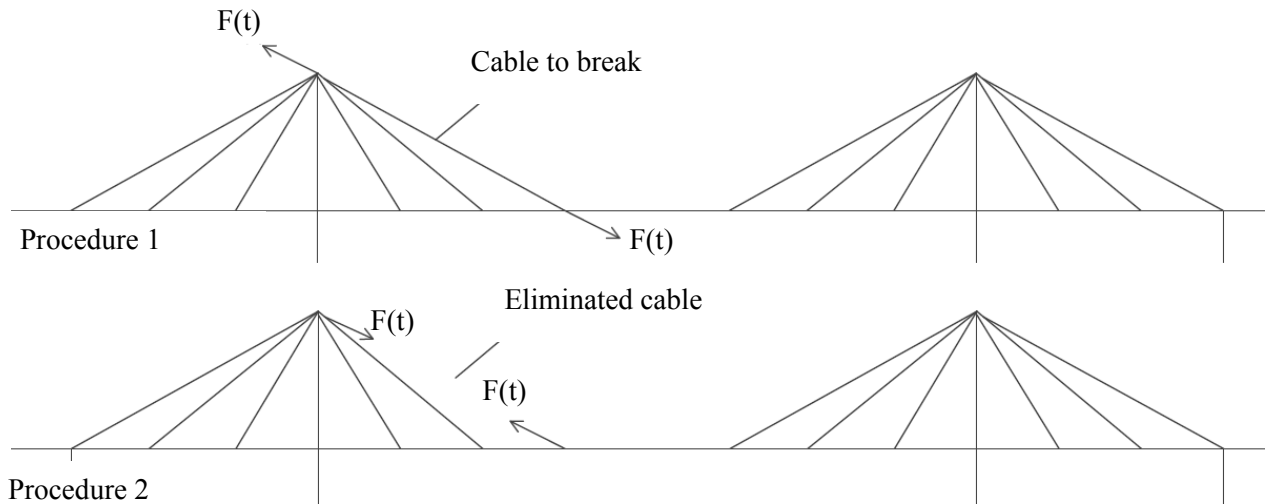


Fig. 2.6 Demonstration of different approaches for the modeling of cable failure (Zhou and Chen 2014)

In Fig. 2.7, the envelopes of vertical bending moments along the bridge girder using different methods are demonstrated.

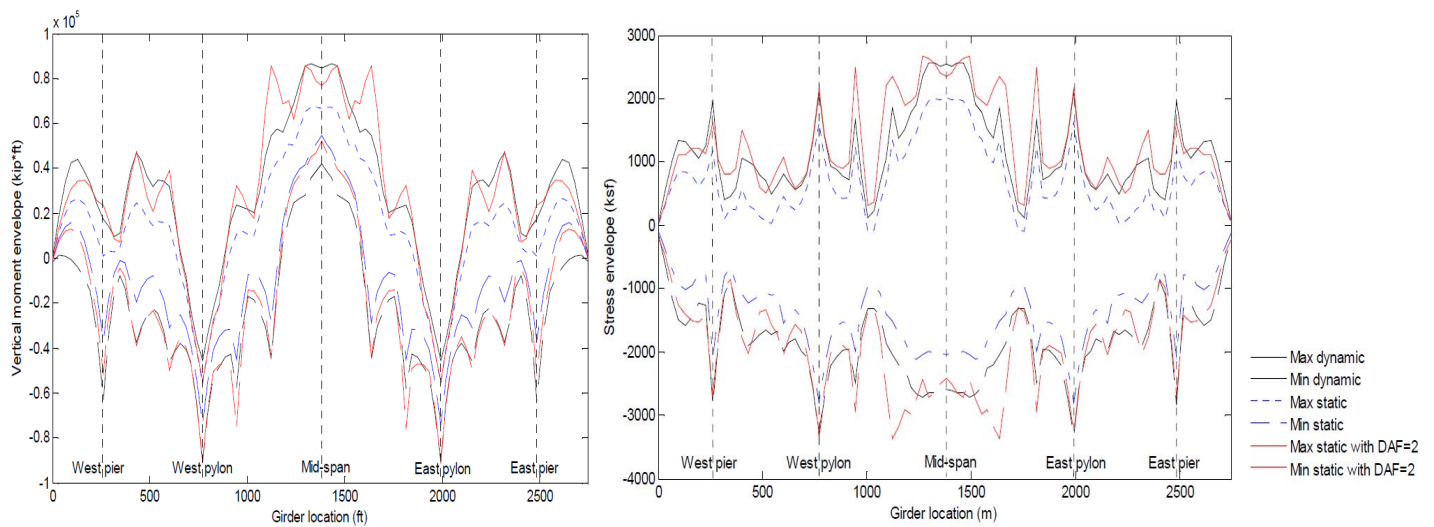


Fig. 2.7 Envelopes of vertical bending moments and stresses along the bridge girder using different methods- Zhou and Chen (2014)

They stated that the consideration of stochastic traffic loads during cable rupture events is essential and the stochastic traffic loads may cause larger bridge response than that of the static traffic loads.

Qiu et al. (2014) performed nonlinear static and nonlinear dynamic analyses and studied the responses of an actual self-anchored suspension bridge (Zhuanghe Jianshe Bridge) to the sudden breakage of hangers. In Fig. 2.8, the layout of the bridge is demonstrated. Their results showed that the sudden breakage of a hanger produces considerable vibrations and causes large changes in the internal forces of the structural elements. For example, the maximum tension force of the critical hanger due to the breakage of the adjacent hanger exceeds 2.22 times of its original force before the cable rupture.

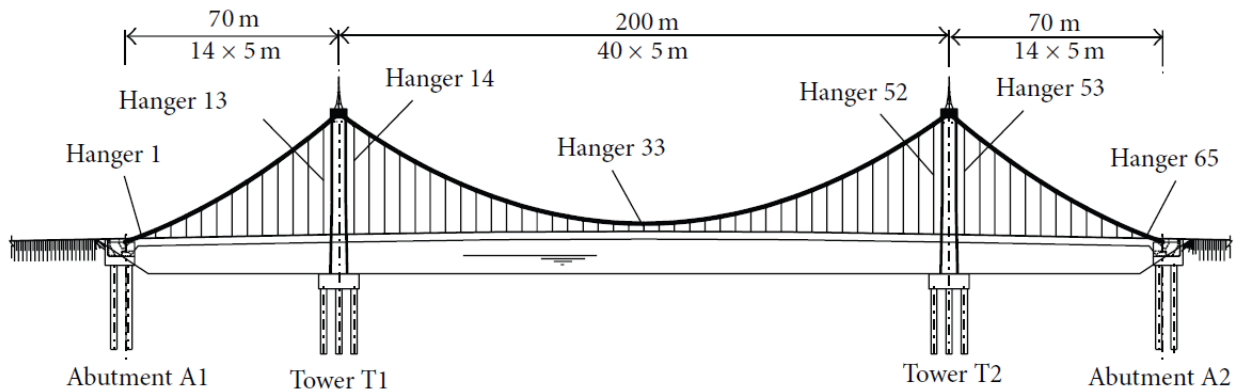


Fig. 2.8 Layout of Zhuanghe Jianshe Bridge-Qiu et al. (2014)

Das et al. (2016) investigated the nonlinear behavior of a cable-stayed bridge during different cable-loss scenarios. Their results showed that the sudden failure of stay cables at the center of the bridge span is more critical.

Miao and Ghosn (2016) proposed a methodology for performing probabilistic progressive collapse analyses and calibrating incremental analysis criteria for highway bridges accounting for the uncertainties in the applied loads and the load-carrying capacities of the members as well as the system. Their results showed that how the results from several reliability analyses can be implemented to develop criteria that would lead to consistent levels of safety and reliability. Bi et al. (2015) studied the mechanism of progressive collapse in a multi-span simply-supported bridge. They investigated the collapse of Hongqi Viaduct Bridge as a case study.

Wolf and Starossek (2009 and 2010) investigated the collapse behavior of a cable-stayed bridge in a cable-loss scenario. It was shown that the initial failure of three adjacent short cables, which were responsible for the stabilization of the bridge girder in compression, caused the lack of bracing in the girder. The girder began to buckle in the vertical direction as a result of high normal forces, and finally, an instability-type collapse occurred in the girder.

A parametric study has also been conducted on the dynamic response of cable-stayed bridges to the sudden failure of a cable (Mozos and Aparicio (2010a, b)). They examined the effects

of different layouts of the stays and the stiffness of the deck on the structural response of the bridge during sudden cable failure. It was shown that the sudden failure of a cable produced large bending moments on pylons.

Hashemi et al. (2016) studied the dynamic response of a cable-stayed bridge under a blast load considering the effects of cable loss on the behavior of the bridge. Their research showed that cable anchorage loss in the case of medium and large explosions are expected, and that shorter cables within the vicinity of the pylon are more vulnerable to rupturing.

Lonetti and Pascuzzo (2014) studied the structural behavior of hybrid cable-stayed suspension bridges in a cable-loss scenario. Their results showed that the hybrid scheme guarantees a proper degree of robustness against cable failure.

2.6.1 Determination of dynamic amplification factor (DAF)

Cable failure occurs in a very short period of time and is of dynamic nature. Using the nonlinear dynamic analysis is the most accurate method for the investigation of the behavior of the structure in such cases. However, it requires much more time and effort than a static analysis, which makes this method more costly. In addition, the application and the interpretation of the results of the nonlinear dynamic analysis are very complex and could be easily misleading. Therefore, it should be done only by expert engineers with related experience. Using linear static analysis with a DAF is a common approach in practical projects to solve the aforementioned problems. Obviously, an accurate estimation of the DAF in the case of using linear static analysis is very important.

DAF is a dimensionless factor, defined in Equation 2.1, by which the structural response obtained from linear static analysis should be multiplied to get the actual response of the structure under dynamic loading.

$$DAF = \frac{S_{dyn} - S_0}{S_{stc} - S_0} \quad (2.1)$$

where S denotes any state variable, S_{dyn} is the dynamic structural response, S_{stc} is the static structural response, and S_0 is the structural response in the initial state before the cable rupture happens.

The investigation of the DAF has been carried out in several studies (Hyttinen et al. (1994), Zoli and Woodward (2005), Park et al. (2007), Ruiz-Teran and Aparicio (2007 and 2009), Wolf and Starossek (2009), Tsai (2010), Mozos and Aparicio (2009, and 2010a, b), Tsai and You (2012), Khuyen and Iwasaki (2016), and Trong-Nghia and Samec. (2016)).

Hyttinen et al. (1994) studied the sudden failure of a stay cable on the Saame Bridge and concluded that the maximum value of DAF is equal to 1.8.

The investigation of the dynamic response of a single degree of freedom system (SDOF) subjected to a rectangular pulse load, studied in several classical references such as Chopra (2001), shows that the maximum value of the DAF is equal to two. Since cable-stayed bridges are complex structural systems with many degrees of freedom, their dynamic behavior is different from the behavior of a SDOF system, and using a constant DAF in all situations for all structural elements is questionable. In this regard, Mozos and Aparicio (2009) studied the dynamic response of a multiple degree of freedom system (MDOF) subjected to a pulse load of infinite durations and showed that under certain conditions, the DAF of a MDOF system could reach values larger than two.

In another study, Tasi (2010) conducted an analytical study and investigated the DAF of an inelastic SDOF model subjected to downward step loadings. Tsai and You (2012) performed a further development of the previous study and devised a small-scale test setup to investigate the inelastic DAF for structures subjected to sudden support loss.

Trong-Nghia and Samec (2016) investigated the cable rupture in cable-stayed bridges and stated that the DAF depends on several factors, such as the location of stay-cable rupture, structural damping, and the stiffness of structural elements. In addition, they concluded that the DAF could surpass the value of two, especially in pylon elements.

Zhou and Chen (2014) compared the results of the linear static and nonlinear dynamic analyses. They showed that using a DAF of two in the static analysis cannot capture the extreme values for both the moments and the stresses.

Khuyen and Iwasaki (2016) proposed an empirical equation to calculate the DAF for steel truss bridges in the case of the sudden failure of a structural member. In the following paragraphs, the results of two studies that investigated this issue more comprehensively will be presented.

Wolf and Starossek (2009) studied the dynamic behavior of cable-stayed bridges and investigated the realistic values of the DAF for different structural members. They concluded that DAF depends on the location of the failed cable as well as the type and location of the considered state variable. Therefore, a unique DAF for all structural members cannot be specified. Their results showed that the value of the DAF for the deflections and the bending moments of the stiffening girder vary in a very wide range. Fig. 2.9 shows the bending moment on the girder at different sections and corresponding values of DAF.

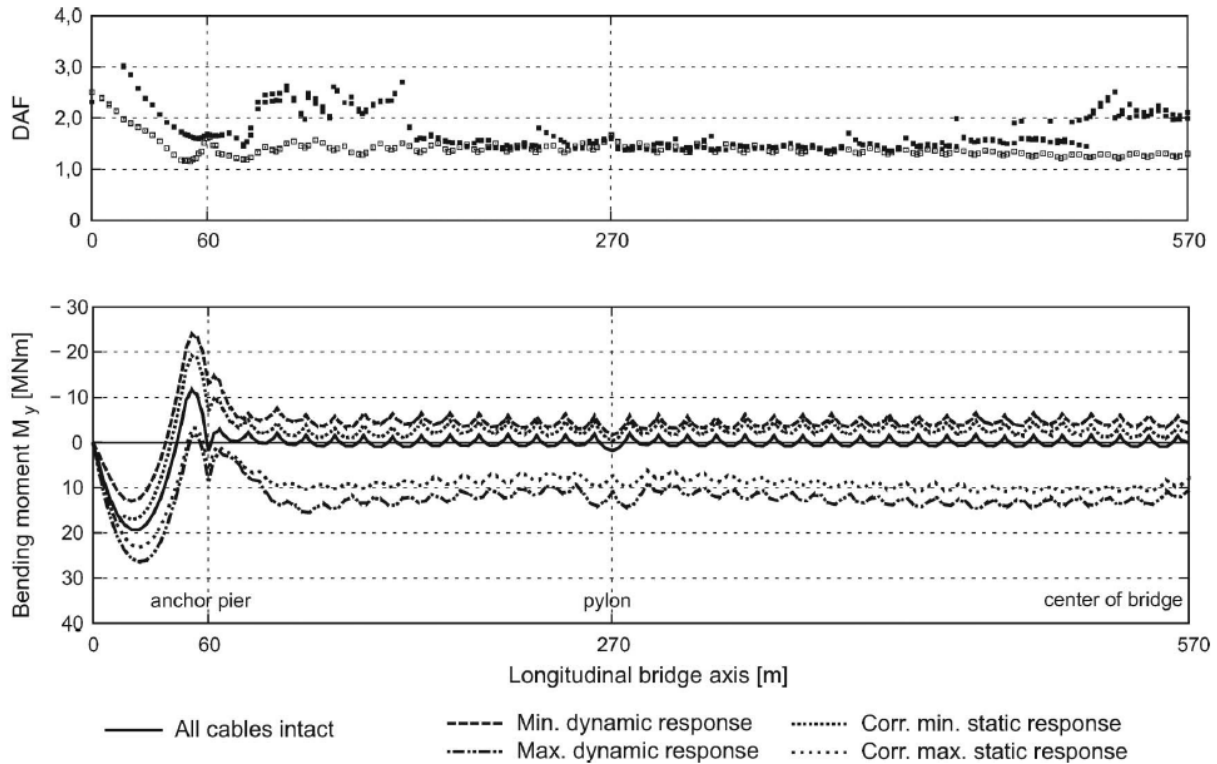


Fig. 2.9 The envelop of the bending moments as well as corresponding DAF of a cable-stayed bridge subjected to a cable failure-Wolf and Starossek (2009)

They found that for the positive bending moments of the girder, the DAF lies between 1.3 and 1.6. Investigating the negative bending moments showed that DAF varies from 1.4 to 2.7. An interesting aspect of their research was finding that the DAF of the bending moments on the girder at locations further away from the failed cable is significantly higher than two. However, because the static responses in these locations are very small, the large value of the DAF is irrelevant.

Investigating the axial force of the cables revealed that the DAF of the critical cable is between 1.35 and 2. This shows that using a DAF of two is safe for the design of the cables. They also found that the DAF of the bending moments in the pylons is significantly larger than two. Therefore, they concluded that, in this case, using static analysis with a DAF is not safe at all, and dynamic time-history analyses are highly recommended.

In another comprehensive study, Mozos and Aparicio (2010a, b) performed a parametric study to investigate the dynamic response of cable-stayed bridges to the sudden loss of a stay. Their main target was to determine the safety level provided by using a linear static analysis with a DAF of 2.0. For this purpose, they analyzed ten cable-stayed bridges and investigated

the effect of different characteristics of the structural system, such as the layout of the stays (fan or harp pattern), the number of planes of stays, and the stiffness of the deck, on the DAF. In Fig. 2.10, the longitudinal layouts of the studied bridges are depicted.

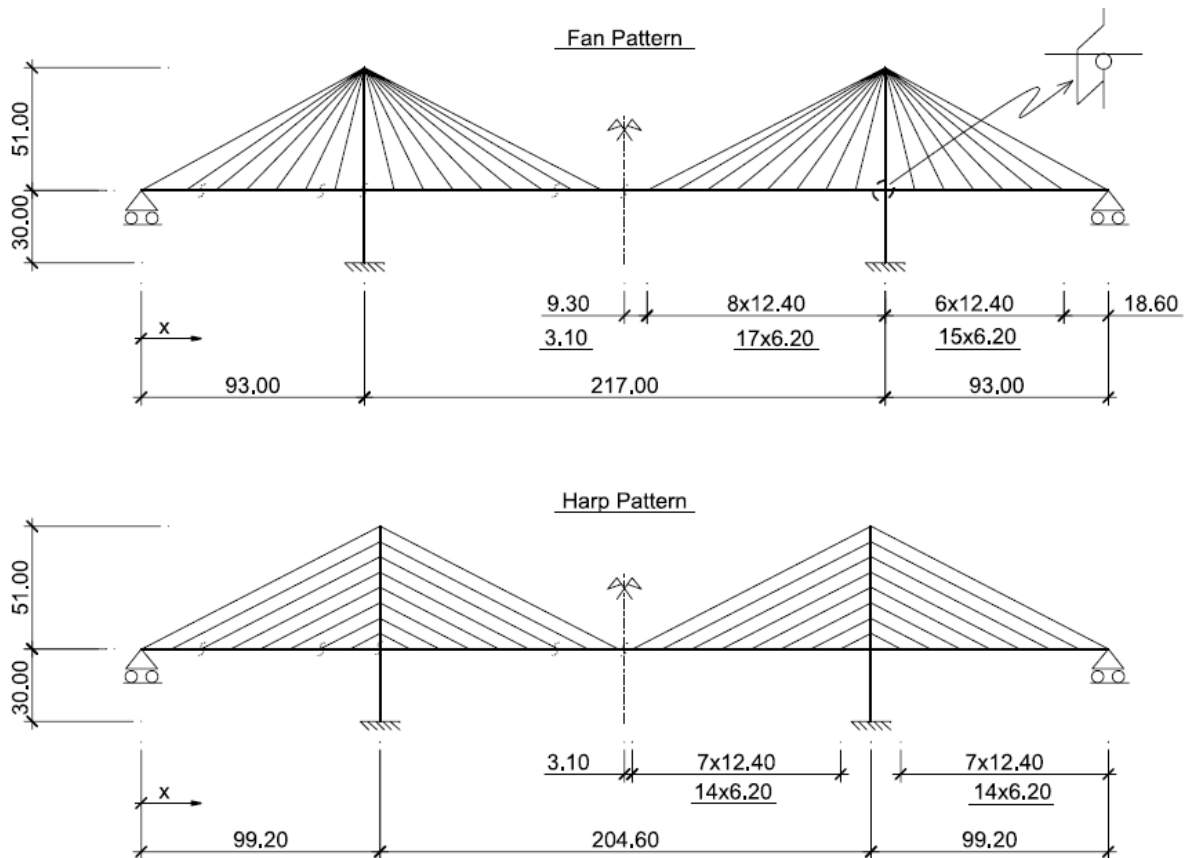


Fig. 2.10 Longitudinal layout of the studied bridges by Mozos and Aparicio (2010a, b)

Their results regarding the bending moments on the girder showed that using a fan pattern generates a larger DAF. Regarding the negative bending moments on the girder, the value of the DAF is significantly larger than two. In this case, the averages of DAF for damped and undamped systems were equal to 2.52 and 3.35, respectively. On the other hand, investigating the positive bending moments on the girder showed that the average value of the DAF is equal to 1.4 and 1.7 for the damped and undamped systems, respectively. They concluded that using a dynamic analysis for the design of the deck in a cable-loss scenario is necessary.

Studying the dynamic behavior of the pylons showed that the sudden failure of a cable produces large bending moments in the pylons. Regarding both negative and positive bending moments, the obtained DAF was larger than two in most cases. In addition, their results showed that using a fan pattern and a stiffer girder are two factors that increase the DAF. Consequently, they concluded that using a DAF of two is a very unsafe approach for evaluating the bending moments on the pylons due to cable failure.

Finally, the investigation of the dynamic response of the cable showed that only the dynamic response of the cables close to the failed cable is important, and the most critical cable is the cable adjacent to the failed cable. The average of the obtained DAF of the axial force in the cables due to the cable rupture was 1.68. Thus, they concluded that using static analysis with a DAF of two is a safe method for evaluating the axial forces in the cables during a cable-loss scenario.

2.6.2 Cable breakage duration

In this section, the related studies regarding the realistic value of cable breakage duration will be briefly reviewed. There are two methods for modeling cable failure either the elimination of the cable tension force or the reduction of the elastic modulus of the cable to zero. In Fig. 2.11, both of these methods are shown. Cable rupture occurs in a very short period of time. According to the basic principles of dynamics, as the duration of the cable failure (Δt) decreases, the maximum response of the structure increases.

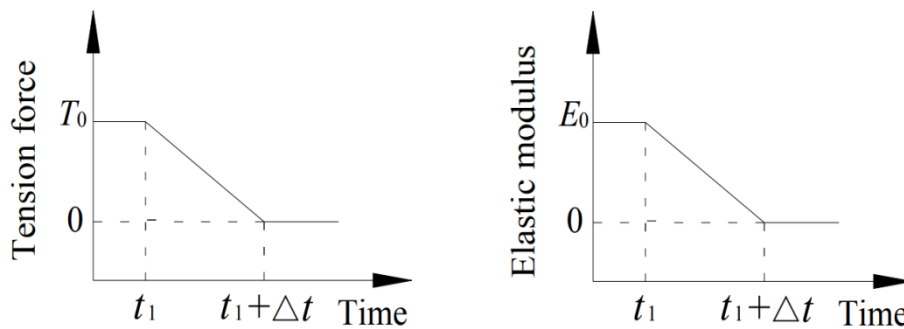


Fig. 2.11 Time history curve of the broken hanger-Wu and Qiu (2018)

In numerical studies, a realistic estimation of the cable breakage duration is essential and has an important effect on the final results. However, there are very few studies regarding the investigation of a realistic duration of cable failure. Some researchers, including Ruiz-Teran and Aparicio (2009), Mozos and Aparicio (2010a, 2011), and Zhou and Chen (2014), discussed this issue and suggested some values for the estimation of the cable breakage duration.

Mozos and Aparicio (2011) performed an experimental study on the rupture time of a seven-wire strand made of specific steel type with a nominal diameter of 0.6 inches. They concluded that the average rupture times for damaged and undamaged wires are 0.00375 s and 0.0055 s, respectively.

In another study, Hoang et al. (2015) conducted an experimental study to simulate the cable rupture event in cable-stayed bridges. They examined the rupture time of steel wires while being tensioned by an autograph tensile testing machine. They considered two rupture

scenarios. In the first one, the cross-section area of the testing specimen was reduced to reproduce the rupture of a stay cable damaged by corrosion. Fig. 2.12 shows a testing specimen with reduced cross-section area.

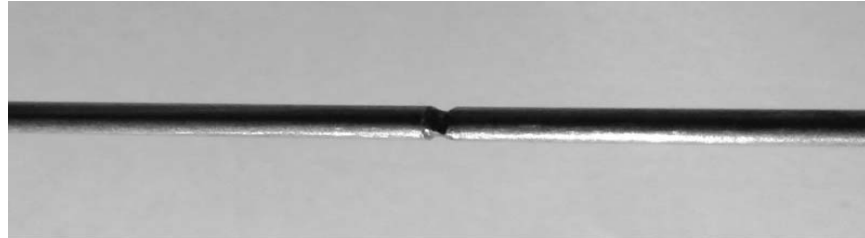


Fig. 2.12 Reduction of the cross-section of the testing wire-Hoang et al. (2015)

The second scenario was cutting the sample with a pair of pliers while being tensioned by an autograph tensile testing machine. This simulates a working cable in cable-stayed bridge broken due to an aggressive external shearing force. Fig. 2.13 shows the relationship between the rupture time and DAF. They showed that the rupture time in the second scenario is shorter and is equal to 0.0007 s.

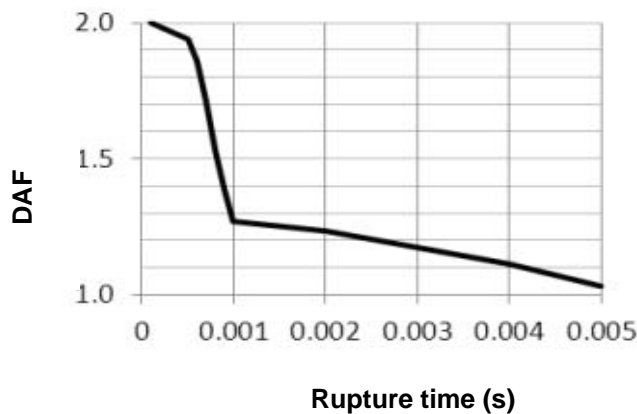


Fig. 2.13 Relationship between rupture time and DAF-Hoang et al. (2015)

Aoki (2014) claimed that the duration of the cable failure is in a range between 1 ms to 10 ms. Zhou and Chen (2014) and Xiang et al. (2018) reviewed the related studies and chose the cable breakage duration to be 0.01 s for their numerical studies. Wu and Qiu (2018) did the same and chose the cable breakage duration to be 0.005 s.

In a more general approach, Ruiz-Teran and Aparicio (2009) performed a parametric study and investigated the structural robustness of under-deck cable-stayed bridges to the sudden breakage of stay cables when 100% of the traffic load is applied. They considered several parameters, such as the type of breakage, the time over which breakage occurs, the number of failed cables, and the type of deviators. The most interesting result of this study was finding the relation between the breakage time of the cables and the dynamic response of the bridge. They considered the breakages from 1/10000 to 10 times of the fundamental period of the bridge and showed that the maximum dynamic response of the bridge is reached when the breakage time is less than 1/100 of the fundamental period of the bridge. In Fig. 2.14, the relationship between the breakage time of the cables and DAF is shown.

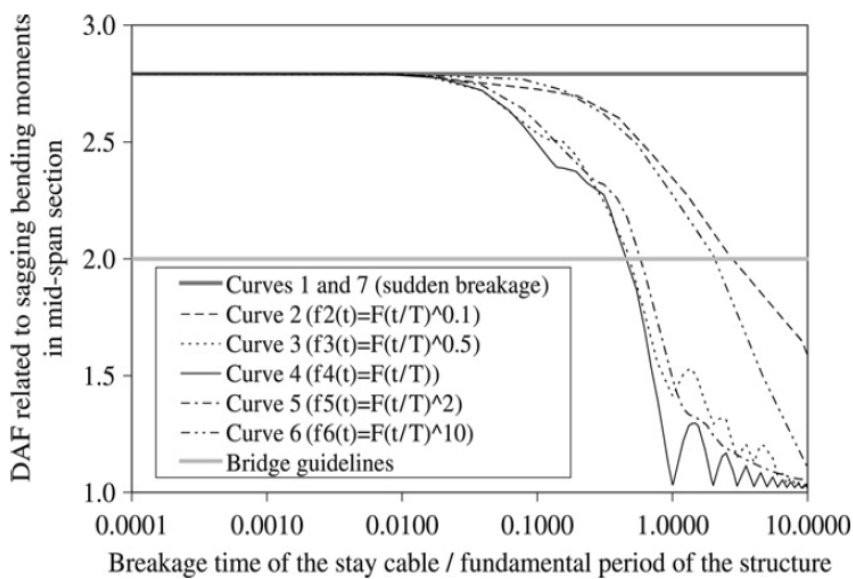


Fig. 2.14 The relationship between the breakage time of the cables and DAF- Ruiz-Teran and Aparicio (2009)

2.7 Mathematical models for the analysis of suspension bridges

In this section, some of the mathematical models suggested for the analysis of suspension bridges will be briefly reviewed. A detailed review and further developments of the classic mathematical models of suspension bridges have been presented by Gazzola (2015).

The French engineer and mathematician Navier (1823) was the first person who developed a mathematical framework for the analysis of suspension bridges. His work was, for more than five decades, the only tool for engineers to analyze suspension bridges and to have a better understanding of their structural behavior. This work is described in the literature, Kawada (2010), as “a Bible for engineers for almost half a century”. The proposed mathematical model by Navier was a simplified model and only considered the static of the cables and their interaction with the towers. He described the flexural behavior of a suspension bridge with

second order differential equations and solved them. His model was oversimplified in several aspects. However, considering the lack of prior history of mathematical models, his work was a masterpiece at that time.

The Italian mathematician and engineer Castigliano (1879) presented a theory named “theorem of the derivatives of internal work of deformation” for elastic systems. One of the applications of this theory is to calculate the deflection of a beam, which had an important role for further development of mathematical models for the analysis of suspension bridges.

Melan (1906) applied the Castigliano Theorem to the calculation of the deflection of the beam and studied different kinds of suspension bridges using the static of the cables and the beam. He investigated the effects of different parameters such as the number of spans, the stiffened or unstiffened structure, and temperature on the suspension bridges. He simplified a suspension bridge as an elastic beam suspended from several cables. In Fig. 2.15, the simplified model used by Melan is depicted. Melan's theory is certainly a milestone in developing mathematical models for suspension bridges. He suggested the following fourth order differential equation for describing the behavior of a suspension bridge:

$$EIw''''(x) - (H + h)w''(x) - hy''(x) = p(x) \quad (2.2)$$

It is denoted by:

EI the flexural rigidity of the beam; L the length of the beam (the distance between the towers); $p=p(x)$ is the live loads per unit length applied to the beam; $y=y(x)$ the downwards distance of the cable from the horizontal line connecting the endpoints of the cable due to the dead load; $w=w(x)$ the downwards displacement of the beam and, hence, the additional displacement of the cable due to the live load; H the horizontal tension in the cable, when subject to the dead load only; $h=h(w)$ the additional tension in the cable produced by the live load.

The function w describes the displacements of the beam and the hangers. It should be noted that Melan neglected the elastic deformations of the hangers. Therefore, the downwards displacements of the beam and the hangers were assumed to be the same. Although this assumption is not always correct, it was a generally acceptable simplification in the scientific community at that time. This assumption is justifiable when the bending stiffness of the beam is relatively small and only the lower modes of the bridge are critical. Luco and Turmo (2010) showed that the flexibility of the hangers has a significant effect on the frequencies of the higher modes when the stiffness of the girder is important.

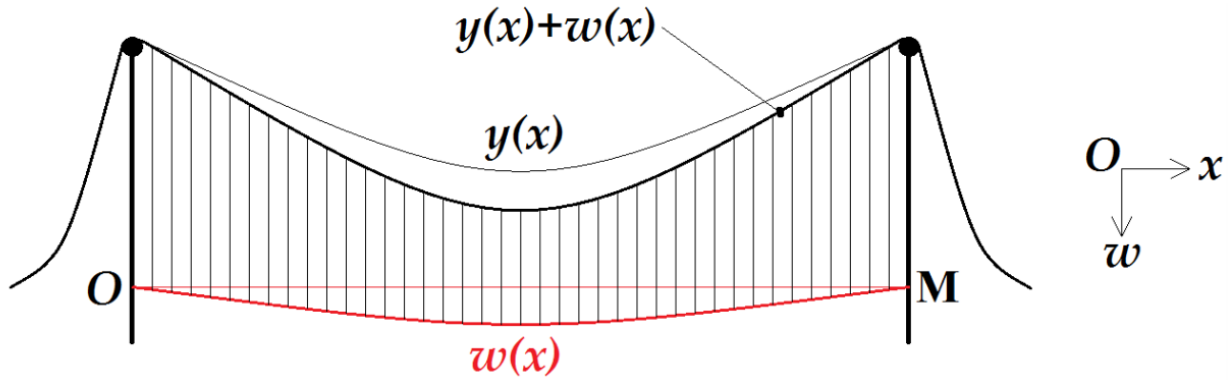


Fig. 2.15 Beam (red) sustained by a cable (black) through parallel hangers-Gazzola (2015).

In Fig. 2.15, the point O is defined as the origin of the orthogonal coordinate system and positive displacements are oriented downwards. The position of the main cable when the dead load is applied can be defined by $y(x)$. The segment connecting the two points of O and M is the unloaded beam.

Melan assumed that dead loads do not produce any bending moments in the beam. It means that the first adjustment of the main cable should be made in such a way that it carries all the dead loads, including its own weight, the hangers' weight and the beam weight. Therefore, all additional deformations of the main cable and the beam due to the live loads are small and negligible.

Melan calculated the downwards displacements of the cable due to the dead load, and derived the following equations:

$$y'(x) = \frac{q}{H} \left(\frac{L}{2} - x \right) \quad (2.3)$$

$$y''(x) = -\frac{q}{H} \quad (2.4)$$

$$EIw''''(x) - (H + h)w''(x) = p(x) - \frac{hq}{H} \quad (2.5)$$

where q is the dead load per unit length applied to the beam. Neglecting the elastic deformation of the hangers allowed him to use one single equation for describing the deflection of the beam and the main cable. After the collapse of the Tacoma Bridge due to the excessive vibration of the bridge in a strong wind, the engineering community tried to modify the Melan equation to find an explanation for the collapse of the Tacoma Bridge. For this purpose, time variables were introduced in mathematical models. Smit and Vincent (1950) and Bleich (1950) carried out two important works addressing this issue. They assumed a hinged beam at its two ends and considered the downwards displacement of the beam as a time variable. Then, they derived the following partial differential equation:

$$mu_{tt} + \delta u_t + EIu_{xxxx} - (H + h(u))u_{xx} + \frac{q}{H}h(u) = P \quad (2.6)$$

where $u=u(x,t)$ is the downwards displacement, m denotes the mass per unit length, q is the dead load which is equal to $q=mg$, $P=P(x,t)$ is the live load per unit length which is also defined as a time variable to take into account the effects of the wind on the bridge behavior, and δ is the damping parameter. They assumed that the live load and the displacement function have a periodic pattern and solve Equation 2.6.

$$P=P(x,t)=P(x) \sin(\omega t) \quad (2.7)$$

$$u=u(x,t)=w(x)\sin(\omega t) \quad (2.8)$$

where ω is the frequency and $w(x)$ is the maximum deflection at any point. However, these assumptions are not correct. The recorded vibration frequencies at the Tacoma Bridge show a different pattern of vibration.

Robinson (1967) stated that neglecting the extension of the hangers was the main reason for the inaccuracy of the mathematical models. McKenna (1987) was the first person who developed nonlinear mathematical models for describing the behavior of suspension bridges. In fact, the Melan equation has relatively acceptable accuracy when a suspension bridge has small oscillations. However, it loses its accuracy when large oscillations are involved.

In addition to the vertical components of the bridge vibration, its torsional component is also essential. Como et al. (2005) considered both of these components and derived the following linearized equations to describe the bridge behavior:

$$mu_{tt} + EIu_{xxxx} - Hu_{xx} + \frac{q^2}{H^2} + \frac{EI}{L_c} \int_0^L u(z,t) dz = f(x,t) \quad (2.9)$$

$$I_0\theta_{tt} + C_1\theta_{xxxx} - (C_2 + Hl^2)\theta_{xx} + \frac{l^2q^2}{H^2} + \frac{EI}{L_c} \int_0^L \theta(z,t) dz = g(x,t) \quad (2.10)$$

Where C_1 and C_2 are the warping and torsional stiffness of the beam, respectively. I_0 is the polar moment of inertia of the beam, $2l$ is the widths of the roadway, and $u(x,t)$ and $\theta(x,t)$ are the vertical and torsional components of the vibration, respectively. The rest of the parameters are defined before.

Gazzola (2015) modified the Melan equation and calculated the additional tension of the cables due to the live loads. He calculated the length of the main cable at rest (L_c) and the increment of the length due to the deformation as follows:

$$L_c = \int_0^L \sqrt{1 + y'(x)^2} dx \quad (2.11)$$

$$\Delta L_c = \int_0^L \sqrt{1 + (w'(x) + \frac{q}{H}(\frac{L}{2} - x))^2} dx - L_c \quad (2.12)$$

By using the aforementioned equations, the additional tension in the cable due to the live load can be calculated as follows:

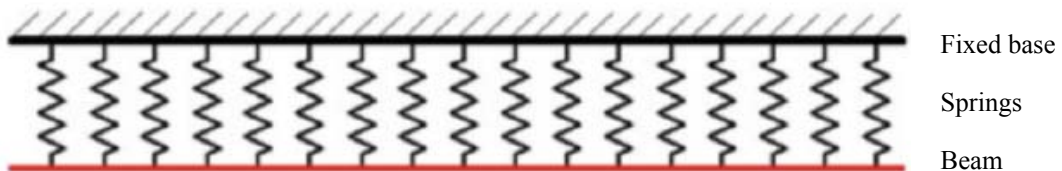
$$h = \frac{EA}{L_c} \Delta L_c \quad (2.13)$$

where A is the cross sectional area of the cable.

In addition to the exact value of the additional tension load in the cable, Gazzola (2015) reviewed three different ways in the literature for finding its approximation.

2.7.1 Conceptual models of suspension bridges

Suspension bridges are complicated structural systems with many degrees of freedom. Hence, developing a mathematical model for an actual suspension bridge is difficult. In order to make the mathematical procedures easier, engineers and mathematicians tried to develop some conceptual models. In this section, some of the conceptual models for the analysis of suspension bridges are briefly reviewed.



2.16 *Beam suspended from possibly slackening hangers*

The collapse of Tacoma Narrows Bridge showed that the slackening of hangers during a strong vibration is possible. Ammann (1941) studied the collapse of the Tacoma Narrows Bridge and mentioned that “one of the four suspenders in its group was permanently slack.”

Fig. 2.16 demonstrates a simplified model that has been presented in the literature to consider the possible slacking of the hangers. The simplified model consists of a beam suspended from large numbers of nonlinear springs. The nonlinear springs do not tolerate any compression forces. McKenna and Walter (1987) derived the following equation to describe the simplified model:

$$mu_{tt} + Elu_{xxxx} + ku^+ = f(x, t) \quad (2.14)$$

Where u is the downwards displacement of the beam, u^+ is the positive part of the displacement, k is the stiffness of the springs, and $f(x, t)$ is the acting force on the beam (dead load and live load), including the weight of the beam per unit length, the wind load, and the traffic loads. They used the boundary conditions of the system and solved the aforementioned differential equation. Lazer and McKenna (1990) developed the previous analytical solution and found a very interesting fact. They showed that strengthening a bridge can lead to its destruction in some situations when the stiffness of the hangers is sufficiently large. They used a simplified model, without modeling the towers, damping, and flexible cables. However, if this simplified model shows a distinct phenomenon, a similar phenomenon in more sophisticated models can also be expected. Fonda et al. (1994) added the damping coefficient (δ) to the previous equation and derived Equation 2.15. They solved the mentioned equation by assuming a periodic force acting on the beam.

$$mu_{tt} + Elu_{xxxx} + \delta u_t + ku^+ = f(x, t) \quad (2.15)$$

In Fig. 2.16, it was assumed that the beam is suspended from a fixed base through a large number of springs. In the next model, Gazzola (2015) assumed that the fixed base is replaced by an extensible cable. The simplified model is similar to the model depicted in Fig 2.15. The cable is fixed at its two endpoints, and the beam is hinged. The length of the main cable can be increased if it is forced by a load. By introducing the time, the following equations are derived:

$$m_c v_{tt} - H v_{xx} + \delta_c v_t - k(u - v)^+ = q_c + f_c(x, t) \quad (2.16)$$

$$m_b u_{tt} + Elu_{xxxx} + \delta_b u_t + k(u - v)^+ = q_b + f_b(x, t) \quad (2.17)$$

where $u(x, t)$ and $v(x, t)$ are the downwards displacements of the beam and the cable, respectively. Other parameters are the same as the previous equations highlighting that the indexes of c and b are abbreviations for cable and beam, and the positive part of $(u-v)^+$ emphasizes the fact that hangers exert a restoring force only under extension.

In the previous models, the deck of the bridge was modeled as a beam suspended from some hangers. Modeling the deck as a beam fails to capture the two degrees of freedom of the deck, namely, longitudinal and torsional degrees of freedom. In order to study the torsional behavior of the bridge, a two-dimensional model of the deck should be used. McKenna (1999) simplified the cross section of the deck as a beam suspended by two lateral hangers. His model showed that when the hangers lose tension, a large torsional oscillation occurs in the beam. A further numerical study performed by Doole and Hogan (2000) demonstrated that a

purely vertical periodic force on the deck might create a torsional response. Arioli and Gazzola (2015) investigated a further development of the McKenna model. Their model consists of a whole set of coupled cross sections suspended from a large number of oscillators. This model will be discussed in the next paragraph.

The next conceptual model that can describe the torsional oscillations of the deck is called the Fish-Bone model. In Fig. 2.17, the Fish-Bone model is shown. The grey part is the bridge deck, the length of the main span is L and the width of the deck is $2l$, the two thick black cross sections are fixed and the plate is hinged there. The red line contains the centers of the cross sections. The green orthogonal lines are virtual cross sections, and the angle of the torsion of the cross section is θ . Gazzola (2015) considers the following equations for describing the Fish-Bone model and solved them using the boundary conditions of the system and applying several simplifications.

$$my_{tt} + Ely_{xxxx} + f(y + l\sin\theta) + f(y - l\sin\theta) = 0 \tag{2.18}$$

$$\frac{ml^2}{3}\theta_{tt} - \mu l^2\theta_{xx} + l\cos\theta(f(y + l\sin\theta) - f(y - l\sin\theta)) = 0 \tag{2.19}$$

where $\mu > 0$ is a constant depending on the shear modulus and the moment of the inertia of the pure torsion. The other parameters are as described in the previous sections. The target of his study was to find the mathematical reason for appearing torsional oscillations in suspension bridges. He found that “when enough energy is present within the structure, a sudden transition between vertical and torsional oscillations may occur.” In fact, an internal resonance, which is a structural problem, causes the instability of the bridge. He also estimated the energy threshold of instability.

Benci et al. (2017) developed Gazzola’s study and proved the existence of solitons in suspension bridges. A soliton is a self-reinforcing wave packet that maintains its form during the propagation at a constant velocity. They also showed that in the case of existing large tension in the sustaining cables, solitons have nontrivial torsional components, which increase the risk of the instability of the bridge.

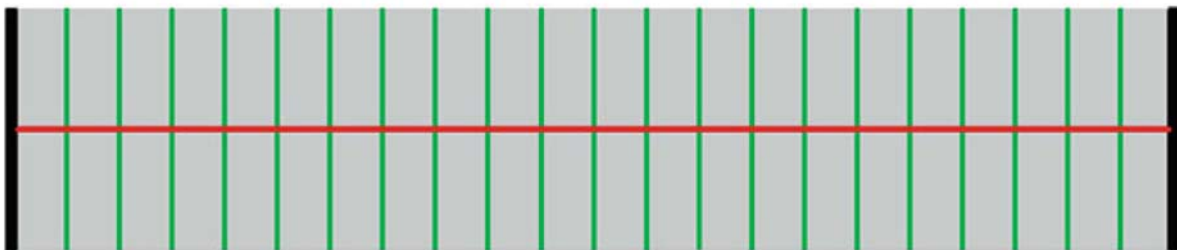


Fig. 2.17 A Fish-Bone model (Gazzola 2015)

Gazzolla (2015) defined three requirements for a good mathematical model of an engineering system. It should be as close as possible to the actual structure and reproduce the response of the real system in different scenarios. In addition, it should be theoretically tractable. Finally, it should be practical and usable for actual engineering projects. He developed four conceptual models as the mathematical models of suspension bridges. The first conceptual model, depicted in Fig. 2.18, consists of a continuous beam subjected to the restoring forces of several nonlinear two-sided springs. Considering the nonlinear restoring force of the springs and a uniform downwards load applied on the beam (e.g., dead load), he described the behavior of a suspension bridge. He showed that if $0 \leq T < 2\sqrt{kEI}$, the following equation describes the behavior of suspension bridges:

$$EIw''''(x) - Tw''(x) + kw(x) = P \quad (2.20)$$

where T is the constant tension in the beam, which is usually small, P is a uniform downwards load acting on the beam, and k is the stiffness of the springs. He solved Equation 2.20 and found a general form of the function $w(x)$. Besides, he showed that an unbounded beam subjected to the superlinear restoring forces has a natural tendency to vibrate with self-excited oscillations, which is very dangerous for the structure.

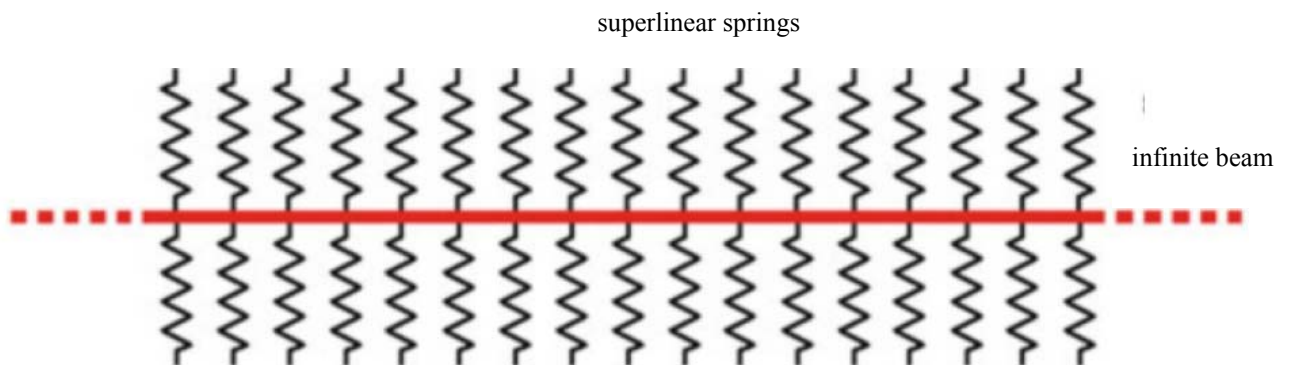


Fig. 2.18 The conceptual model of a suspension bridge developed by Gazzolla (2015)

In the second conceptual model, Gazzolla considered a hinged beam subjected to the superlinear restoring forces and performed a similar approach. The simplified model is shown in Fig. 2.19.

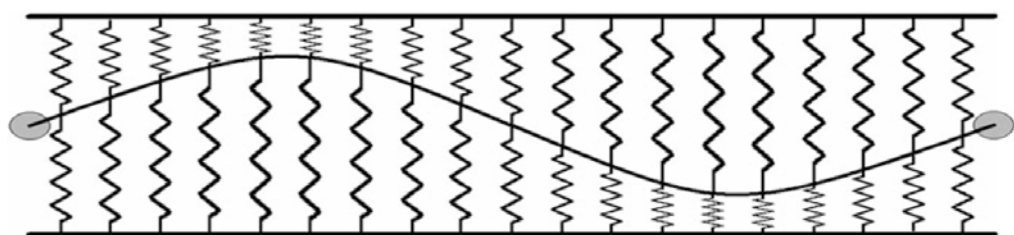


Fig. 2.19 The conceptual model of a suspension bridge developed by Gazzolla (2015)

In another effort for modeling a suspension bridge, Gazzola (2015) stated that when the space between hangers is very small, and the mass of the cable is neglected, the hangers can be considered as a continuous sheet or a membrane. Hence, he developed a conceptual model consisting of a beam suspended from the main cable through a membrane. The corresponding conceptual model is depicted in Fig. 2.20.

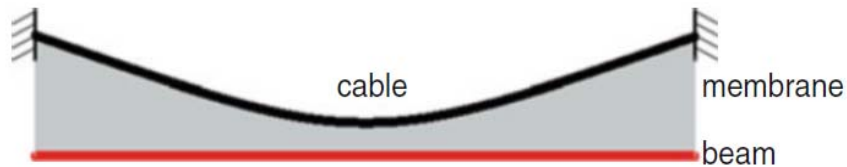


Fig. 2.20 Conceptual model of suspension bridges consists of a beam sustained by the main cable through a membrane (grey)-Gazzola (2015)

Arioli and Gazzola (2015) proposed a more sophisticated model to investigate the reason for the collapse of the Tacoma Narrows Bridge. In order to display the torsional oscillations of the deck, they modeled the deck of the bridge as a rod having two degrees of freedom. These degrees of freedom are the vertical displacement of the deck, y , and the angle of deflection from horizontal position, θ . The model is shown in Fig. 2.21. They modeled the bridge as a combination of several cross sections which are linked by linear forces. The red lines are the oscillators, which are linked to the hangers (nonlinear springs). The grey part is a membrane element which connects two adjacent oscillators.

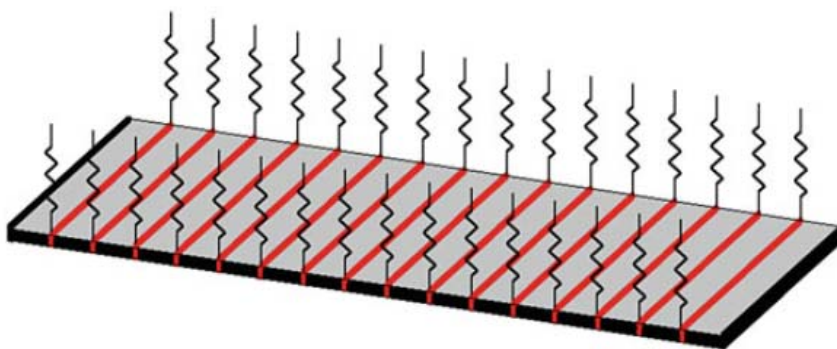


Fig. 2.21 The discretized model of a suspension bridge-Arioli and Gazzola (2015)

As demonstrated, the cross section of the bridge is modeled as two coupled oscillators (vertical and torsional). They used Newton's equation and described the vertical-torsional oscillations of the rod for each section as follows:

$$\frac{ml^2}{3} \ddot{\theta} = l \cos \theta (f(y + l \sin \theta) - f(y - l \sin \theta)) \quad (2.21)$$

$$m \ddot{y} = f(y - l \sin \theta) + f(y + l \sin \theta) \quad (2.22)$$

where the mass of the rod is m , the length of the rod is $2l$, and the angular velocity of the rod is $\dot{\theta}$. It is assumed that the center of the cross section of each rod behaves as an oscillator and the forces are applied through two hangers. The aforementioned equations are derived based on one cross section. They considered n parallel rods; each rod interacts with two adjacent rods, to model the length of the bridge.

Their model explains why torsional oscillations can occur independently of the applied force. Gazzolla (2015) reviewed several mathematical models of suspension bridges and stated that there is still a considerable gap between the mathematical models and the actual suspension bridges, which has not been filled even in recent years.

2.7.2 Considering the cable failure in the mathematical models of cable-supported bridges

The mentioned mathematical models in the previous section are mostly intended to capture the vertical and torsional vibrations of the deck and do not consider the failure of the cables. To the author's knowledge, Starossek (2011, unpublished) was the first person who developed a conceptual model considering the failure of a hanger.

In Fig. 2.22, the conceptual model developed by Starossek is shown. The conceptual model consists of a continuous beam suspended from tension elements (cables).

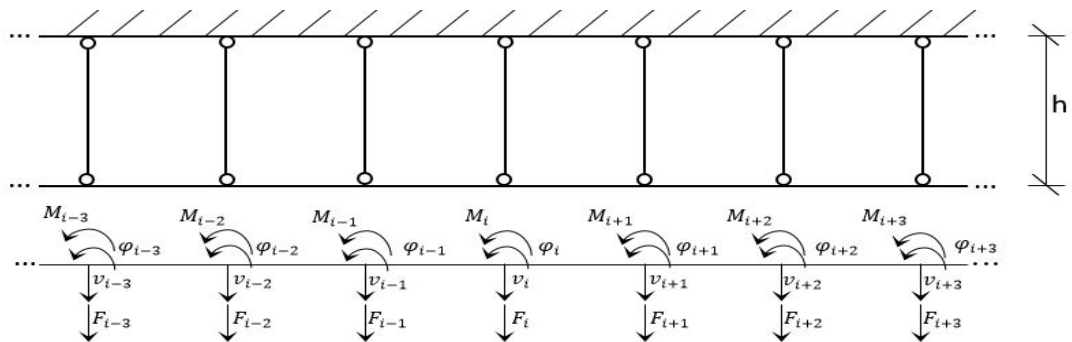


Fig. 2.22 A parallel load-bearing system developed by Starossek (2011)

His idea was to develop a measure of robustness by comparing the stiffness and the flexibility matrices of the intact and damaged system. To calculate the stiffness matrix of the intact system, he used the reduced form of the stiffness matrix. The reduced stiffness matrix is then inverted to obtain the flexibility matrix. The conceptual model is continuous. Hence, the

stiffness matrix is an infinite matrix. For converting an infinite matrix, Starossek used an innovative mathematical solution.

To make analytical calculations straightforward, he defined parameter η as the stiffness ratio of the system ($\eta = \frac{k_{cable}}{k_{beam}}$), and derived the reduced form of the stiffness matrix for an intact system as follows:

$$\underline{F} = \underline{\underline{K^{vv,red}}} * \underline{v} \quad (2.23)$$

$$\underline{F} = (\dots, F_{i-2}, F_{i-1}, F_i, F_{i+1}, F_{i+2}, \dots) \quad (2.24)$$

$$\underline{v} = (\dots, v_{i-2}, v_{i-1}, v_i, v_{i+1}, v_{i+2}, \dots) \quad (2.25)$$

$$\underline{\underline{K^{vv,red}}} = 3\sqrt{3}k_b \begin{pmatrix} \vdots & \vdots & \vdots & \vdots & \vdots & \vdots & \vdots \\ \dots & \frac{k_2}{3\sqrt{3}} & \frac{k_1}{3\sqrt{3}} & \frac{k_2}{3\sqrt{3}} & \varepsilon^2 & (-\varepsilon)^3 & \dots \\ \dots & \varepsilon^2 & \frac{k_2}{3\sqrt{3}} & \frac{k_1}{3\sqrt{3}} & \frac{k_2}{3\sqrt{3}} & \varepsilon^2 & \dots \\ \dots & (-\varepsilon)^3 & \varepsilon^2 & \frac{k_2}{3\sqrt{3}} & \frac{k_1}{3\sqrt{3}} & \frac{k_2}{3\sqrt{3}} & \dots \\ \vdots & \vdots & \vdots & \vdots & \vdots & \vdots & \vdots \end{pmatrix} \quad (2.26)$$

where $\varepsilon = \sqrt{3} - 2$, $k_1 = \eta - 4 + 3\sqrt{3}$, and $k_2 = \frac{1}{2}(19 - 12\sqrt{3})$.

Kempski (2016) performed a further development of this model by calculating the stiffness and flexibility matrices of the damaged systems. In Fig. 2.23, the procedures of the calculation of the stiffness matrix for damaged and intact systems are shown.

Kempski showed that there are certain stiffness ratios that must be avoided. She concluded that the calculation of the stiffness and the flexibility matrix is very complex and even the system with a failing tension element can only be determined by software program Maple with a long calculation time.

In this dissertation, the developed model by Starossek has been considered, and a different approach for solving the problem has been performed.

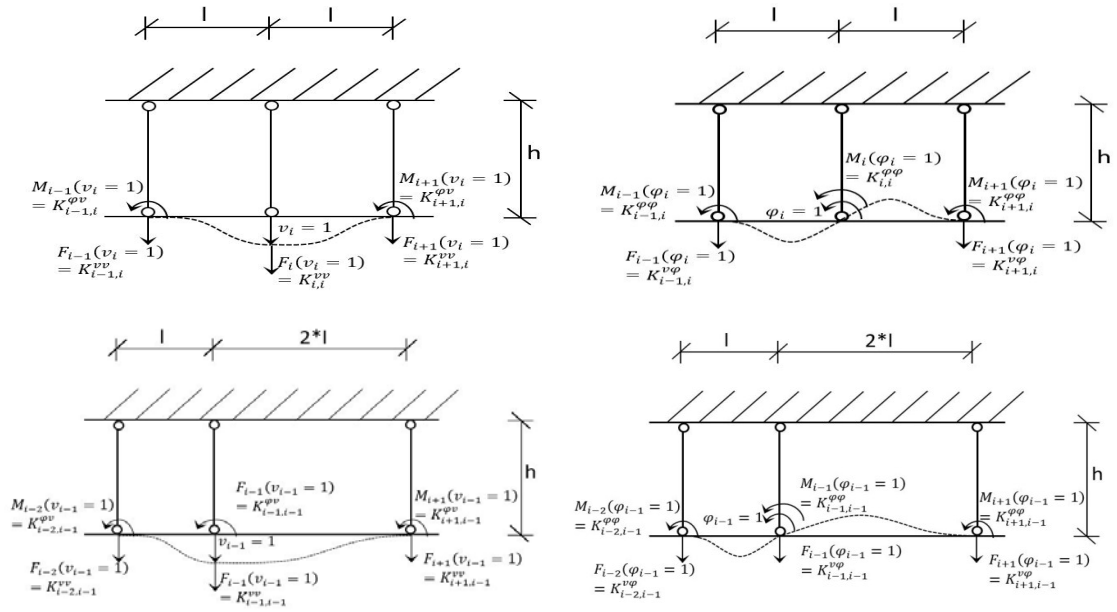


Fig. 2.23 The procedure of the calculation of the stiffness matrix for damaged and intact systems-Kempski (2016)

Chapter 3

Developing an Analytical Method for the Investigation of Cable Failure in Long-Span Cable-Supported Bridges

3.1 Introduction

Parallel load-bearing systems are structural systems with load-bearing members that are similar in type and function. These systems are distinguished by their ability to constitute alternative load paths. Cable-supported bridges, including suspension bridges and cable-stayed bridges, are good examples of such a structural system. In suspension bridges, the parallel load-bearing members are usually referred to as hangers, and in cable-stayed bridges, the parallel load-bearing elements are the stay cables. In this study, the word “cable” stands for both of them.

In this chapter, the structural behavior of a long-span cable-supported bridge after the sudden rupture of some of its cables will be investigated. The load carried by the failed cable must be redistributed to the remaining structure. In this situation, the cable adjacent to the failed cables receives most of the redistributed load and becomes the critical cable. If this cable can tolerate the redistributed load, the structure is robust, meaning that the collapse will not progress to the next members and the remaining structure stays intact. Hence, because of the vital role of the critical cable in the robustness of the structural system, the focus of this chapter is on this structural element. The main target is to find the “stress increase ratio” of the critical cable in a cable-loss scenario.

In the first section, a parallel-load bearing system is considered as a conceptual model of a long-span cable-supported bridge. Then, an analytical approach based on differential equations of the system is used, and an approximation function for a general parallel load-bearing system, in the case of the rupture of one of its cables, is derived. Afterward, the number of failed cables is increased to achieve an analytical method concerning the failure of any arbitrary number of cables. Then, the structural robustness of a system segmented by zipper-stoppers is investigated, and the stress increase ratio of the zipper-stopper in a cable-loss scenario is examined. Finally, the developed approximation function is employed to derive a reserve-based robustness index. It is shown that the proposed approximation function and the results of numerical models are in good agreement.

3.2 Conceptual model

To use the analytical approach, a conceptual bridge model is considered. The conceptual model is based on a mathematical model of suspension bridges developed by Starossek. In Fig. 3.1, the simplification procedure is depicted. The simplified model consists of a beam suspended from tension elements (cables).

In this study, only a part of the bridge is considered. Therefore, there are interferences in the border regions. The borders to account for the additional regions of the girder are investigated on the one hand as fixed supports, and on the other hand, as hinged supports. By doing so, two extreme values limiting the real behavior of actual systems are determined. The investigation of these two extreme conditions for long-span systems showed relatively similar results regarding the absorbed load in the critical cable as well as the maximum bending moment on the girder due to cable failure. It should be noted that the critical cable and the critical section of the girder are in the center of the system and far from border regions. Therefore, to make the analytical approach easier, a hinge is assumed at the border regions. In this study, a conceptual approach is applied. Hence, some differences between an accurate bridge model and the simplified model used here are unavoidable. For instance, assuming rigid upper cable supports does not exactly correspond to the actual structures.

Besides, because only a part of the bridge is considered, and for a selected part of the bridge, the stiffness of cables are close to each other, assuming the same cable stiffness is reasonable.

It should be mentioned that in some cases, torsion can be neglected. For example, in mono cable plane systems with box girder or systems with two cable planes with edge girders, the torsion effect is negligible. In this study, torsion is neglected.

It is worth highlighting that although the main idea comes from a suspension bridge, the simplified model can be used for any parallel load-bearing system, including cable-stayed bridges. It is assumed that all cables have the same axial stiffness and the stiffness of the girder is the same in all cross-sections. The axial stiffness of the cables should be determined considering the entire structural system of the actual bridge. The target is to find a general equation for the stress increase ratio of the critical member due to cable failure. Therefore, the number of cables is variable. In the first step, it is assumed that only one cable fails, and then an equation for the stress increase ratio of the critical cable is derived. In the second step, the number of failed cables is increased. Finally, an equation for a system including $2n$ cables in the case of the failure of m cables is derived.

In the simplified model, the distance between two adjacent cables is L , the axial stiffness of the cable is K and the bending stiffness of the girder is $K_b=12EI/L^3$. The failing cable is in the

center and the whole system is symmetrical. The load carried by the failing cable is F , the absorbed load in the critical cable due to the cable rupture is F_1 , and the corresponding absorbed loads in other cables on both sides from the center are F_2 to F_n (corresponding to K_2 to K_n). The calculated forces in cables and, consequently, the calculated bending moment in the girder are increased cable force and increased bending moment due to the cable rupture.

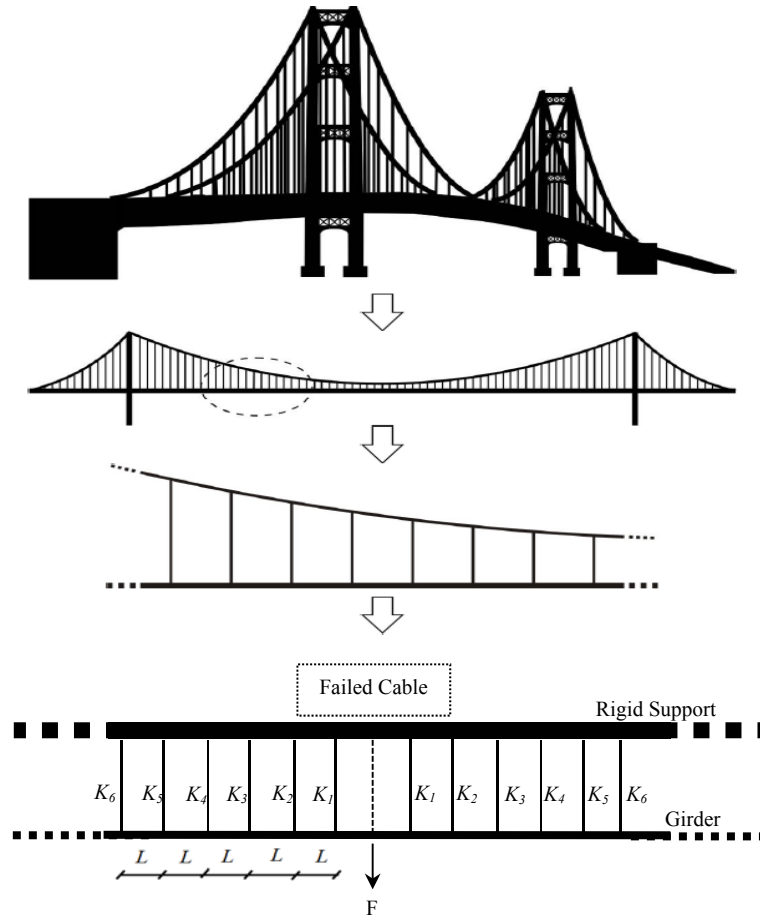


Fig. 3.1 From bridge to model, based on Haberland et al. 2012

3.3 Analytical approach for the determination of the stress increase ratio of the critical cable due to cable loss

The simplified system in Fig. 3.1 is a symmetric system and could be solved by superposition principle and boundary conditions taking into account the symmetry of the system. The elastic behavior of the girder is expressed as follows:

$$M(x) = EI \frac{d^2v}{dx^2} \tag{3.1}$$

where EI is the flexural stiffness of the girder, I is moment of inertia of the girder, v is the vertical displacement, and x is the distance of the section from the left end of the beam. $M(x)$

is the bending moment as a function of x due to the failure of the central cable, which could be found as follows:

$$0 \leq x \leq L \quad M(x) = F_n x \quad (3.2)$$

$$L \leq x \leq 2L \quad M(x) = F_n x + F_{n-1}(x - L) \quad (3.3)$$

$$2L \leq x \leq 3L \quad M(x) = F_n x + F_{n-1}(x - L) + F_{n-2}(x - 2L) \quad (3.4)$$

$$(n - 1)L \leq x \leq nL \quad M(x) = F_n x + F_{n-1}(x - L) + F_{n-2}(x - 2L) + \dots + F_1(x - (n - 1)L) \quad (3.5)$$

By taking the integral of Equation 3.1 for different sections, a system of linear equations will be found. For example, for $0 \leq x \leq L$:

$$\int M(x)dx = \int F_n x dx = F_n \frac{x^2}{2} + C_1 = EI \frac{dv}{dx} \quad (3.6)$$

$$\iint M(x)dx = \iint F_n x dx = F_n \frac{x^3}{6} + C_1 x + C_2 = EI v \quad (3.7)$$

where C_1 and C_2 are integration constants and are found by the boundary conditions of the system. Boundary conditions are the vertical displacements at the location of corresponding cables (v_i).

$$C_1 = \frac{EI v_n - EI v_{n-1} - \frac{F_n L^3}{6}}{L}, \quad v_i = \frac{F_i}{K_i}, \quad i = 1 \text{ to } n \quad (3.8)$$

$$C_2 = -EI v_n \quad (3.9)$$

A similar approach is performed for $L \leq x \leq 2L$ as follows:

$$\int M(x)dx = \int (F_n x + F_{n-1}(x - L))dx = F_n \frac{x^2}{2} + F_{n-1} \frac{x^2}{2} - F_{n-1} xL + D_1 = EI \frac{dv}{dx} \quad (3.10)$$

where D_1 is integration constant, and is found by the boundary conditions of the system:

$$D_1 = \frac{EI v_{n-1} - EI v_{n-2} - \frac{7F_n L^3}{6} + \frac{F_{n-1} L^3}{3}}{L} \quad (3.11)$$

Because the system is continuous, the slope of the girder is the same at $x=L$. Therefore, Equation 3.6 and Equation 3.10 have the same values at $x=L$. Therefore, the next equation can be derived.

$$(F_n \frac{x^2}{2} + C_1)_{x=L} = (F_n \frac{x^2}{2} + F_{n-1} \frac{x^2}{2} - F_{n-1}xL + D_1)_{x=L} \quad (3.12)$$

By repeating the same procedure for other sections, a system of linear equations can be derived. Solving the derived system of linear equations yields the axial force in each cable.

For a better understanding of the mathematical approach, in the following, an eight-cable system will be solved as an example. In Fig. 3.2, the eight-cable system and its structural specifications are shown.

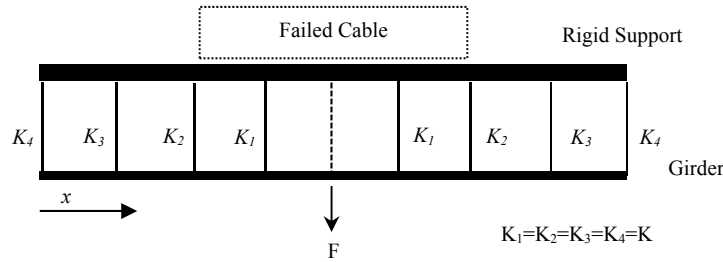


Fig. 3.2 The eight-cable system and its structural specifications

Solving the eight-cable system:

$$0 \leq x \leq L \quad M(x) = F_4 x = EI \frac{d^2 v}{dx^2} \quad (3.13)$$

Taking the integral of Equation 3.13:

$$\int M(x) dx = \int F_4 x dx = F_4 \frac{x^2}{2} + C_1 = EI \frac{dv}{dx} \quad (3.14)$$

Taking the integral of Equation 3.14:

$$\iint M(x) dx = \iint F_4 x dx = F_4 \frac{x^3}{6} + C_1 x + C_2 = EI v \quad (3.15)$$

where C_1 and C_2 are integration constants and are found by the boundary conditions of the system. Boundary conditions are the vertical displacements at the location of corresponding cables (v_i).

Boundary condition 1: $v_{x=0} = -y_4$

Boundary condition 2: $v_{x=L} = -y_3$

$$C_1 = \frac{EIy_4 - EIy_3 - \frac{F_4L^3}{6}}{L} \quad (3.16)$$

$$C_2 = -EIy_4 \quad (3.17)$$

A similar approach is performed for $L \leq x \leq 2L$ as follows:

$$\int M(x)dx = \int (F_4x + F_3(x - L))dx = F_4 \frac{x^2}{2} + F_3 \frac{x^2}{2} - F_3xL + D_1 = EI \frac{dv}{dx} \quad (3.18)$$

$$\iint M(x)dx = \iint (F_4x + F_3(x - L)) dx = F_4 \frac{x^3}{6} + F_3 \frac{x^3}{6} - F_3 \frac{Lx^2}{2} + D_1x + D_2 = EIv \quad (3.19)$$

where D_1 and D_2 are integration constants and are found by the boundary conditions of the system.

Boundary condition 1: $v_{x=L} = -y_3$

Boundary condition 2: $v_{x=2L} = -y_2$

Using the boundary conditions as mentioned above in Equation 3.19 yields the following system of equations:

$$\begin{cases} F_4 \frac{L^3}{6} + F_3 \frac{L^3}{6} - F_3 \frac{L^3}{2} + D_1L + D_2 = -EIy_3 \\ F_4 \frac{8L^3}{6} + F_3 \frac{8L^3}{6} - 2F_3L^3 + 2D_1L + D_2 = -EIy_2 \end{cases} \quad (3.20)$$

Solving the aforementioned system of equations yields:

$$D_1 = \frac{EIy_3 - EIy_2 - \frac{7F_4L^3}{6} + \frac{F_3L^3}{3}}{L} \quad (3.21)$$

$2L \leq x \leq 3L$:

$$\begin{aligned} \int M(x)dx &= \int (F_4x + F_3(x - L) + F_2(x - 2L))dx = F_4 \frac{x^2}{2} \\ &+ F_3 \frac{x^2}{2} - F_3xL + F_2 \frac{x^2}{2} - 2F_2Lx + G_1 = EI \frac{dv}{dx} \end{aligned} \quad (3.22)$$

$$\begin{aligned} \iint M(x)dx &= \iint (F_4x + F_3(x - L) + F_2(x - 2L)) dx = \\ &= F_4 \frac{x^3}{6} + F_3 \frac{x^3}{6} - F_3 \frac{Lx^2}{2} + F_2 \frac{x^3}{6} - F_2Lx^2 + G_1x + G_2 = EIv \end{aligned} \quad (3.23)$$

where G_1 and G_2 are integration constants, and are found by the boundary conditions of the system.

Boundary condition 1: $v_{x=2L} = -y_2$

Boundary condition 2: $v_{x=3L} = -y_1$

Applying the boundary conditions as mentioned above in Equation 3.23 yields the following system of equations:

$$\begin{cases} F_4 \frac{8L^3}{6} + F_3 \frac{8L^3}{6} - 2F_3L^3 + F_2 \frac{8L^3}{6} - 4F_2L^3 + 2G_1L + G_2 = -EIy_2 \\ F_4 \frac{27L^3}{6} + F_3 \frac{27L^3}{6} - F_3 \frac{9L^3}{2} + F_2 \frac{27L^3}{6} - 9F_2L^3 + 3G_1L + G_2 = -EIy_1 \end{cases} \quad (3.24)$$

Solving the aforementioned system of equations yields:

$$G_1 = \frac{6EIy_2 - 6EIy_1 - 19F_4L^3 - 4F_3L^3 + 11F_2L^3}{6L} \quad (3.25)$$

$3L \leq x \leq 4L$:

$$\begin{aligned} \int M(x)dx &= \int (F_4x + F_3(x-L) + F_2(x-2L) + F_1(x-3L))dx = F_4 \frac{x^2}{2} \\ &+ F_3 \frac{x^2}{2} - F_3xL + F_2 \frac{x^2}{2} - 2F_2Lx + F_1 \frac{x^2}{2} - 3F_1Lx + H_1 = EI \frac{dv}{dx} \end{aligned} \quad (3.26)$$

where H_1 is integration constant. Since at $x = 4L$ the slope of the girder is equal to zero (middle of the girder), here another boundary condition will be employed.

Boundary condition 1: $\dot{v}_{x=4L} = 0$

H_1 can be found by using the mentioned boundary condition in Equation 3.26 and solving the derived equation as follows:

$$F_4 \frac{(4L)^2}{2} + F_3 \frac{(4L)^2}{2} - F_3(4L)L + F_2 \frac{(4L)^2}{2} - 2F_2L(4L) + F_1 \frac{(4L)^2}{2} - 3F_1L(4L) + H_1 = 0 \quad (3.27)$$

$$H_1 = -8F_4L^2 - 4F_3L^2 + 4F_1L^2 \quad (3.28)$$

After calculating the integration constants for all sections of the girder, a system of equations is created. By doing so, the axial forces in all cables could be calculated. For creating a system of equations, other kinds of boundary conditions should be employed. Because the system is continuous, the slope of the girder at each section of the girder is the same. It means

that calculating the slope of the girder at the left (l) and right (r) side of each section gives us the same value.

$$x = L \quad \dot{V}_l = \dot{V}_r$$

$$F_4 \frac{x^2}{2} + C_1 = F_4 \frac{x^2}{2} + F_3 \frac{x^2}{2} - F_3 xL + D_1 \quad (3.29)$$

Equation 3.30 is created by replacing the calculated values of C_l and D_l in Equation 3.29.

$$C_1 = \frac{EIy_4 - EIy_3 - \frac{F_4 L^3}{6}}{L}$$

$$D_1 = \frac{EIy_3 - EIy_2 - \frac{7F_4 L^3}{6} + \frac{F_3 L^3}{3}}{L}$$

$$F_4 \frac{x^2}{2} + \frac{EIy_4 - EIy_3 - \frac{F_4 L^3}{6}}{L} = F_4 \frac{x^2}{2} + F_3 \frac{x^2}{2} - F_3 xL + \frac{EIy_3 - EIy_2 - \frac{7F_4 L^3}{6} + \frac{F_3 L^3}{3}}{L} \quad (3.30)$$

Solving the aforementioned equation for $x=L$ yields the following equation, which is the second equation in the final system of equations:

$$6F_4 L^3 + F_3 L^3 + 6EIy_4 - 12EIy_3 + 6EIy_2 = 0 \quad (3.31)$$

In the following, the same approach will be performed for other sections.

$$x = 2L \quad \dot{V}_l = \dot{V}_r$$

$$F_4 \frac{x^2}{2} + F_3 \frac{x^2}{2} - F_3 xL + D_1 = F_4 \frac{x^2}{2} + F_3 \frac{x^2}{2} - F_3 xL + F_2 \frac{x^2}{2} - 2F_2 Lx + G_1 \quad (3.32)$$

$$\text{where } G_1 = \frac{6EIy_2 - 6EIy_1 - 19F_4 L^3 - 4F_3 L^3 + 11F_2 L^3}{6L}$$

Equation 3.33 is created by replacing the calculated values of D_l and G_l in Equation 3.32.

$$\begin{aligned} F_4 \frac{x^2}{2} + F_3 \frac{x^2}{2} - F_3 xL + \frac{EIy_3 - EIy_2 - \frac{7F_4 L^3}{6} + \frac{F_3 L^3}{3}}{L} = \\ = F_4 \frac{x^2}{2} + F_3 \frac{x^2}{2} - F_3 xL + F_2 \frac{x^2}{2} - 2F_2 Lx + \frac{6EIy_2 - 6EIy_1 - 19F_4 L^3 - 4F_3 L^3 + 11F_2 L^3}{6L} \end{aligned} \quad (3.33)$$

Solving the aforementioned equation for $x=2L$ yields the following equation, which is the third equation in the final system of equations.

$$12F_4L^3 + 6F_3L^3 + F_2L^3 + 6EIy_3 - 12EIy_2 + 6EIy_1 = 0 \quad (3.34)$$

$$x = 3L \quad \dot{v}_l = \dot{v}_r$$

$$\begin{aligned} F_4 \frac{x^2}{2} + F_3 \frac{x^2}{2} - F_3xL + F_2 \frac{x^2}{2} - 2F_2Lx + G_1 &= \\ &= F_4 \frac{x^2}{2} + F_3 \frac{x^2}{2} - F_3xL + F_2 \frac{x^2}{2} - 2F_2Lx + F_1 \frac{x^2}{2} - 3F_1Lx + H_1 \end{aligned} \quad (3.35)$$

$$\text{where } H_1 = -8F_4L^2 - 4F_3L^2 + 4F_1L^2$$

Equation 3.36 is created by replacing the calculated values of G_l and H_l in Equation 3.35.

$$\begin{aligned} F_4 \frac{x^2}{2} + F_3 \frac{x^2}{2} - F_3xL + F_2 \frac{x^2}{2} - 2F_2Lx + \frac{6EIy_2 - 6EIy_1 - 19F_4L^3 - 4F_3L^3 + 11F_2L^3}{6L} &= \\ = F_4 \frac{x^2}{2} + F_3 \frac{x^2}{2} - F_3xL + F_2 \frac{x^2}{2} - 2F_2Lx + F_1 \frac{x^2}{2} - 3F_1Lx - 8F_4L^2 - 4F_3L^2 + 4F_1L^2 \end{aligned} \quad (3.36)$$

Solving the aforementioned equation for $x=3L$ yields the following equation, which is the last equation in the final system of equations.

$$29F_4L^3 + 20F_3L^3 + 11F_2L^3 + 3F_1L^3 + 6EIy_2 - 6EIy_1 = 0 \quad (3.37)$$

In this example, there are four unknown variables (F_i). Therefore, four equations are needed to solve the system. In the previous steps, three equations are derived. The final equation comes from equilibrium as follows:

$$F_1 + F_2 + F_3 + F_4 = \frac{F}{2} \quad (3.38)$$

where F_i is the axial force in each cable and F is the external force at the location of the failed cable. Because the system is symmetrical, only half of the system is considered. In the following, the final system of equations for an eight-cable system is created.

$$\begin{cases} F_1 + F_2 + F_3 + F_4 = \frac{F}{2} \\ 6F_4L^3 + F_3L^3 + 6EIy_4 - 12EIy_3 + 6EIy_2 = 0 \\ 12F_4L^3 + 6F_3L^3 + F_2L^3 + 6EIy_3 - 12EIy_2 + 6EIy_1 = 0 \\ 29F_4L^3 + 20F_3L^3 + 11F_2L^3 + 3F_1L^3 + 6EIy_2 - 6EIy_1 = 0 \end{cases} \quad (3.39)$$

By defining parameter β as the stiffness ratio of the system ($\beta = \frac{EI}{KL^3}$) and replacing the corresponding value of $y_i = \frac{F_i}{K}$, the above system of equations can be rewritten as follows:

$$\left\{ \begin{array}{l} F_1 + F_2 + F_3 + F_4 = \frac{F}{2} \\ F_4(6 + 6\beta) + F_3(1 - 12\beta) + F_2(6\beta) = 0 \\ F_4(12) + F_3(6 + 6\beta) + F_2(1 - 12\beta) + F_1(6\beta) = 0 \\ F_4(29) + F_3(20) + F_2(11 + 6\beta) + F_1(3 - 6\beta) = 0 \end{array} \right. \quad (3.40)$$

Solving the aforementioned system of equations gives us the axial forces of all cables due to cable failure. In the following, the stress increase ratio of the critical cable as a function of β is presented for eight-cable system:

$$\frac{F_1}{F} = \frac{173 + 3540\beta + 6264\beta^2 + 216\beta^3}{232 + 5976\beta + 18288\beta^2 + 1728\beta^3} \quad (3.41)$$

Finding the aforementioned system of equations is the key to solve the problem. However, performing the analytical approach for large systems requires lots of mathematical calculations, which is quite time consuming. Therefore, it is decided to perform the analytical approach for several small systems and find a mathematical pattern in the final system of equations. If such a mathematical pattern can be recognized, the final system of equations of any arbitrary large system can be derived by following a simple pattern without taking too much time.

In the following, the explained analytical approach is performed for several systems with different numbers of cables. The target is to find the final system of equations for each system.

Four-cable system:

$$\left\{ \begin{array}{l} F_1 + F_2 = \frac{F}{2} \\ F_2(11 + 6\beta) + F_1(3 - 6\beta) = 0 \end{array} \right. \quad (3.42)$$

Six-cable system:

$$\begin{cases} F_1 + F_2 + F_3 = \frac{F}{2} \\ F_3(6 + 6\beta) + F_2(1 - 12\beta) + F_1(6\beta) = 0 \\ F_3(20) + F_2(11 + 6\beta) + F_1(3 - 6\beta) = 0 \end{cases} \quad (3.43)$$

Eight-cable system:

$$\begin{cases} F_1 + F_2 + F_3 + F_4 = \frac{F}{2} \\ F_4(6 + 6\beta) + F_3(1 - 12\beta) + F_2(6\beta) = 0 \\ F_4(12) + F_3(6 + 6\beta) + F_2(1 - 12\beta) + F_1(6\beta) = 0 \\ F_4(29) + F_3(20) + F_2(11 + 6\beta) + F_1(3 - 6\beta) = 0 \end{cases} \quad (3.44)$$

10-cable system:

$$\begin{cases} F_1 + F_2 + F_3 + F_4 + F_5 = \frac{F}{2} \\ F_5(6 + 6\beta) + F_4(1 - 12\beta) + F_3(6\beta) = 0 \\ F_5(12) + F_4(6 + 6\beta) + F_3(1 - 12\beta) + F_2(6\beta) = 0 \\ F_5(18) + F_4(12) + F_3(6 + 6\beta) + F_2(1 - 12\beta) + F_1(6\beta) = 0 \\ F_5(38) + F_4(29) + F_3(20) + F_2(11 + 6\beta) + F_1(3 - 6\beta) = 0 \end{cases} \quad (3.45)$$

12-cable system:

$$\begin{cases} F_1 + F_2 + F_3 + F_4 + F_5 + F_6 = \frac{F}{2} \\ F_6(6 + 6\beta) + F_5(1 - 12\beta) + F_4(6\beta) = 0 \\ F_6(12) + F_5(6 + 6\beta) + F_4(1 - 12\beta) + F_3(6\beta) = 0 \\ F_6(18) + F_5(12) + F_4(6 + 6\beta) + F_3(1 - 12\beta) + F_2(6\beta) = 0 \\ F_6(24) + F_5(18) + F_4(12) + F_3(6 + 6\beta) + F_2(1 - 12\beta) + F_1(6\beta) = 0 \\ F_6(47) + F_5(38) + F_4(29) + F_3(20) + F_2(11 + 6\beta) + F_1(3 - 6\beta) = 0 \end{cases} \quad (3.46)$$

14-cable system:

$$\left\{ \begin{array}{l} F_1 + F_2 + F_3 + F_4 + F_5 + F_6 + F_7 = \frac{F}{2} \\ F_7(6 + 6\beta) + F_6(1 - 12\beta) + F_5(6\beta) = 0 \\ F_7(12) + F_6(6 + 6\beta) + F_5(1 - 12\beta) + F_4(6\beta) = 0 \\ F_7(18) + F_6(12) + F_5(6 + 6\beta) + F_4(1 - 12\beta) + F_3(6\beta) = 0 \\ F_7(24) + F_6(18) + F_5(12) + F_4(6 + 6\beta) + F_3(1 - 12\beta) + F_2(6\beta) = 0 \\ F_7(30) + F_6(24) + F_5(18) + F_4(12) + F_3(6 + 6\beta) + F_2(1 - 12\beta) + F_1(6\beta) = 0 \\ F_7(56) + F_6(47) + F_5(38) + F_4(29) + F_3(20) + F_2(11 + 6\beta) + F_1(3 - 6\beta) = 0 \end{array} \right. \quad (3.47)$$

16-cable system:

$$\left\{ \begin{array}{l} F_1 + F_2 + F_3 + F_4 + F_5 + F_6 + F_7 + F_8 = \frac{F}{2} \\ F_8(6 + 6\beta) + F_7(1 - 12\beta) + F_6(6\beta) = 0 \\ F_8(12) + F_7(6 + 6\beta) + F_6(1 - 12\beta) + F_5(6\beta) = 0 \\ F_8(18) + F_7(12) + F_6(6 + 6\beta) + F_5(1 - 12\beta) + F_4(6\beta) = 0 \\ F_8(24) + F_7(18) + F_6(12) + F_5(6 + 6\beta) + F_4(1 - 12\beta) + F_3(6\beta) = 0 \\ F_8(30) + F_7(24) + F_6(18) + F_5(12) + F_4(6 + 6\beta) + F_3(1 - 12\beta) + F_2(6\beta) = 0 \\ F_8(36) + F_7(30) + F_6(24) + F_5(18) + F_4(12) + F_3(6 + 6\beta) + F_2(1 - 12\beta) + F_1(6\beta) = 0 \\ F_8(65) + F_7(56) + F_6(47) + F_5(38) + F_4(29) + F_3(20) + F_2(11 + 6\beta) + F_1(3 - 6\beta) = 0 \end{array} \right. \quad (3.48)$$

18-cable system:

$$\left\{ \begin{array}{l} F_1 + F_2 + F_3 + F_4 + F_5 + F_6 + F_7 + F_8 + F_9 = \frac{F}{2} \\ F_9(6 + 6\beta) + F_8(1 - 12\beta) + F_7(6\beta) = 0 \\ F_9(12) + F_8(6 + 6\beta) + F_7(1 - 12\beta) + F_6(6\beta) = 0 \\ F_9(18) + F_8(12) + F_7(6 + 6\beta) + F_6(1 - 12\beta) + F_5(6\beta) = 0 \\ F_9(24) + F_8(18) + F_7(12) + F_6(6 + 6\beta) + F_5(1 - 12\beta) + F_4(6\beta) = 0 \\ F_9(30) + F_8(24) + F_7(18) + F_6(12) + F_5(6 + 6\beta) + F_4(1 - 12\beta) + F_3(6\beta) = 0 \\ F_9(36) + F_8(30) + F_7(24) + F_6(18) + F_5(12) + F_4(6 + 6\beta) + F_3(1 - 12\beta) + F_2(6\beta) = 0 \\ F_9(42) + F_8(36) + F_7(30) + F_6(24) + F_5(18) + F_4(12) + F_3(6 + 6\beta) + F_2(1 - 12\beta) + F_1(6\beta) = 0 \\ F_9(74) + F_8(65) + F_7(56) + F_6(47) + F_5(38) + F_4(29) + F_3(20) + F_2(11 + 6\beta) + F_1(3 - 6\beta) = 0 \end{array} \right. \quad (3.49)$$

20-cable system:

$$\left\{ \begin{array}{l}
 F_1 + F_2 + F_3 + F_4 + F_5 + F_6 + F_7 + F_8 + F_9 + F_{10} = \frac{F}{2} \\
 F_{10}(6 + 6\beta) + F_9(1 - 12\beta) + F_8(6\beta) = 0 \\
 F_{10}(12) + F_9(6 + 6\beta) + F_8(1 - 12\beta) + F_7(6\beta) = 0 \\
 F_{10}(18) + F_9(12) + F_8(6 + 6\beta) + F_7(1 - 12\beta) + F_6(6\beta) = 0 \\
 F_{10}(24) + F_9(18) + F_8(12) + F_7(6 + 6\beta) + F_6(1 - 12\beta) + F_5(6\beta) = 0 \\
 F_{10}(30) + F_9(24) + F_8(18) + F_7(12) + F_6(6 + 6\beta) + F_5(1 - 12\beta) + F_4(6\beta) = 0 \quad (3.50) \\
 F_{10}(36) + F_9(30) + F_8(24) + F_7(18) + F_6(12) + F_5(6 + 6\beta) + F_4(1 - 12\beta) + F_3(6\beta) = 0 \\
 F_{10}(42) + F_9(36) + F_8(30) + F_7(24) + F_6(18) + F_5(12) + F_4(6 + 6\beta) + F_3(1 - 12\beta) + F_2(6\beta) = 0 \\
 F_{10}(48) + F_9(42) + F_8(36) + F_7(30) + F_6(24) + F_5(18) + F_4(12) + F_3(6 + 6\beta) + F_2(1 - 12\beta) + F_1(6\beta) = 0 \\
 F_{10}(83) + F_9(74) + F_8(65) + F_7(56) + F_6(47) + F_5(38) + F_4(29) + F_3(20) + F_2(11 + 6\beta) + F_1(3 - 6\beta) = 0
 \end{array} \right.$$

A comparison of the derived systems of equations for different structural systems shows a mathematical pattern. The first equation in the final system of equations comes from equilibrium, the last equation comes from boundary condition at the location of the failed cable, and other equations, following a simple rule, come from the boundary conditions of other intact cables.

After recognizing the mathematical pattern in the final system of equations, the following system of linear equations is derived as a general representation for a structural system with an arbitrary number of cables:

$$\left\{ \begin{array}{l}
 F_n + F_{n-1} + F_{n-2} + \dots + F_1 = \frac{F}{2} \\
 F_n(6 + 6\beta) + F_{n-1}(1 - 12\beta) + F_{n-2}(6\beta) = 0 \\
 F_n(12) + F_{n-1}(6 + 6\beta) + F_{n-2}(1 - 12\beta) + F_{n-3}(6\beta) = 0 \\
 F_n(18) + F_{n-1}(12) + F_{n-2}(6 + 6\beta) + F_{n-3}(1 - 12\beta) + F_{n-4}(6\beta) = 0 \\
 F_n(24) + F_{n-1}(18) + F_{n-2}(12) + F_{n-3}(6 + 6\beta) + F_{n-4}(1 - 12\beta) + F_{n-5}(6\beta) = 0 \quad (3.51) \\
 \vdots \\
 F_n(6n - 12) + F_{n-1}(6(n - 1) - 12) + \dots + F_3(6 + 6\beta) + F_2(1 - 12\beta) + F_1(6\beta) = 0 \\
 F_n(9n - 7) + F_{n-1}(9(n - 1) - 7) + \dots + F_2(11 + 6\beta) + F_1(3 - 6\beta) = 0
 \end{array} \right.$$

It is worth highlighting that because the system is symmetric, in all the above calculations, just half of the system is considered.

In Fig. 3.3, the stress increase ratio of the critical cable, also referred to as relative force increase, for different systems is demonstrated.

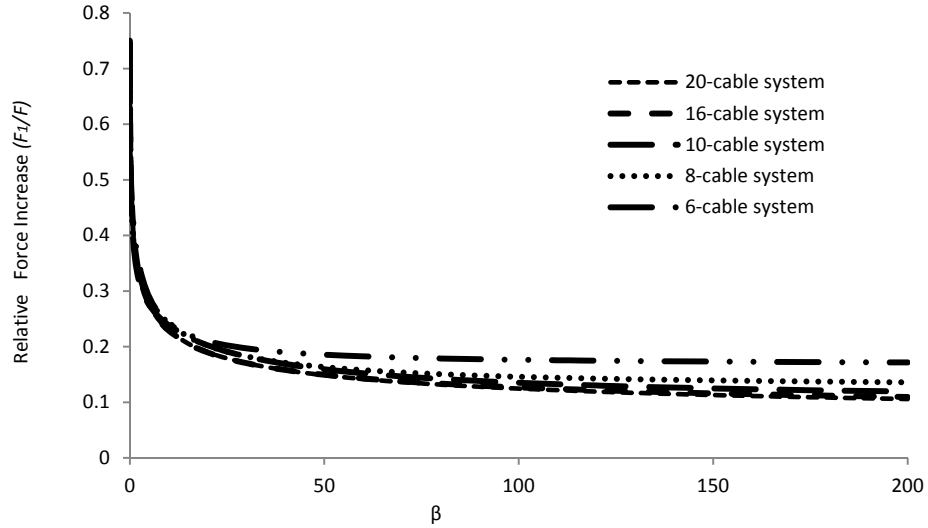


Fig. 3.3 The stress increase ratio of the critical cable for different systems.

Fig. 3.3 reveals that by increasing the β -value, the stress increase ratio of the critical cable decreases.

The next step is to find a general solution for the derived system of linear equations. The target is to find the stress increase ratio of the critical cable ($\frac{F_1}{F}$) as a function of β .

To solve this system of equations, a step by step method is applied. The main approach is similar to the previous step. The plan is to solve the system of linear equations for several small systems and find a mathematical pattern. This pattern, if found, could be used for any arbitrary system. Found below are the results of the calculations of the stress increase ratios of the critical cable, as a function of β , for several systems:

Four-cable system:

$$\frac{F_1}{F} = \frac{11 + 6\beta}{16 + 24\beta} \quad (3.52)$$

Six-cable system:

$$\frac{F_1}{F} = \frac{23 + 171\beta + 18\beta^2}{31 + 372\beta + 108\beta^2} \quad (3.53)$$

Eight-cable system:

$$\frac{F_1}{F} = \frac{173 + 3540\beta + 6264\beta^2 + 216\beta^3}{232 + 5976\beta + 18288\beta^2 + 1728\beta^3} \quad (3.54)$$

10-cable system:

$$\frac{F_1}{F} = \frac{323 + 14100\beta + 168021\beta^2 + 649836\beta^3 + 399168\beta^4 + 5832\beta^5}{433 + 21237\beta + 294408\beta^2 + 1407996\beta^3 + 1472256\beta^4 + 58320\beta^5} \quad (3.55)$$

It is worth mentioning that by considering the applied method, the calculation of the stress increase ratio of all cables is possible. However, only the stress increase ratio of the critical cable is of interest here. To check the correctness of the analytical solution, the results obtained from the applied method are compared to the numerical models using the software package SAP2000. As expected, because of the geometric simplicity of the model and the application of the linear static analysis, there are very small differences between the analytical and numerical solutions. In Fig. 3.4, the comparison of the analytical and numerical results for a 10-cable system is shown.

According to Equations 3.52 through 3.55, the general form of equation is as follows:

$$\frac{F_1}{F} = \frac{a' + b'\beta + c'\beta^2 + d'\beta^3 + \dots}{a'' + b''\beta + c''\beta^2 + d''\beta^3 + \dots} \quad (3.56)$$

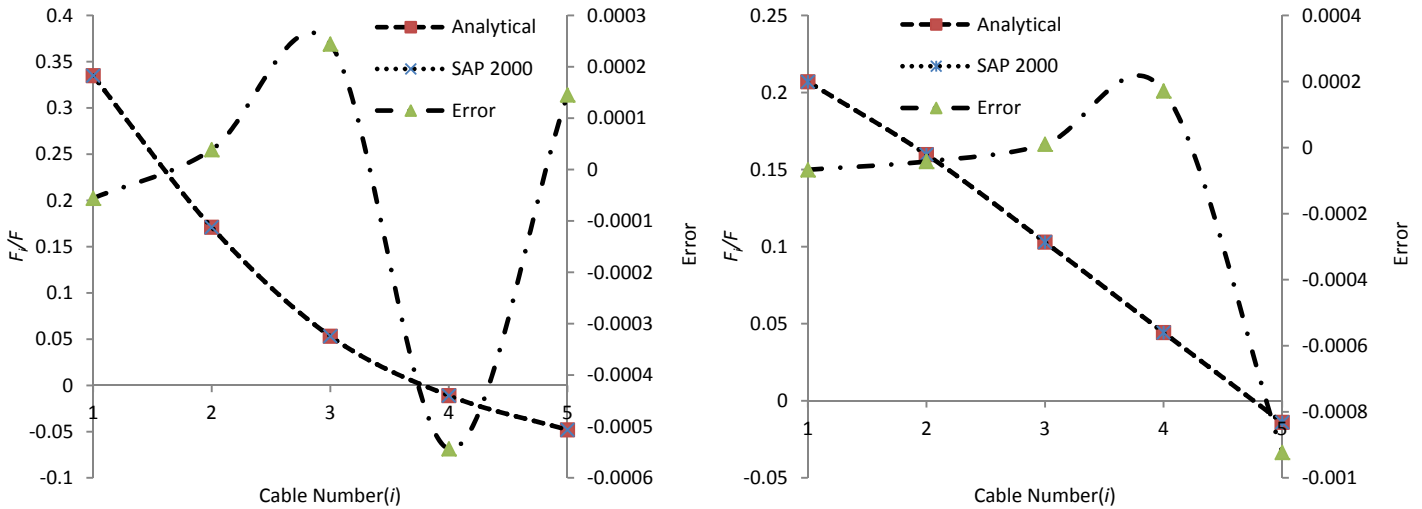


Fig. 3.4 Comparison of analytical and numerical solutions for a 10 cable system - $\beta=1.83$ (left) and $\beta=18.3$ (right)

As mentioned, the target is to find a mathematical pattern for the calculation of the stress increase ratio of the critical cable to be used for any arbitrary system. However, the examination of the above equations does not show any practical and straightforward relationship between different coefficients of β in different systems.

In addition, the form of Equation 3.56 is not appropriate for our purpose to find an equation for a general system. This is because for a system with $2n$ cables, $2n$ coefficients must be found. It means that for solving large systems, lots of mathematical effort is required, which makes the calculation process time consuming and costly. To overcome this problem, it is decided to find an approximation function based on the mathematical characteristics of Equation 3.56. The main idea is to approximate Equation 3.56 with a function having as few unknown coefficients as possible. For this purpose, different kinds of nonlinear equations have been investigated and it was found that the following equation has an acceptable compatibility with the mathematical specifications of the original equation.

$$\frac{F_1}{F} = a + \frac{b - a}{1 + \left(\frac{\beta}{c}\right)^d} \quad (3.57)$$

In other words, Equation 3.57 approximates Equation 3.56 if appropriate parameters (a , b , c , and d) could be found. By this method, the number of unknown coefficients has been reduced to four. For a system including $2n$ cables, parameter “ a ” stands for the minimum stress increase ratio, which occurs when $\beta = \infty$ and equals $1/2n$, and parameter “ b ” stands for the maximum stress increase ratio that occurs when $\beta = 0$. From Equations 3.52 to 3.55, the maximum stress increase ratio ($\frac{F_1}{F}$) is found to be close to 0.75 for all systems when $2n \geq 6$. Therefore, the general form of the approximation function will be as follows:

$$\frac{F_1}{F} = \frac{1}{2n} + \frac{\frac{3}{4} - \frac{1}{2n}}{1 + \left(\frac{\beta}{c}\right)^d} \quad (3.58)$$

For finding the other two parameters, a regression analysis method is employed. Regression analysis is a statistical process that estimates the relationships between a dependent variable and one or more independent variables. There are different methods of regression analysis, namely, ordinary least squares, generalized least squares, regularized least squares, least absolute deviations, and least squares method. The simplest form of regression analysis is linear regression. In linear regression, the analyst finds the line that most closely fits the data.

In this study, the least squares method (LSM) is applied. The LSM method defines the estimate of unknown parameters (here parameters “ c ” and “ d ”) as the values which minimize the sum of the squares between the exact and the approximation values (in this case, function T) (Rawlings et al. 1998). For this purpose, the derivative of T with respect to parameters c and d is set to zero (Equations 3.65 and 3.66). The procedure of calculations used for a data set consisting of x matching points (y_i and f_i) is presented in the following equations:

$$f_i = a + \frac{b - a}{1 + \left(\frac{\beta}{c}\right)^d} \quad (3.59)$$

$$\Delta_i = y_i - f_i = y_i - \left(a + \frac{b - a}{1 + \left(\frac{\beta}{c}\right)^d} \right) \quad (3.60)$$

$$\Delta_i^2 = (y_i - a)^2 + \frac{(b - a)^2}{1 + \left(\frac{\beta}{c}\right)^{2d} + 2\left(\frac{\beta}{c}\right)^d} - \frac{2(b - a)(y_i - a)}{1 + \left(\frac{\beta}{c}\right)^d} \quad (3.61)$$

$$\frac{\partial(\Delta_i^2)}{\partial d} = \frac{-(b - a)^2 \left(2\left(\frac{\beta}{c}\right)^{2d} \ln\left(\frac{\beta}{c}\right) + 2\left(\frac{\beta}{c}\right)^d \ln\left(\frac{\beta}{c}\right) \right)}{\left(1 + \left(\frac{\beta}{c}\right)^{2d} + 2\left(\frac{\beta}{c}\right)^d \right)^2} - \frac{-2(b - a)(y_i - a)\left(\frac{\beta}{c}\right)^d \ln\left(\frac{\beta}{c}\right)}{\left(1 + \left(\frac{\beta}{c}\right)^d \right)^2} \quad (3.62)$$

$$\frac{\partial(\Delta_i^2)}{\partial c} = \frac{(b - a)^2 (2d\beta^{2d}c^{-2d-1} + 2d\beta^d c^{-d-1})}{\left(1 + \left(\frac{\beta}{c}\right)^{2d} + 2\left(\frac{\beta}{c}\right)^d \right)^2} - \frac{2(b - a)(y_i - a)d\beta^d c^{-d-1}}{\left(1 + \left(\frac{\beta}{c}\right)^d \right)^2} \quad (3.63)$$

$$T = \sum_{i=1}^x \Delta_i^2 \quad (3.64)$$

$$\frac{\partial T}{\partial d} = 0 \quad (3.65)$$

$$\frac{\partial T}{\partial c} = 0 \quad (3.66)$$

where y_i and f_i are the exact and approximate stress increase ratio values $\left(\frac{F_1}{F}\right)$ for different β -values, respectively.

For solving the aforementioned equations, an iterative method has been used. In the first step, Equation 3.65 is solved for different values of parameter c and corresponding values of parameter d are calculated. In the next step, the calculated values of parameter d are used in Equation 3.66 and corresponding values of parameter c are calculated. Investigated systems showed that there is only one pair of parameters c and d that satisfy both equations.

In Fig. 3.5, the calculation of parameters c and d for 10 and 20-cable systems are shown. In Table 3.1, the calculated parameters of the approximation function for different systems after the rupture of one cable is shown. In Fig. 3.6, parameters c and d for different systems are shown. As demonstrated, parameter c has an upward limit of one (it will be checked in the following section).

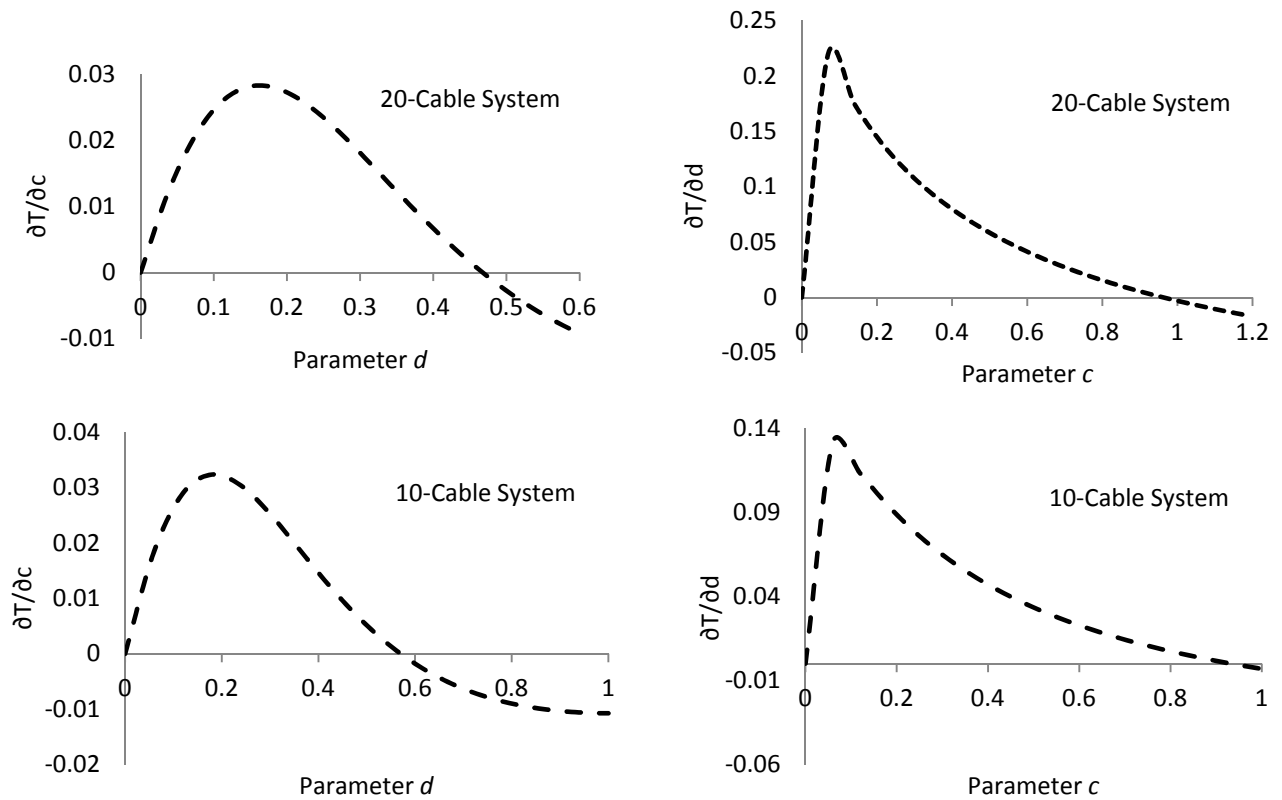


Fig. 3.5 Calculation of parameters c and d for 10 and 20-cable systems

Table 3.1 The calculated parameters of the approximation function-one failed cable

	a	b	c	d
4-cable system	0.250	0.69	0.666	1.000
6-cable system	0.167	0.75	0.700	0.710
8-cable system	0.125	0.75	0.840	0.620
10-cable system	0.100	0.75	0.920	0.580
12-cable system	0.083	0.75	0.948	0.540
14-cable system	0.071	0.75	0.962	0.510
16-cable system	0.063	0.75	0.972	0.490
18-cable system	0.056	0.75	0.980	0.475
20-cable system	0.050	0.75	0.985	0.460

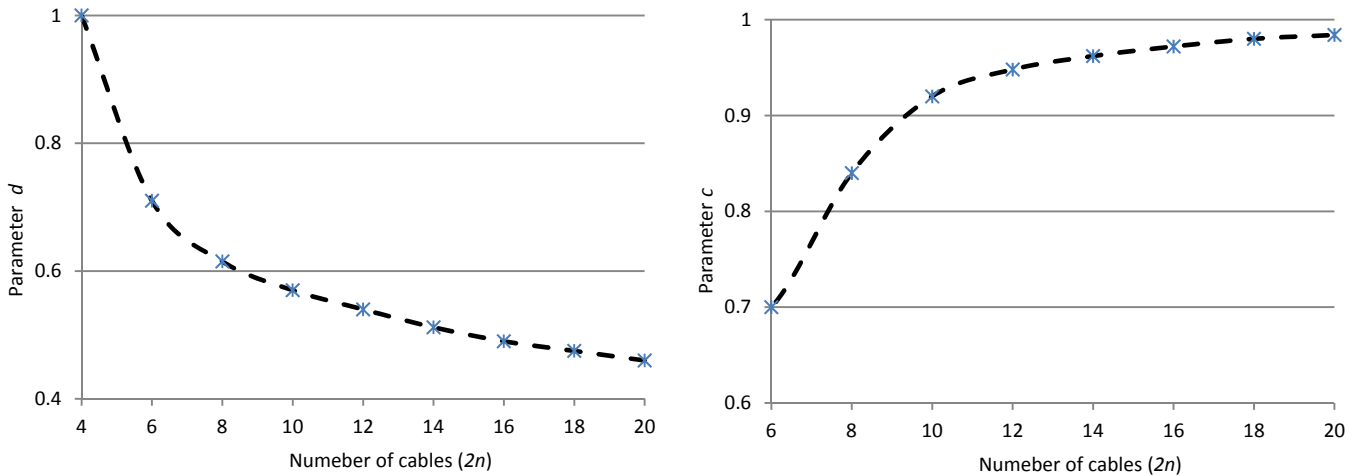


Fig. 3.6 Parameters c and d for different systems

For finding an equation for parameter d , the LSM method is used once again. To reduce the complexity of the equation and increase its accuracy for larger systems, only systems with more than 12 cables are considered. Parameter d can be expressed by the following equation:

$$d = 0.35 + \frac{0.65}{1 + (\frac{2n}{5})^{1.1}} \quad 2n \geq 12 \quad (3.67)$$

According to the aforementioned equation, parameter d is equal to 0.35 for large values of n . The mathematical calculation is the same as Equations 3.59 through 3.66 and is not repeated. In Fig. 3.7, the accuracy of Equation 3.67 is checked by the calculated values resulting from the LSM method. As can be seen, the proposed equation can express the exact value of parameter d with reasonable accuracy, and the maximum error is less than 1%.

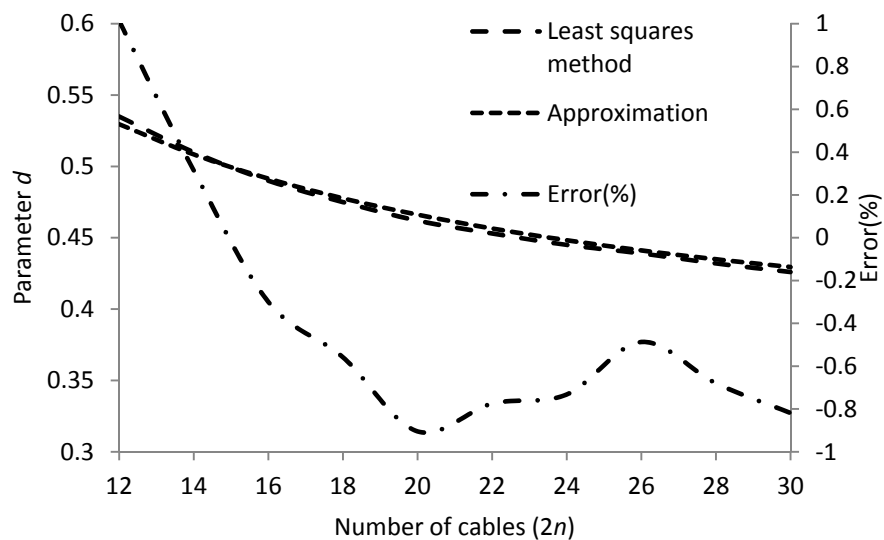


Fig. 3.7 Comparison of the calculation of parameter d by two methods

Considering the previously mentioned findings, the approximation function could be rewritten for a general system as follows:

$$\frac{F_1}{F} = \frac{1}{2n} + \frac{\frac{3}{4} - \frac{1}{2n}}{1 + \left(\frac{\beta}{c}\right)^d} \quad \delta_i = 1 \quad (i = 1 \text{ to } n) \quad (3.68)$$

And for large values of n :

$$\frac{F_1}{F} \cong \frac{\frac{3}{4}}{1 + \beta^d} \quad (3.69)$$

where parameter d should be calculated by Equation 3.67.

In Fig. 3.8, the exact curves of the stress increase ratio as well as the curves calculated from the approximation function for different systems are shown. It is seen that the curves depicted from the approximation function express the exact values of the stress increase ratio with good accuracy. Except for small β -values, the error of approximation is less than 5%.

It is worth highlighting that the maximum stress increase ratio is equal to 0.75, which is larger than 0.50. The parameter R-squared (R^2), also known as the coefficient of determination, shown in Fig. 3.8, is the ratio of variation that is explained by the approximation function to the total variation in the model. R-squared is a statistical measure that gives some information about the accuracy of an approximation function. It shows how accurate the regression method approximates the actual data points. R-squared is equal to one for a perfect fit and tends towards zero for a bad fit (Rawlings et al. 1998). For a data set consisting of x matching points (y_i and f_i), R-squared is calculated as follows:

$$\bar{y} = \frac{1}{x} \sum_{i=1}^x y_i \quad (3.70)$$

$$SS_{tot} = \sum_{i=1}^x (y_i - \bar{y})^2 \quad (3.71)$$

$$SS_{res} = \sum_{i=1}^x (y_i - f_i)^2 \quad (3.72)$$

$$R^2 = 1 - \frac{SS_{res}}{SS_{tot}} \quad (3.73)$$

where y_i and f_i are the exact and approximate values, respectively. In Table 3.2, a summary of calculations of R-squared for different systems is presented.

Equation 3.68 is the approximation function for the stress increase ratio of the critical cable after the rupture of one cable. In the next section, the failure of several cables will be investigated.

Table 3.2 Calculation of R-squared for different systems

	R-squared (R^2)	$\sum_{i=1}^x y_i$	\bar{y}	SS_{tot}	SS_{res}
4-cable system	0.999	7.94	0.417	0.543	3.45E-07
6-cable system	0.992	7.28	0.383	0.74	0.0056
8-cable system	0.985	6.93	0.36	0.815	0.012
10-cable system	0.988	6.80	0.358	0.859	0.010
12-cable system	0.992	6.27	0.33	0.797	0.006
14-cable system	0.994	6.69	0.352	0.905	0.0049
16-cable system	0.995	6.66	0.35	0.918	0.0046
18-cable system	0.995	6.63	0.349	0.927	0.0045
20-cable system	0.995	6.62	0.348	0.934	0.005

3.4 Determination of the stress increase ratio of the critical cable due to the failure of several cables

The target of this section is to calculate the stress increase ratio of the critical cable after the failure of any arbitrary number of cables in a cable-loss scenario. For solving this problem, a step by step method is performed.

In the first step, it is assumed that only one cable is failed, and then an equation for the stress increase ratio of the critical cable is derived. In the next steps, the number of failed cables increases. It means that in the second and third steps, the failure of two and three cables will be considered, respectively. Finally, a general equation for a system including $2n$ cables in the case of the failure of m cables will be derived. The simplified model is depicted in Fig. 3.9.

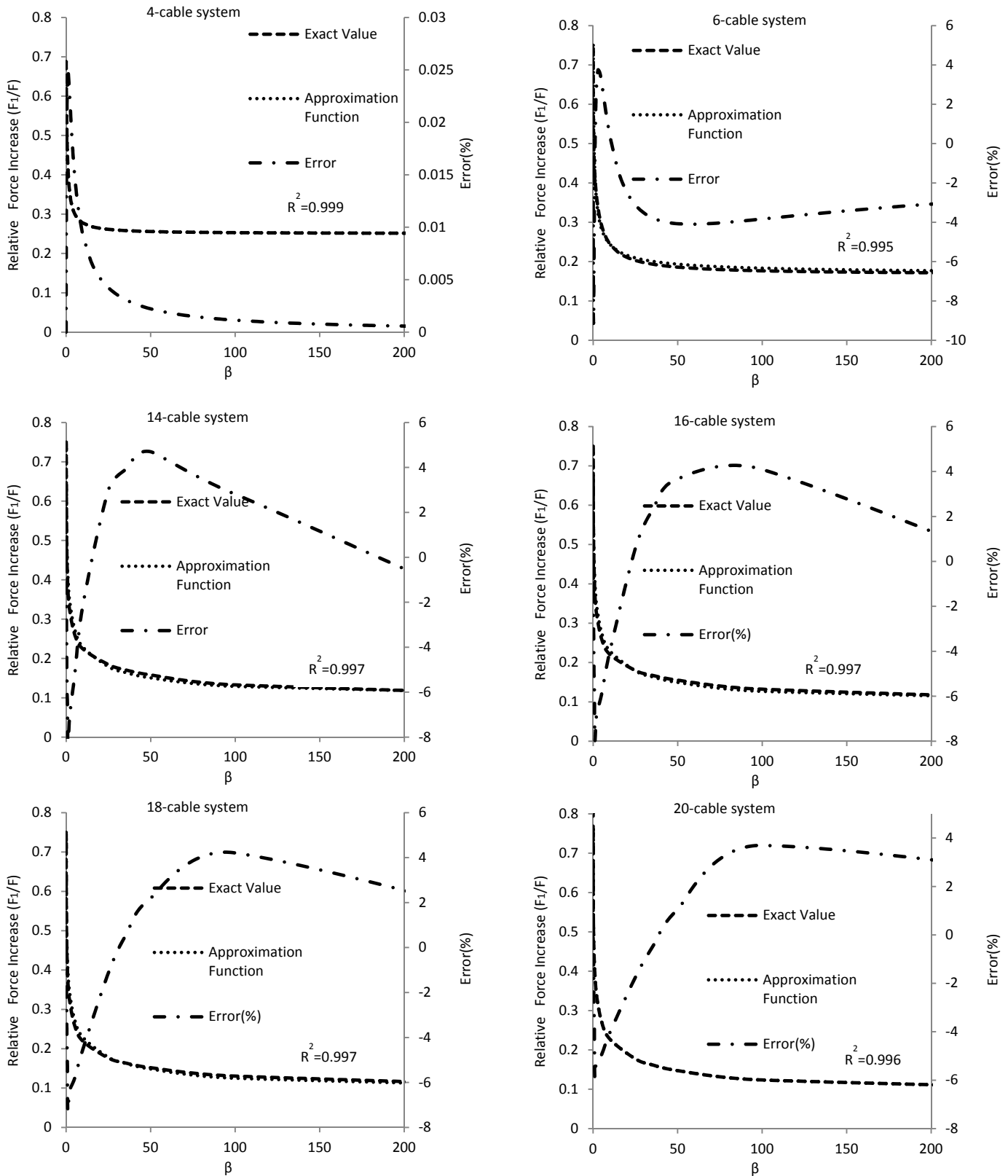


Fig. 3.8 Exact and approximate values of stress increase ratios in different systems-one failed cable

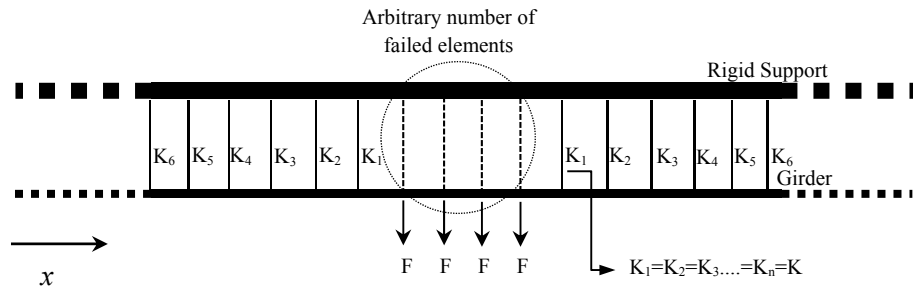


Fig. 3.9 The simplified model of a long-span cable-supported bridge after the failure of several cables

The first step is to calculate the stress increase ratio of the critical cable after the failure of one cable, which has been done in the previous section. The second step is considering the failure of two cables. Performing the analytical approach is similar to the previous section. As mentioned, the key point is to find the final system of linear equations. First, the problem will be solved for several small systems to find a mathematical pattern. Then, the found pattern will be used to derive a general equation.

As mentioned, the final system of equations consists of three kinds of equations. The first equation comes from equilibrium, the last equation comes from boundary condition at the location of the failed cable, and other equations come from the boundary conditions of other intact cables. Investigation of a system after the rupture of two cables shows that only the boundary conditions at the locations of the failed cables are different from the first step. Therefore, the only differences in the final system of equations are the first and the last equations. In the following, the final systems of equations for several systems after the failure of two cables are derived.

Eight-cable system:

$$\left\{ \begin{array}{l} F_1 + F_2 + F_3 + F_4 = F \\ F_4(6 + 6\beta) + F_3(1 - 12\beta) + F_2(6\beta) = 0 \\ F_4(12) + F_3(6 + 6\beta) + F_2(1 - 12\beta) + F_1(6\beta) = 0 \\ F_4(173) + F_3(125) + F_2(77 + 24\beta) + F_1(33 - 24\beta) - 9F = 0 \end{array} \right. \quad (3.74)$$

10-cable system:

$$\left\{ \begin{array}{l} F_1 + F_2 + F_3 + F_4 + F_5 = F \\ F_5(6 + 6\beta) + F_4(1 - 12\beta) + F_3(6\beta) = 0 \\ F_5(12) + F_4(6 + 6\beta) + F_3(1 - 12\beta) + F_2(6\beta) = 0 \\ F_5(18) + F_4(12) + F_3(6 + 6\beta) + F_2(1 - 12\beta) + F_1(6\beta) = 0 \\ F_5(221) + F_4(173) + F_3(125) + F_2(77 + 24\beta) + F_1(33 - 24\beta) - 9F = 0 \end{array} \right. \quad (3.75)$$

12-cable system:

$$\left\{ \begin{array}{l} F_1 + F_2 + F_3 + F_4 + F_5 + F_6 = F \\ F_6(6 + 6\beta) + F_5(1 - 12\beta) + F_4(6\beta) = 0 \\ F_6(12) + F_5(6 + 6\beta) + F_4(1 - 12\beta) + F_3(6\beta) = 0 \\ F_6(18) + F_5(12) + F_4(6 + 6\beta) + F_3(1 - 12\beta) + F_2(6\beta) = 0 \\ F_6(24) + F_5(18) + F_4(12) + F_3(6 + 6\beta) + F_2(1 - 12\beta) + F_1(6\beta) = 0 \\ F_6(269) + F_5(221) + F_4(173) + F_3(125) + F_2(77 + 24\beta) + F_1(33 - 24\beta) - 9F = 0 \end{array} \right. \quad (3.76)$$

16-cable system:

$$\left\{ \begin{array}{l} F_1 + F_2 + F_3 + F_4 + F_5 + F_6 + F_7 + F_8 = F \\ F_8(6 + 6\beta) + F_7(1 - 12\beta) + F_6(6\beta) = 0 \\ F_8(12) + F_7(6 + 6\beta) + F_6(1 - 12\beta) + F_5(6\beta) = 0 \\ F_8(18) + F_7(12) + F_6(6 + 6\beta) + F_5(1 - 12\beta) + F_4(6\beta) = 0 \\ F_8(24) + F_7(18) + F_6(12) + F_5(6 + 6\beta) + F_4(1 - 12\beta) + F_3(6\beta) = 0 \\ F_8(30) + F_7(24) + F_6(18) + F_5(12) + F_4(6 + 6\beta) + F_3(1 - 12\beta) + F_2(6\beta) = 0 \\ F_8(36) + F_7(30) + F_6(24) + F_5(18) + F_4(12) + F_3(6 + 6\beta) + F_2(1 - 12\beta) + F_1(6\beta) = 0 \\ F_8(365) + F_7(317) + F_6(269) + F_5(221) + F_4(173) + F_3(125) + F_2(77 + 24\beta) + F_1(33 - 24\beta) - 9F = 0 \end{array} \right. \quad (3.77)$$

Similar to the previous step, a comparison of the derived systems of equations shows a mathematical pattern. The following system of linear equations is derived for a system after the rupture of two cables:

$$\left\{ \begin{array}{l}
 F_n + F_{n-1} + F_{n-2} + \dots + F_1 = F \\
 F_n(6 + 6\beta) + F_{n-1}(1 - 12\beta) + F_{n-2}(6\beta) = 0 \\
 F_n(12) + F_{n-1}(6 + 6\beta) + F_{n-2}(1 - 12\beta) + F_{n-3}(6\beta) = 0 \\
 F_n(18) + F_{n-1}(12) + F_{n-2}(6 + 6\beta) + F_{n-3}(1 - 12\beta) + F_{n-4}(6\beta) = 0 \\
 F_n(24) + F_{n-1}(18) + F_{n-2}(12) + F_{n-3}(6 + 6\beta) + F_{n-4}(1 - 12\beta) + F_{n-5}(6\beta) = 0 \quad (3.78) \\
 \vdots \\
 F_n(6n - 12) + F_{n-1}(6(n - 1) - 12) + \dots + F_3(6 + 6\beta) + F_2(1 - 12\beta) + F_1(6\beta) = 0 \\
 F_n(48n - 19) + F_{n-1}(48(n - 1) - 19) + \dots + F_2(77 + 24\beta) + F_1(33 - 24\beta) - 9F = 0
 \end{array} \right.$$

As can be seen, there are no fundamental differences between the final solutions in the first and second steps. Therefore, the general form of the equation for the stress increase ratio in the second step should be similar to the first step.

Equations 3.79 and 3.80 are the exact analytical solutions for the stress increase ratios of four and six-cable systems. As can be seen, the general forms of equations are the same as the previous case (Equation 3.56). Therefore, the chosen approximation function can be used again. In this case, parameters a and b have the same definitions (not the same values) as in the previous case.

4-cable system:

$$\frac{F_1}{F} = \frac{68 + 24\beta}{44 + 48\beta} \quad (3.79)$$

6-cable system:

$$\frac{F_1}{F} = \frac{292 + 1944\beta + 144\beta^2}{172 + 1920\beta + 432\beta^2} \quad (3.80)$$

The maximum stress increase ratio is almost 1.71 for all systems except for the four-cable system with a maximum ratio of 1.54.

In Table 3.3, the parameters of the approximation function adjusted for the elimination of two cables are calculated. It is apparent that parameters c and d do not change. According to Table

3.3, and based on the fact that parameters c and d are the same as in the previous case, the approximation function for the rupture of two cables is derived as follows ($2n \geq 6$):

$$\frac{F_1}{F} = \frac{2}{2n} + \frac{1.71 - \frac{2}{2n}}{1 + \left(\frac{\beta}{c}\right)^d} \quad (3.81)$$

And for large values of n :

$$\frac{F_1}{F} \cong \frac{1.71}{1 + \beta^d} \quad (3.82)$$

where parameter d should be calculated by Equation 3.67. In Fig. 3.10, the exact curves of stress increase ratio as well as the curve calculated from the approximation function for different systems after the rupture of two cables are shown.

Table 3.3 The calculated parameters of the approximation function-two failed cables

	a	b	c	d
4-cable system	0.50	1.54	0.666	1.000
6-cable system	0.333	1.70	0.700	0.710
8-cable system	0.25	1.71	0.840	0.620
10-cable system	0.20	1.71	0.920	0.580
12-cable system	0.167	1.71	0.948	0.540
14-cable system	0.143	1.71	0.962	0.510
16-cable system	0.125	1.71	0.972	0.490
18-cable system	0.111	1.71	0.980	0.475
20-cable system	0.10	1.71	0.985	0.460

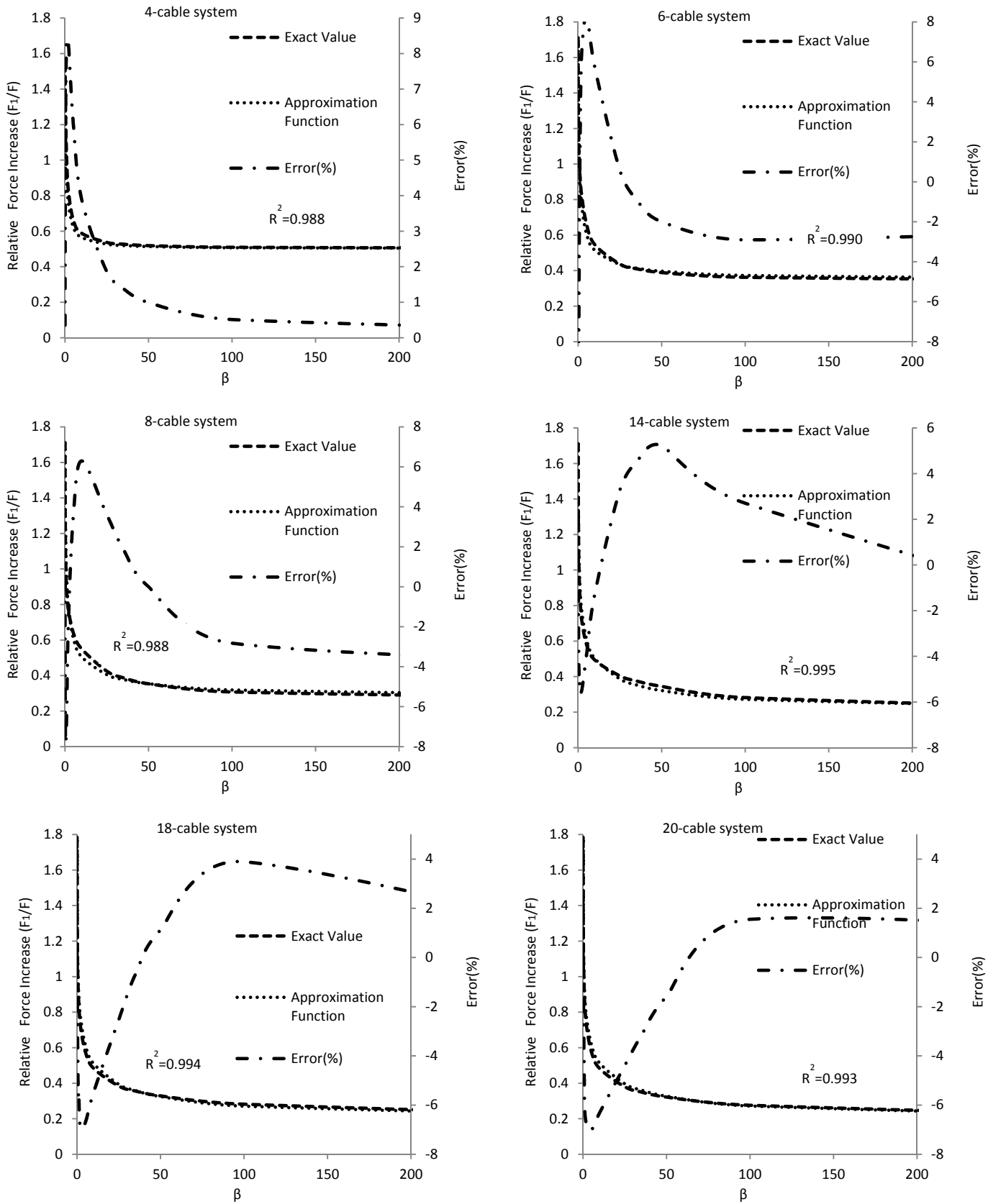


Fig. 3.10 Exact and approximate values of stress increase ratios in different systems-two failed cables

The previous step revealed that parameters c and d do not depend on the number of failed cables. In addition, the calculation of parameter a is straightforward. Therefore, parameter b , which stands for the maximum stress increase ratio, is the only unknown parameter for deriving a general equation. By finding parameter b , a general equation can be derived concerning the failure of any arbitrary number of cables.

In the next step, parameter b will be found, and an approximation function for the rupture of any arbitrary number of cables will be derived.

The accuracy of the final approximation function will be checked by the exact values of a system with three failed cables. For this purpose, the final system of equations of a system with three failed cables will also be derived.

As mentioned, the maximum stress increase ratio occurs when $\beta=0$. Hence, the number of failed cables is the only effective parameter on parameter b . For finding the relationship between parameter b and the number of failed cables, the maximum stress increase ratios of different systems considering different numbers of failed cables are calculated. In Fig. 3.11, the relation between parameter b and the number of failed cables (m) is shown.

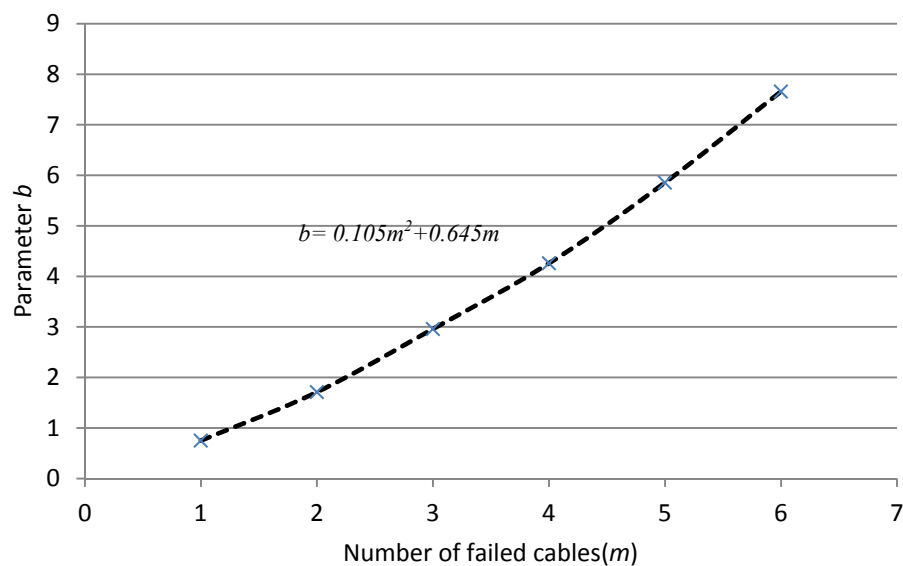


Fig. 3.11 The calculation of parameter b

As shown, parameter b can be expressed by the following equation:

$$b = 0.105m^2 + 0.645m \quad (3.83)$$

Therefore, the general form of the approximation function could be derived as follows:

$$\frac{F_1}{F} = \frac{m}{2n} + \frac{(0.105m^2 + 0.645m) - \frac{m}{2n}}{1 + \left(\frac{\beta}{c}\right)^d} \quad (3.84)$$

Likewise, for large values of n :

$$\frac{F_1}{F} \cong \frac{0.105m^2 + 0.645m}{1 + \beta^d} \quad (3.85)$$

where parameter d should be calculated by Equation 3.67. To verify Equation 3.84, the results of the exact stress increase ratio, and the one calculated from the approximation function for the elimination of three cables, are compared. Performing the analytical approach for a system after the rupture of three cables yields the following system of equations:

$$\left\{ \begin{array}{l} F_1 + F_2 + F_3 + F_4 + F_5 + F_6 + F_7 + F_8 = \frac{3F}{2} \\ F_8(6 + 6\beta) + F_7(1 - 12\beta) + F_6(6\beta) = 0 \\ F_8(12) + F_7(6 + 6\beta) + F_6(1 - 12\beta) + F_5(6\beta) = 0 \\ F_8(18) + F_7(12) + F_6(6 + 6\beta) + F_5(1 - 12\beta) + F_4(6\beta) = 0 \\ F_8(24) + F_7(18) + F_6(12) + F_5(6 + 6\beta) + F_4(1 - 12\beta) + F_3(6\beta) = 0 \\ \vdots \\ F_n(6n - 12) + F_{n-1}(6(n - 1) - 12) + \dots + F_3(6 + 6\beta) + F_2(1 - 12\beta) + F_1(6\beta) = 0 \\ F_n(15n + 2) + F_{n-1}(15(n - 1) + 2) + \dots + F_4(62) + F_3(47) + F_2(32 + 6\beta) + F_1(18 - 6\beta) - 12F = 0 \end{array} \right. \quad (3.86)$$

Because the analytical approach is similar to the first and second steps, mathematical calculations are not repeated. In this section, as a final check, larger systems are also considered. Therefore, the accuracy of parameters c and d can also be checked. For the calculations of systems with more than 20 cables, software package SAP2000 is used. In doing so, the used analytical approach has been checked again. For these systems, parameter c is set equal to one.

In Fig. 3.12, the exact curves of stress increase ratio as well as the curve calculated from the approximation function for different systems after the rupture of three cables are shown. As can be seen, setting parameter c equal to one for systems with more than 20 cables has acceptable accuracy and the maximum error of the approximation function is less than 5%.

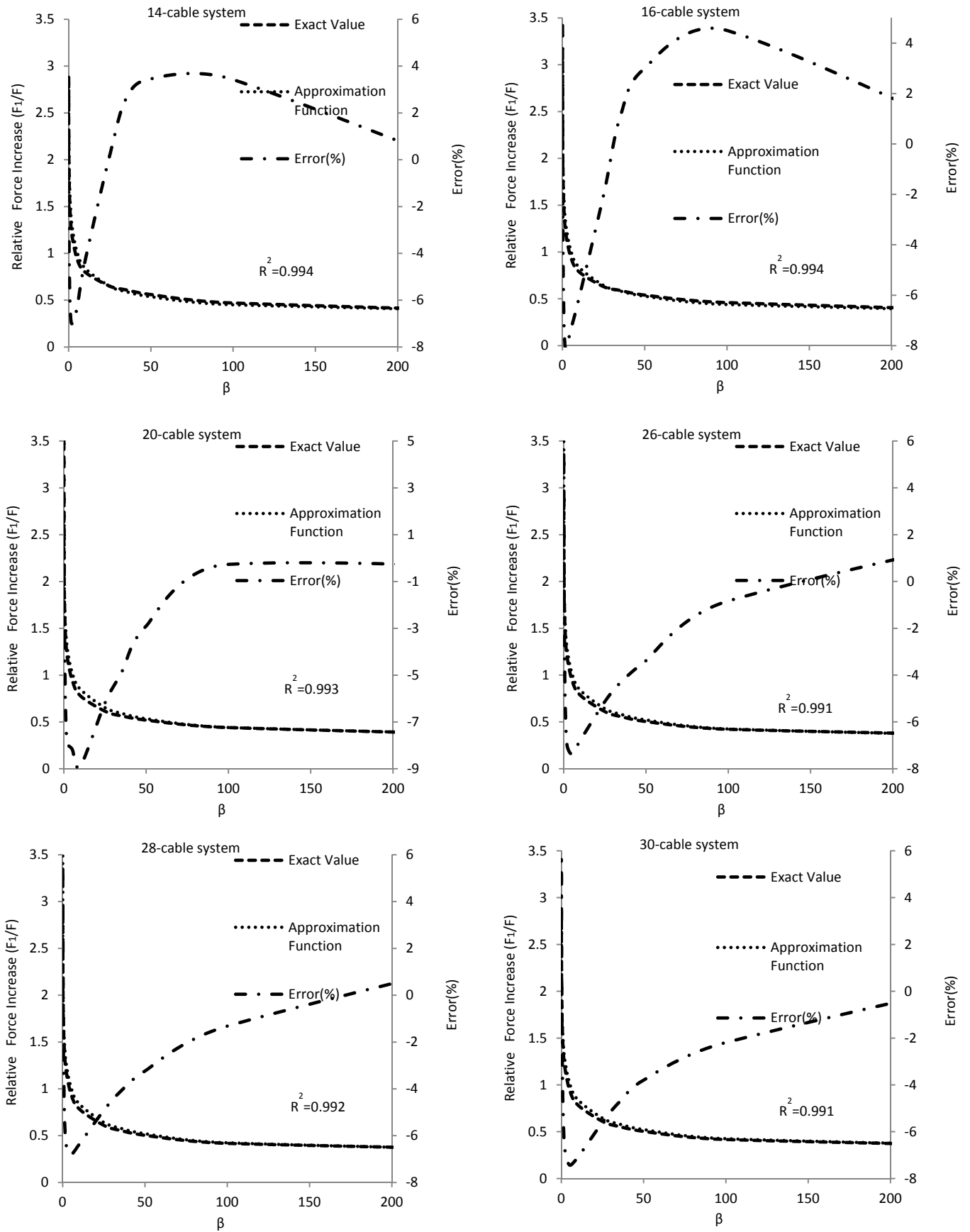


Fig. 3.12 Exact and approximate values of stress increase ratios in different systems-three failed cables

It should be emphasized that the approximation function is derived based on a linear static analysis, and the dynamic nature of the cable failure is not taken into account. Therefore, a DAF of 2, as suggested by PTI (2012), is applied. In addition, nonlinear behavior of the structural system is not considered here. Plastic deformations are, especially in the case of the failure of several cables, very important. Hence, the inadequacy of the analytical model in this respect should be highlighted.

By using Equation 3.85, the design load of a continuous system taking into account the cable-loss scenarios could also be calculated. In Fig. 3.13, a general continuous parallel load-bearing system is shown. It is assumed that all cables have the same axial stiffness, the distance between two adjacent cables is L , and the whole system is symmetric.

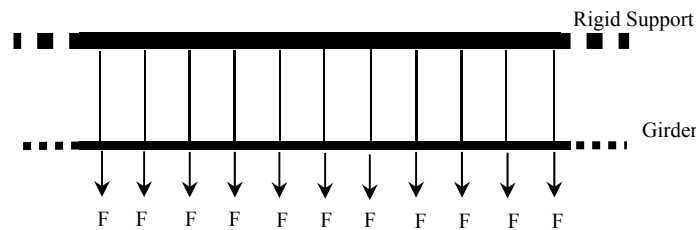


Fig. 3.13 Continuous parallel load bearing system

As mentioned, it is suggested in the literature that the rupture of all cables within a range of 10 m should be considered in the design of bridges (O'Donovan et al. 2003). For example, if the distance between two adjacent cables is $5 < L \leq 10$ m, considering the failure of two cables is necessary. Therefore, the minimum design load of a cable includes its original load plus the load redistributed from the adjacent failed cables in a cable-loss scenario (calculated by Equation 3.85 and multiplied by a DAF of 2) and could be calculated as follows:

$$\text{Cable's Design Load} = F + 2F \left(\frac{0.105m^2 + 0.645m}{1 + \beta^{0.35}} \right) \quad (3.87)$$

It can be seen that the design load of a cable is influenced by β . It means that for systems with larger β -values, smaller design loads are required. For example, according to Equation 3.87, the design loads of two different systems with β -values of 50 and 500 considering the failure of two cables are $1.69F$ and $1.35F$, respectively. This shows a considerable difference of 25 percent. In the case of long-span cable-supported bridges, the bridge could be divided into different zones corresponding to different β -values (small, medium, and large β -values), then the design load for each zone could be calculated. Thus, using the proposed method makes the design of cables in a cable-loss scenario more economical. The optimum design of parallel load-bearing systems will be discussed in detail in chapter 5.

3.5 Developing a reserve-based robustness index

The target of this section is to develop a robustness index for parallel load-bearing systems using the derived approximation function in the previous section. First, a selection of different definitions of robustness in the literature will be provided. Then, different indexes for assessing the structural robustness, or related characteristics of a structural system, will be briefly explained. Finally, a reserve-based robustness index will be derived.

3.5.1 Definition of robustness

The term robustness is used differently by different authors and there is no general agreement to date on its precise meaning (Starossek and Haberland 2010). In Table 3.4, a selection of different definitions of robustness is provided. It is apparent that there are different definitions of robustness in the literature, and there is no consensus on its meaning. Some authors define robustness as a structural property, while others define it as a property of both structure and environment.

Cavaco et al. (2010) investigated different definitions of robustness in the literature and concluded that although there is no agreement on a definitive definition of robustness, there is no doubt that member by member safety verification does not ensure the safety of the structure. A global property defining system safety is desirable.

In this study, robustness is defined as insensitivity to local failure, where “insensitivity” and “local failure” should be quantified by the design objectives, which are part of the design criteria (Starossek 2018).

3.5.2 Assessment of structural robustness

According to guidelines, a structural system should be robust. It means that the extent of structural failure should not be disproportional to the initial failure. However, this statement is not quantitative and does not provide any applicable criteria for design engineers to calculate the level of the robustness of a structure (Baker et al. 2008). Therefore, developing a quantitative measure of robustness would be helpful.

Table 3.4 Different definitions of the term robustness in the literature

Definition of robustness	
GSA (2003)	"Ability of a structure or structural components to resist damage without premature and/or brittle failure due to events like explosions, impacts, fire or consequences of human error, due to its vigorous strength and toughness."
Val and Val (2006)	"Ability of the structure to withstand local damage without disproportionate collapse."
EN 1991-1-7 (2006)	"The ability of a structure to withstand events like fire, explosions, impact or the consequences of human error without being damaged to an extent disproportionate to the original cause."
Bontempi et al. (2007)	"The robustness of a structure, intended as its ability not to suffer disproportionate damages as a result of limited initial failure, is an intrinsic requirement, inherent to the structural system organisation."
Biondini et al. (2008)	"Structural robustness can be viewed as the ability of the system to suffer an amount of damage not disproportionate with respect to the causes of the damage itself."
Agarwal and England (2008)	"Robustness is [...] the ability of a structure to avoid disproportionate consequences in relation to the initial damage."
JCSS (2008)	"The robustness of a system is defined as the ratio between the direct risks and the total risks (total risks is equal to the sum of direct and indirect risks), for a specified time frame and considering all relevant exposure events and all relevant damage states for the constituents of the system."
Vrouwenvelder (2008)	"The notion of robustness is that a structure should not be too sensitive to local damage, whatever the source of damage."
Cavaco et al. (2010)	"Robustness is a structural property which measures the degree of structural performance remaining after damage occurrence."
Starossek and Haberland (2011)	"Robustness is a desirable property of structural systems which mitigate their susceptibility to progressive or disproportionate collapse. It is defined as the insensitivity of a structure to local failure."
Haberland (2012)	"Insensitivity of a structure to an initial damage. A structure is robust if an initial damage does not lead to disproportionate collapse"
Beverly (2013)	"The ability of a structure subject to accidental or exceptional loadings to sustain local damage to some structural components without experiencing a disproportionate degree of overall distress or collapse."

A practical robustness index should have certain characteristics. It should be expressive, simple, calculable, objective, and general (Lind 1995, Haberland 2007, and Starossek 2018). It means that a practical robustness index should completely reflect the robustness of the structural system without being influenced by other aspects. Besides, it should be as simple as possible without the requirement of excessive computational effort. In addition, it should be reproducible and independent of user decisions. Finally, a practical robustness index should be applicable to a wide range of structural systems. However, different structural systems are prone to different types of collapse and respond differently to initial damage. Hence, there is no unique robustness index suitable for all or a wide range of structural systems. In fact, all the mentioned characteristics for a practical robustness index cannot be satisfied to the same level at the same time (Starossek 2018). For instance, a damage-based robustness index can be applied to all kinds of structural systems and has a high level of expressiveness. However, it is computationally costly.

Different approaches have been proposed in the literature for the calculation of the robustness index or related characteristics of a structural system such as reliability, redundancy, vulnerability, and damage tolerance (see, Neves Carneiro and Conceicao Antonio (2019a, b), Maes et al. 2006, Kanno and Ben-Haim 2011, Husain and Tsopelas 2004, Wisniewski et al. 2006, Biondini et al. 2008, Smith 2006, Baker et al. 2008, and Agarwal et al. 2003).

Wang et al. (2017) proposed a reliability index based on uncertainty theory. Neves Carneiro and Conceicao Antonio (2019a) presented a practical procedure for global convergence of the Reliability Index Approach (RIA). Their method is suitable for the design optimization of more complex structures. Zahi and Zhang (2019) introduced a new approach for evaluating structural reliability under twofold uncertainty.

Measures based on structural behavior can be divided into deterministic and probabilistic measures. Frangopol and Curley (1987) studied the effects of damage and redundancy on the reliability of structural systems and proposed deterministic and probabilistic measures. These measures are based on a definition of structural redundancy, including both system reliability and damage assessment concepts. As a deterministic approach, they proposed the following measure of redundancy:

$$R = \frac{L_{Intact}}{L_{Intact} - L_{damaged}} \quad (3.88)$$

Where R is the redundancy index, L_{Intact} is the overall structural collapse load without damage, and $L_{damaged}$ is the overall structural collapse load considering some damage in one, or more, member. The redundancy index is equal to 1 when the damaged structure has no

reserve strength, and it is infinite when the damage has no influence on the reserve structural strength. They also proposed a probabilistic redundancy index, β_R , defined by:

$$\beta_R = \frac{\beta_{Intact}}{\beta_{Intact} - \beta_{damaged}} \quad (3.89)$$

where β_{Intact} is the reliability index of the intact system and $\beta_{damaged}$ is the reliability index of the damaged system. The structure is robust if β_R is close to infinite. Alternatively, when the value of β_R is close to 1, the robustness tends to be null.

Lind (1995) presented quantitative measures of system vulnerability and damage tolerance. He defined vulnerability of a system, V , as:

$$V = \frac{P(r_d, S)}{P(r_0, S)} \quad (3.90)$$

where r_d is the resistance of the damaged system, r_0 is the resistance of the intact system, and S is the loading condition. $P(r, S)$ is the system failure probability as a function of both loading and resistance effects. The vulnerability of a system varies from one, when the damage has no impact on the system resistance, to infinite, when the damage has a large impact on the structural system.

A risk-based assessment of robustness has been developed by Baker et al. (2008). They used probabilistic risk assessment concepts to formulate a new metric for the robustness of an engineered system. Their method incorporates both the probabilities of adverse events and their associated consequences. According to this method, the robustness index can be calculated as follows:

$$RI = \frac{R_{Dir}}{R_{Dir} + R_{Ind}} \quad (3.91)$$

where RI is the robustness index, R_{Dir} is the direct risks, and R_{Ind} is the indirect risks. This index varies between 0 and 1.0 with larger values representing a higher level of robustness.

Maes et al. (2006) also proposed a probabilistic measure of robustness as follow:

$$RI = \min \frac{P_{f_0}}{P_{f_i}} \quad (3.92)$$

where P_{f_0} is the system failure probability of the undamaged system and P_{f_i} is the system failure probability assuming the failure of member i .

Some of the basic deterministic robustness indices are as follows:

1. Damage-based robustness index
2. Stiffness-based robustness index
3. Reserve-based robustness index
4. Energy-based robustness index

These approaches are mostly based on assuming an initial damage and comparing the properties of the damaged and intact structure. The reserve-based robustness index reflects the capability of the structure in load redistribution and providing alternative load paths and can be expressive for structures that are susceptible to the zipper-type collapse (Starossek 2018). However, it does not account for the extension of damage.

According to Starossek (2018), a reserve-based robustness index can be calculated as follows:

$$RI_r = 1 - \max_{i,j} \frac{F_i + \Delta F_{ij}}{F_{i,ult}} \quad (3.93)$$

where RI_r is the reserve-based robustness index, F_i is the original load of an element i , ΔF_{ij} is the absorbed load in element i due to the failure of element j , and $F_{i,ult}$ is the ultimate load capacity of element i . This formulation can be expanded to account for the initial damage of several elements.

This index is referred to as the reserve-based measure of robustness because the redistribution of forces after a local failure is possible only when the system has reserve load-bearing capacity. Hence, the proposed performance index primarily reflects the redundancy of the structural system. It should be noted that an increase in redundancy does not necessarily lead to an increase in robustness. It depends on the structural system. For example, local failure in a building structure may pull down a larger part of the structure when the structural redundancy is high and structural components are tied together too well. For the simplified model, an increase in redundancy leads to an increase in robustness.

Positive values of the reserve-based robustness index indicate a robust structure because no failure progression will occur. A greater robustness index shows a more secure robust structure. On the other hand, negative values show failure progression and the absence of robustness. The maximum possible value of RI_r is of the order of $1 - \Phi$, where Φ is the average resistance safety factor. Hence, RI_r is always smaller than one (Starossek 2018). The reserve-based robustness index is simple, calculable and objective.

In the previous section, an approximation function for the calculation of the stress increase ratio of the critical cable in a cable-loss scenario has been derived. This approximation

function can be used to calculate the absorbed load in the critical cable due to cable failure (ΔF). By incorporating the value of (ΔF) calculated from the derived approximation function into Equation 3.93, the reserve-based robustness index can be rewritten as follows:

$$RI_r^{m,\phi} = 1 - \max_{i,j} \frac{F_i + \left(\frac{m}{2n} + \frac{(0.105m^2 + 0.645m) - \frac{m}{2n}}{1 + \left(\frac{\beta}{c}\right)^d} \right) 2 F_j}{F_{i,ult}} \quad (3.94a)$$

For large values of n :

$$RI_r^{m,\phi} \approx 1 - \max_{i,j} \frac{(0.105m^2 + 0.645m) 2 F_j}{(1 + \beta^{0.35}) F_{i,ult}} \quad (3.94b)$$

Equation 3.94 is a robustness index for a general parallel load-bearing system. It should be noted that a DAF of 2 is incorporated into the proposed robustness index to account for the dynamic nature of cable failure. In the proposed robustness index, the number of failed cables is variable. Hence, the structural robustness can be determined for different cable-loss scenarios and different levels of the initial damage.

3.6 Structural robustness of long-span cable-supported bridges segmented by zipper-stoppers to prevent progressive collapse

In this section, preventing progressive collapse by using zipper-stoppers will be discussed. First, the zipper-stopper will be defined. Then, the structural robustness of a long-span cable-supported bridge segmented by zipper-stoppers will be investigated, and the stress increase ratio of a zipper-stopper in a cable-loss scenario will be determined.

As mentioned, the zipper-type collapse occurs in structural systems with parallel load-bearing elements and starts by the initial failure of one or a few load-bearing members. The load carried by these members must be redistributed to the adjacent members who are similar in type and function to the failing members. If these members become overloaded, they fail in their function of alternative load paths and the failure progresses (Haberland et al. 2012).

Increasing the robustness of the structural system through segmentation is a possible approach to prevent such a progressive collapse. By segmentation, the structure is divided into segments by dedicated segment borders. In this way, failure is isolated within one segment (or, in particular cases, within two segments); thus preventing a failure from spreading disproportionately (Starossek and Haberland 2010).

According to Starossek (2018), different types of segment borders can be classified as follows:

- strong elements to resist the collapse load
- weak elements (structural fuses) to disconnect the failing part from the remaining structure
- elements with high ductility and large energy dissipation capacity

In this study, the first type of segment borders, referred to as zipper-stopper, is of interest. Zipper-stoppers are strong elements, with a larger load-bearing capacity than ordinary elements, and must be designed in a way that they can tolerate the redistributed load of half of the segment.

In Fig. 3.14, the schematic view of the simplified model of a long-span cable-supported bridge segmented by zipper-stoppers is shown. It is assumed that the axial stiffness of the zipper-stopper is $K_I = \delta_I K$, where K is the axial stiffness of other cables, and δ_I is a chosen coefficient.

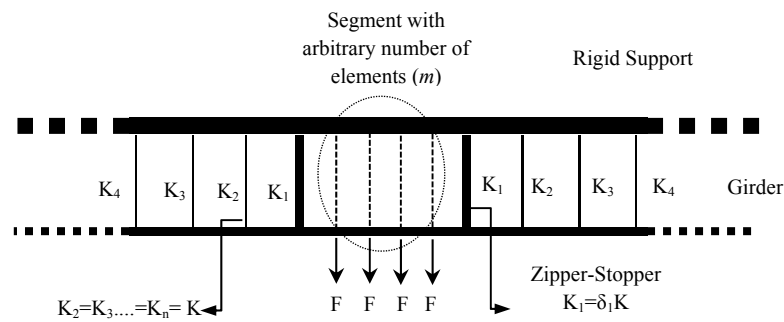


Figure 3.14 A parallel load-bearing system segmented by zipper-stoppers

The base of the analytical approach for the calculation of the stress increase ratio of the zipper-stopper is the same as the previous case. Hence, it is not repeated. For solving this system, a step by step method is applied. In the first step, it is assumed that the segment consists of only one cable and only one cable fails.

Performing the analytical solution leads to the following system of equations (Equation 3.95). This system of equations is solved for different δ_1 -values (see Fig. 3.15). The results show that as δ_1 -value increases, the stress increase ratio of the zipper-stopper increases. As mentioned, δ_1 represents the axial stiffness of the zipper-stopper. Henceforth, increasing the value of δ_1 results in the increase of the axial stiffness of the zipper-stopper; consequently, the zipper-stopper absorbs a larger proportion of the redistributed load.

$$\left\{ \begin{aligned}
 &F_n + F_{n-1} + F_{n-2} + \dots + F_1 = \frac{F}{2} \\
 &F_n(6 + 6\beta) + F_{n-1}(1 - 12\beta) + F_{n-2}(6\beta) = 0 \\
 &F_n(12) + F_{n-1}(6 + 6\beta) + F_{n-2}(1 - 12\beta) + F_{n-3}(6\beta) = 0 \\
 &F_n(18) + F_{n-1}(12) + F_{n-2}(6 + 6\beta) + F_{n-3}(1 - 12\beta) + F_{n-4}(6\beta) = 0 \\
 &F_n(24) + F_{n-1}(18) + F_{n-2}(12) + F_{n-3}(6 + 6\beta) + F_{n-4}(1 - 12\beta) + F_{n-5}(6\beta) = 0 \quad (3.95) \\
 &\vdots \\
 &F_n(6n - 12) + F_{n-1}(6(n - 1) - 12) + \dots + F_3(6 + 6\beta) + F_2(1 - 12\beta) + F_1\left(\frac{6\beta}{\delta_1}\right) = 0 \\
 &F_n(9n - 7) + F_{n-1}(9(n - 1) - 7) + \dots + F_2(11 + 6\beta) + F_1\left(3 - \frac{6\beta}{\delta_1}\right) = 0
 \end{aligned} \right.$$

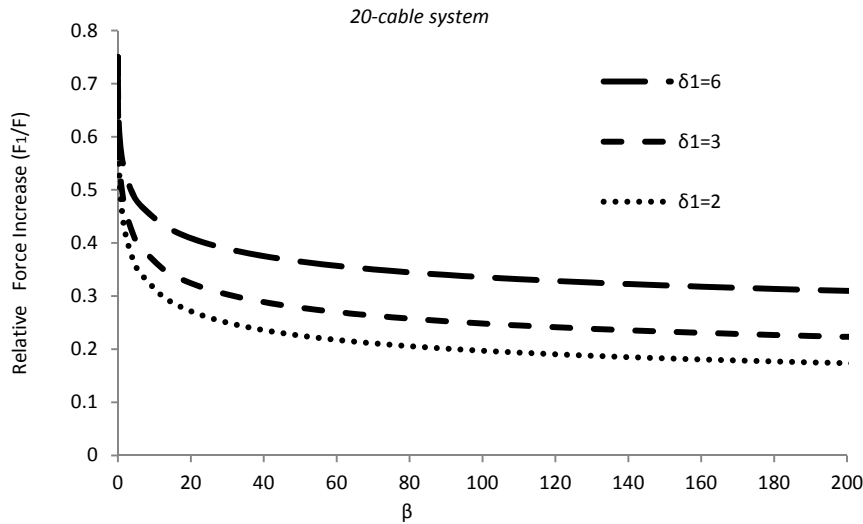


Fig. 3.15 The stress increase ratio of the zipper-stopper for different δ_1 -values

The only difference between this system of equations and the derived system of equations in the previous section is the coefficient of F_1 in the last two equations. Hence, it is expected that the form of the equation for the stress increase ratio, and consequently, the form of the approximation function, remains similar.

The results of the calculations of the aforementioned system of equations for four and six-cable systems are given below.

Four-cable system:

$$\frac{F_1}{F} = \frac{11 + 6\beta}{16 + 12\beta(1 + \frac{1}{\delta_1})} \quad (3.96)$$

Six-cable system:

$$\frac{F_1}{F} = \frac{23 + 171\beta + 18\beta^2}{31 + \beta(288 + \frac{84}{\delta_1}) + \beta^2(36 + \frac{72}{\delta_1})} \quad (3.97)$$

To find the unknown coefficients of the approximation function, their definitions should be recalled. As mentioned before, parameter a stands for the minimum stress increase ratio, which occurs when $\beta = \infty$. This means that the girder is rigid, and all cables have the same displacements. Therefore, parameter a is easily calculated as follows:

$$a = \frac{K_1}{2 \sum_{i=1}^n K_i} = \frac{\delta_1}{2\delta_1 + 2(n - 1)} \quad (3.98)$$

Parameter b is the maximum stress increase ratio, which occurs when β is equal to zero. Hence, δ_1 has no effect on parameter b because beam is rigidly supported. For evaluating parameters c and d for the current configuration, different systems with different δ_1 values are investigated, and appropriate approximation functions are calculated. The results show that parameter c has an upper value equal to δ_1 . It means that the stiffness of other cables has no effect on parameter c . In Fig. 3.16, the calculated values of parameter c for two systems with δ_1 -values of one and two are shown. In Fig. 3.17, parameter d is calculated for a 10-cable system using the LSM method.

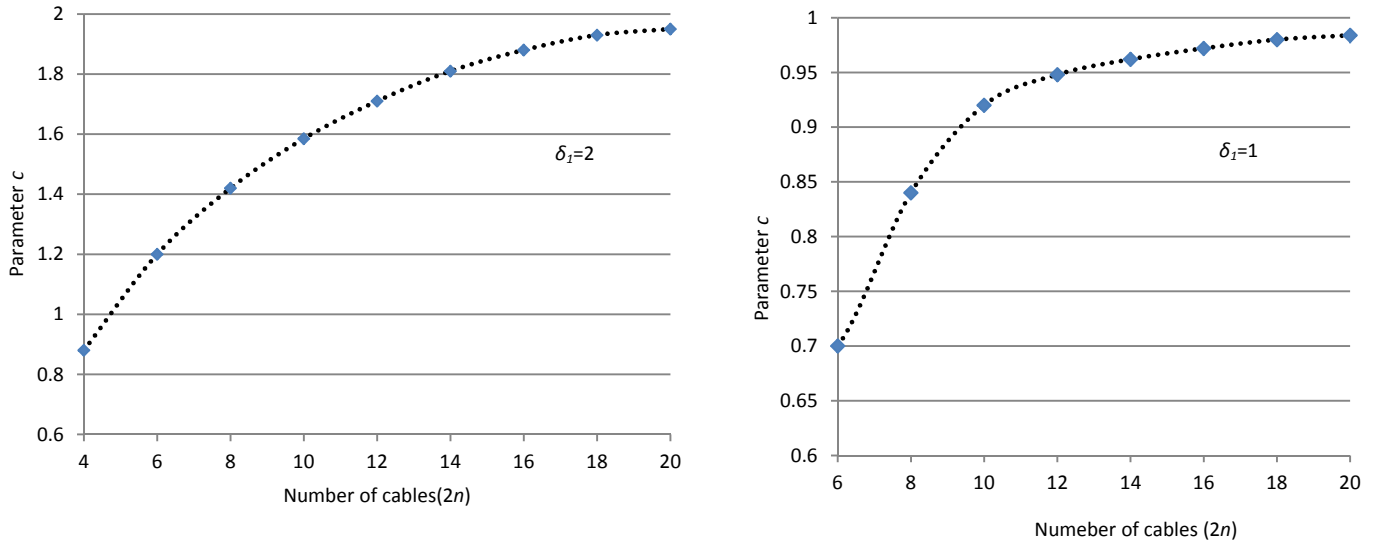


Fig. 3.16 Calculation of parameter c for two systems with different δ_1 -values

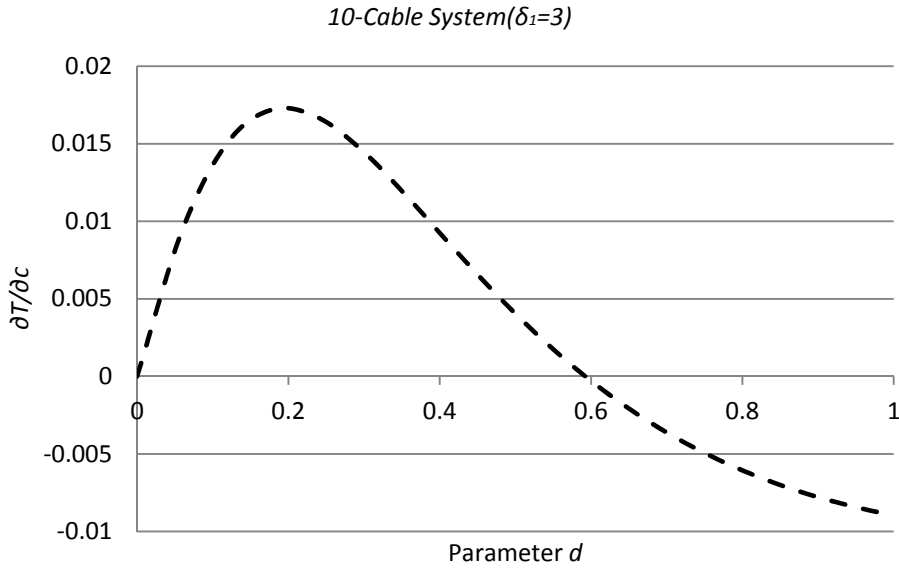


Figure 3.17 Calculation of parameter d for a 10-cable system ($\delta_1=3$)

The comparison of Fig. 3.17 and Fig. 3.5 shows that changing the stiffness of the critical cable has minimal effects on parameter d and, consequently, on the final results. In fact, parameter d is mainly influenced by the number of cables, as well as their stiffness. However, the effects of cable stiffness are fairly insignificant. Furthermore, the main target of this study is to present a practical and simple approximation function. Hence, in order to keep the approximation function as simple as possible, the effect of the cable stiffness on the value of parameter d is ignored.

According to the findings from the previous steps, unknown parameters of the approximation function are defined. The approximation function for the stress increase ratio of the zipper-stopper can be derived as follows:

$$\frac{F_1}{F} = a + \frac{\frac{3}{4} - a}{1 + \left(\frac{\beta}{c}\right)^d} \tag{3.99}$$

where parameter d should be calculated by Equation 3.67.

$$a = \frac{K_1}{2 \sum_{i=1}^n K_i} = \frac{\delta_1}{2\delta_1 + 2(n - 1)} \tag{3.100}$$

And for large values of n :

$$\frac{F_1}{F} = \frac{\frac{3}{4}}{1 + \left(\frac{\beta}{\delta_1}\right)^{0.35}} \tag{3.101}$$

To check the accuracy of the presented approximation function, different systems with different δ_1 -values are investigated.

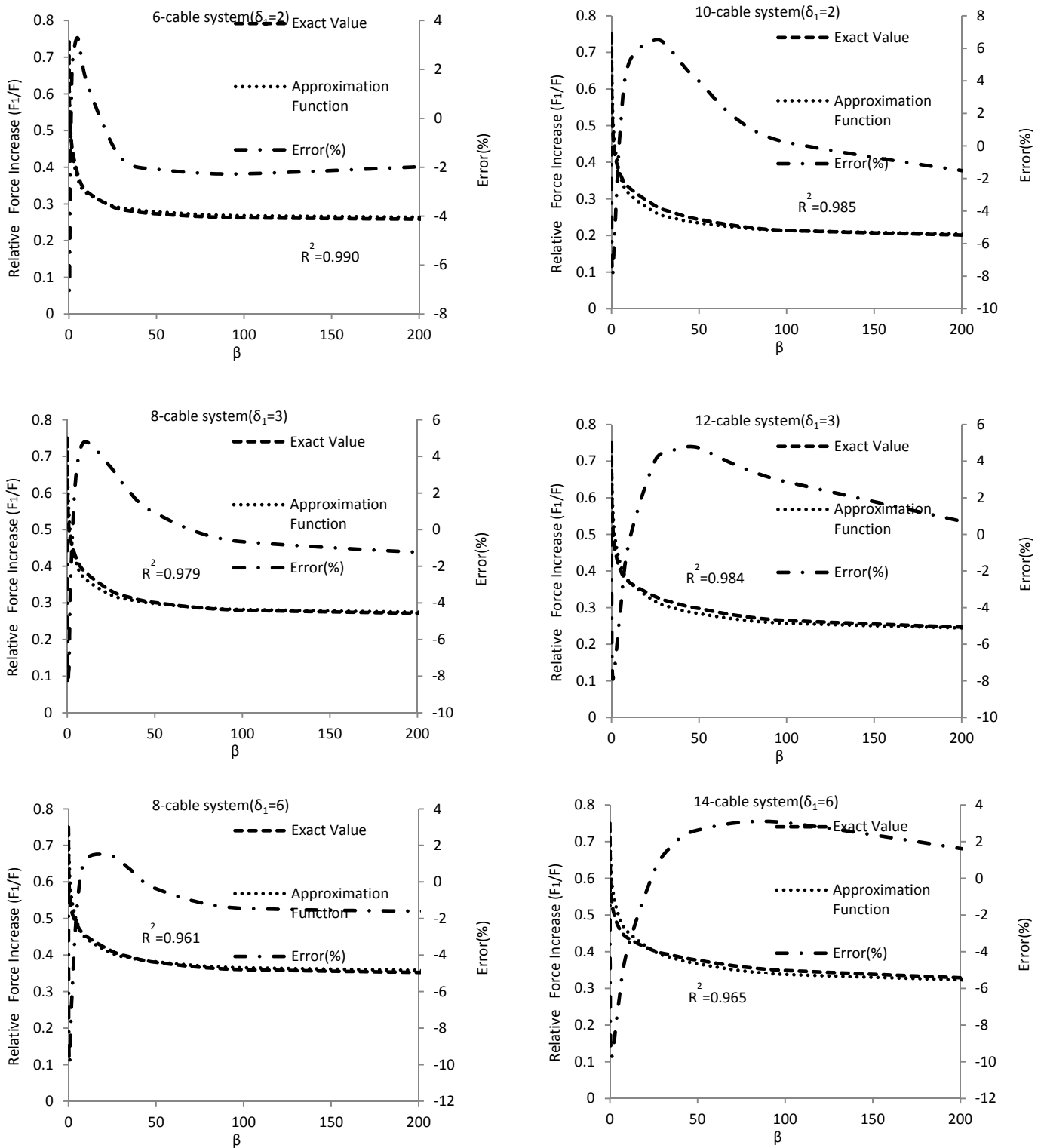


Fig. 3.18 Exact and approximate values for the stress increase ratio of the zipper-stopper in different systems

In Fig. 3.18, the comparison of the exact analytical results and approximate values for different systems and different values of δ_1 after the elimination of one cable is presented.

The results show that when the δ_l -value increases, the parameter R^2 , as a measure of the accuracy of the approximation function, decreases slightly. This is because the effect of the δ_l -value on the calculation of parameter d is ignored. However, as mentioned earlier, it does not have an important effect on the final results.

In the next step, the eliminations of two and three cables are considered. Found below are the final systems of equations for these systems.

The final system of equations for a segmented system with two failed cables:

$$\left\{ \begin{array}{l} F_n + F_{n-1} + F_{n-2} + \dots + F_1 = F \\ F_n(6 + 6\beta) + F_{n-1}(1 - 12\beta) + F_{n-2}(6\beta) = 0 \\ F_n(12) + F_{n-1}(6 + 6\beta) + F_{n-2}(1 - 12\beta) + F_{n-3}(6\beta) = 0 \\ F_n(18) + F_{n-1}(12) + F_{n-2}(6 + 6\beta) + F_{n-3}(1 - 12\beta) + F_{n-4}(6\beta) = 0 \\ F_n(24) + F_{n-1}(18) + F_{n-2}(12) + F_{n-3}(6 + 6\beta) + F_{n-4}(1 - 12\beta) + F_{n-5}(6\beta) = 0 \quad (3.102) \\ \vdots \\ F_n(6n - 12) + F_{n-1}(6(n - 1) - 12) + \dots + F_3(6 + 6\beta) + F_2(1 - 12\beta) + F_1\left(\frac{6\beta}{\delta_1}\right) = 0 \\ F_n(48n - 19) + F_{n-1}(48(n - 1) - 19) + \dots + F_2(77 + 24\beta) + F_1\left(33 - \frac{24\beta}{\delta_1}\right) - 9F = 0 \end{array} \right.$$

The final system of equations for a segmented system with three failed cables:

$$\left\{ \begin{array}{l} F_n + F_{n-1} + F_{n-2} + \dots + F_1 = \frac{3F}{2} \\ F_8(6 + 6\beta) + F_7(1 - 12\beta) + F_6(6\beta) = 0 \\ F_8(12) + F_7(6 + 6\beta) + F_6(1 - 12\beta) + F_5(6\beta) = 0 \\ F_8(18) + F_7(12) + F_6(6 + 6\beta) + F_5(1 - 12\beta) + F_4(6\beta) = 0 \\ F_8(24) + F_7(18) + F_6(12) + F_5(6 + 6\beta) + F_4(1 - 12\beta) + F_3(6\beta) = 0 \quad (3.103) \\ F_8(30) + F_7(24) + F_6(18) + F_5(12) + F_4(6 + 6\beta) + F_3(1 - 12\beta) + F_2(6\beta) = 0 \\ F_n(6n - 12) + F_{n-1}(6(n - 1) - 12) + \dots + F_3(6 + 6\beta) + F_2(1 - 12\beta) + F_1\left(\frac{6\beta}{\delta_1}\right) = 0 \\ F_n(15n + 2) + F_{n-1}(15(n - 1) + 2) + \dots + F_4(62) + F_3(47) + F_2(32 + 6\beta) + F_1\left(18 - \frac{6\beta}{\delta_1}\right) - 12F = 0 \end{array} \right.$$

According to the findings of the previous steps, parameter c and parameter d do not depend on the number of failed cables. Hence, parameter b is the only unknown parameter for the calculation of the stress increase ratio of the zipper-stopper in the case of the failure of all cables in a segment with an arbitrary number of cables.

In addition, it was also found that parameter b represents the maximum stress increase ratio of the system and occurs when $\beta=0$. Hence, the δ_1 -value has no effect on parameter b and the number of failed cables is the only influential factor on parameter b .

The relationship between parameter b and the number of failed cables has been calculated in the previous section. Therefore, the final approximation function for the calculation of the stress increase ratio of the zipper-stopper can be derived as follows:

$$\frac{F_1}{F} = a + \frac{(0.105m^2 + 0.645m) - a}{1 + \left(\frac{\beta}{c}\right)^d} \quad (3.104)$$

And for large values of n :

$$\frac{F_1}{F} = \frac{0.105m^2 + 0.645m}{1 + \left(\frac{\beta}{\delta_1}\right)^{0.35}} \quad (3.105)$$

where parameter a should be calculated by the following equation:

$$a = \frac{mK_1}{2 \sum_{i=1}^n K_i} = \frac{m\delta_1}{2\delta_1 + 2(n-1)} \quad (3.106)$$

To verify the final approximation function, the result of the exact stress increase ratio of the zipper-stopper and the one calculated from the approximation function for the elimination of two and three cables for different systems are compared (see Fig. 3.19).

The results show a good agreement between the exact and approximate values. Except for small β -values, the error of the proposed approximation function is less than 5% in the investigated systems. In addition, it can be seen that by increasing the β -value, the stress increase ratio of the zipper-stopper decreases.

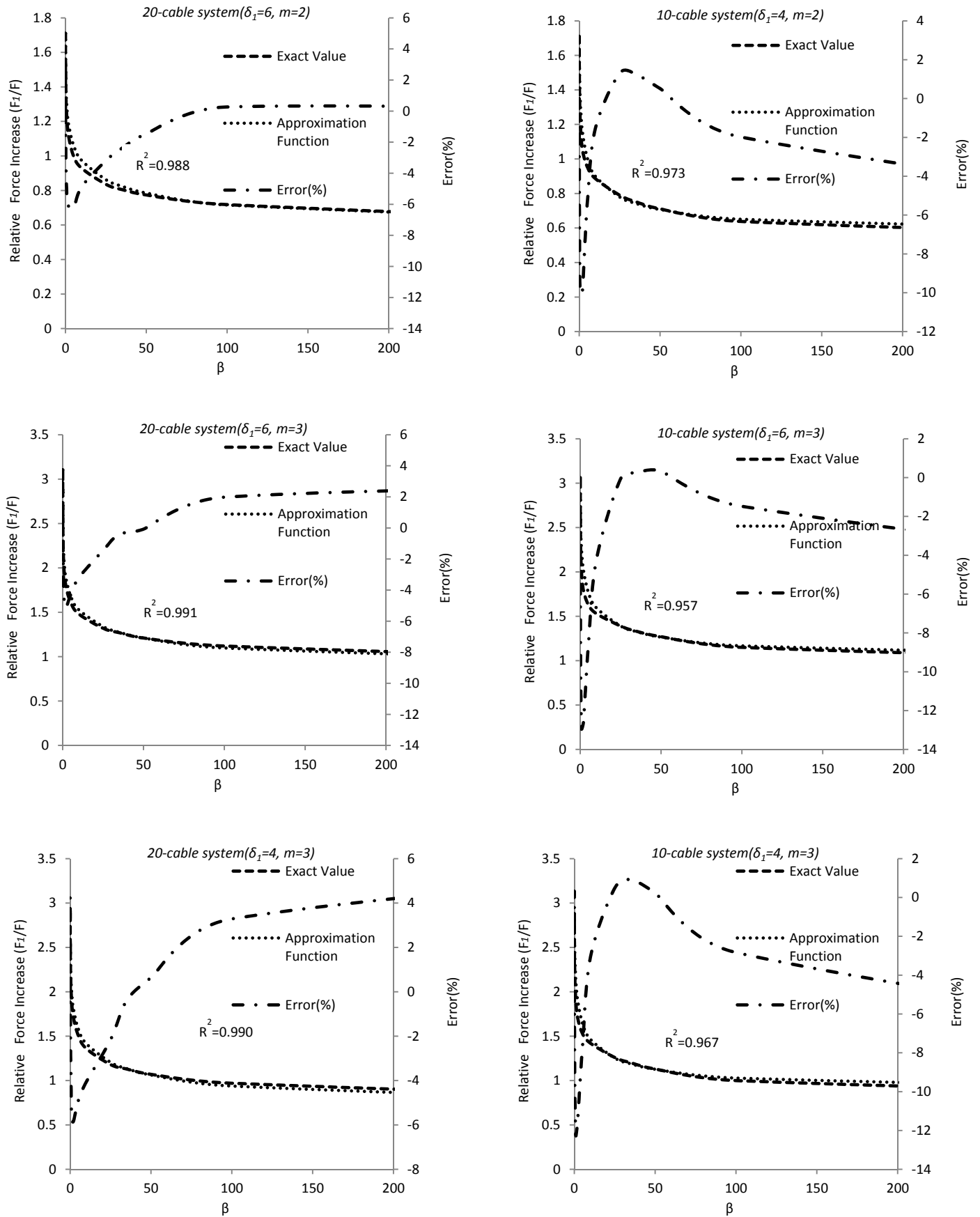


Figure 3.19 Exact and approximate values for the stress increase ratio of the zipper-stopper in different systems

3.7 Modifying the approximation function for a more detailed conceptual model

In the previous sections, it was assumed that the axial stiffness of all cables is the same. However, this assumption is not accurate in actual structures. For example, in cable-supported bridges each cable has a specific length, and consequently, a unique axial stiffness. To make the conceptual model one step closer to reality, in this section, it is assumed that the axial stiffness of each cable is unique. In Fig. 3.20, the schematic view of the considered model is depicted.

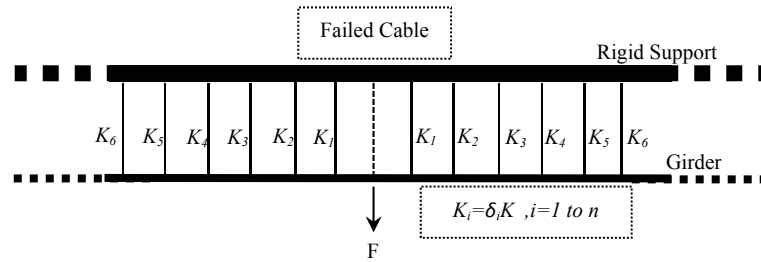


Fig. 3.20 The schematic view of a more detailed model

As shown in Fig. 3.20, the new conceptual model considers a unique axial stiffness in each cable. To render the mathematical procedure straightforward, a reference axial stiffness (K) is used and the stiffness of the cables is expressed as a multiple of the reference stiffness ($K_i = \delta_i K$). The symmetry of the model is kept and it is assumed that only one cable fails. Considering the failure of several cables is also possible, but because the main mathematical procedure is the same as the previous sections, it is not further considered here.

To solve the new model, an analytical approach similar to the one performed in the previous sections has been performed and a system of equations has been derived (Equation 3.107).

For solving this system of equations, a step by step method is applied. In the first step, it is assumed that all cables have the same stiffness ($K_1 = K_2 = \dots = K_n$ or $\delta_1 = \delta_2 = \dots = \delta_n = 1$). Then, the system of linear equations is solved for different cable-systems, and unknown parameters of the approximation function are calculated. In the second step, the stiffness of the critical cable is changed. Therefore, in this step, all cables have the same stiffness except for the critical cable ($\delta_2 = \delta_3 = \dots = \delta_n = 1$). Finally, in the last step, the stiffness of all cables is changed. Therefore, all cables have a unique axial stiffness.

The first and second steps have been done in the previous sections. In fact, finding the parameters of the approximation function for a segmented system revealed the relationship among these parameters, and showed the role of the cable-configuration on the approximation function. This gave the author the idea to consider a unique axial stiffness for each cable.

$$\left\{ \begin{array}{l} F_n + F_{n-1} + F_{n-2} + \dots + F_1 = \frac{F}{2} \\ F_n \left(6 + \frac{6\beta}{\delta_n} \right) + F_{n-1} \left(1 - \frac{12\beta}{\delta_{n-1}} \right) + F_{n-2} \left(\frac{6\beta}{\delta_{n-2}} \right) = 0 \\ F_n(12) + F_{n-1} \left(6 + \frac{6\beta}{\delta_{n-1}} \right) + F_{n-2} \left(1 - \frac{12\beta}{\delta_{n-2}} \right) + F_{n-3} \left(\frac{6\beta}{\delta_{n-3}} \right) = 0 \\ F_n(18) + F_{n-1}(12) + F_{n-2} \left(6 + \frac{6\beta}{\delta_{n-2}} \right) + F_{n-3} \left(1 - \frac{12\beta}{\delta_{n-3}} \right) + F_{n-4} \left(\frac{6\beta}{\delta_{n-4}} \right) = 0 \\ F_n(24) + F_{n-1}(18) + F_{n-2}(12) + F_{n-3} \left(6 + \frac{6\beta}{\delta_{n-3}} \right) + F_{n-4} \left(1 - \frac{12\beta}{\delta_{n-4}} \right) + F_{n-5} \left(\frac{6\beta}{\delta_{n-5}} \right) = 0 \\ \vdots \\ F_n(6n - 12) + F_{n-1}(6(n - 1) - 12) + \dots + F_3 \left(6 + \frac{6\beta}{\delta_3} \right) + F_2 \left(1 - \frac{12\beta}{\delta_2} \right) + F_1 \left(\frac{6\beta}{\delta_1} \right) = 0 \\ F_n(9n - 7) + F_{n-1}(9(n - 1) - 7) + \dots + F_2 \left(11 + \frac{6\beta}{\delta_2} \right) + F_1 \left(3 - \frac{6\beta}{\delta_1} \right) = 0 \end{array} \right. \quad (3.107)$$

According to the definitions of each parameter of the approximation function and based on the findings of the previous steps, it can be concluded that:

1) Parameter a stands for the minimum stress increase ratio, which occurs when $\beta = \infty$, the girder is rigid, and all cables have the same displacements. Therefore, parameter a could be easily calculated as follows:

$$a = \frac{K_1}{2 \sum_{i=1}^n K_i} = \frac{\delta_1}{2 \sum_{i=1}^n \delta_i} \quad , K_i = \delta_i K \quad (3.108)$$

2) Parameter b stands for the maximum stress increase ratio that occurs when $\beta=0$. Hence, the number of failed cables is the only effective parameter on parameter b . It was shown that in the case of the failure of one cable, parameter b is equal to 0.75.

3) Parameter c depends only on the axial stiffness of the critical cable and has an upward value equal to δ_1 .

4) Investigation of several systems showed that parameter d is mainly influenced by the number of cables, as well as their stiffness. However, the effects of cable stiffness are fairly insignificant. Hence, in order to keep the approximation function as simple as possible, the effect of the cable stiffness on the value of parameter d is ignored.

Considering the aforementioned facts, the approximation function can be derived as follows:

$$\frac{F_1}{F} = a + \frac{\frac{3}{4} - a}{1 + \left(\frac{\beta}{c}\right)^d} \quad (3.109)$$

And for large values of n :

$$\frac{F_1}{F} = \frac{\frac{3}{4}}{1 + \left(\frac{\beta}{\delta_1}\right)^{0.35}} \quad (3.110)$$

where parameter d should be calculated by Equation 3.67. To check the accuracy of the presented approximation function, three different systems, each with two different cable-configurations, are investigated (see Fig. 3.21).

In Table 3.5, the structural specifications of each system are presented. The results also show that ignoring the effect of cables' stiffness on parameter d has negligible effects on the accuracy of the final approximation function. Similar to the previous results, with an exception for small β -values, the error of approximation is less than 5%. The calculated values of R-square for all systems are larger than 0.970, which is acceptable. The exact values for 12 and 16-cable systems are calculated by solving the corresponding system of linear equations, and for 22-cable systems, the exact values are calculated using the software package SAP2000. In doing so, the analytical approach has been checked once again.

Table 3.5 Structural specifications of the investigated systems

Cable-Stiffness	12-cable system (a)	12-cable system (b)	16-cable system (a)	16-cable system (b)	22-cable system (a)	22-cable system (b)
K₁	K	3K	K	4.5K	K	2K
K₂	1.4K	2.6K	1.5K	4K	1.1K	1.9K
K₃	1.8K	2.2K	2K	3.5K	1.2K	1.8K
K₄	2.2K	1.8K	2.5K	3K	1.3K	1.7K
K₅	2.6K	1.4K	3K	2.5K	1.4k	1.6K
K₆	3K	K	3.5K	2K	1.5K	1.5k
K₇	-	-	4K	1.5K	1.6K	1.4K
K₈	-	-	4.5K	K	1.7k	1.3K
K₉	-	-	-	-	1.8K	1.2K
K₁₀	-	-	-	-	1.9K	1.1K
K₁₁	-	-	-	-	2K	K

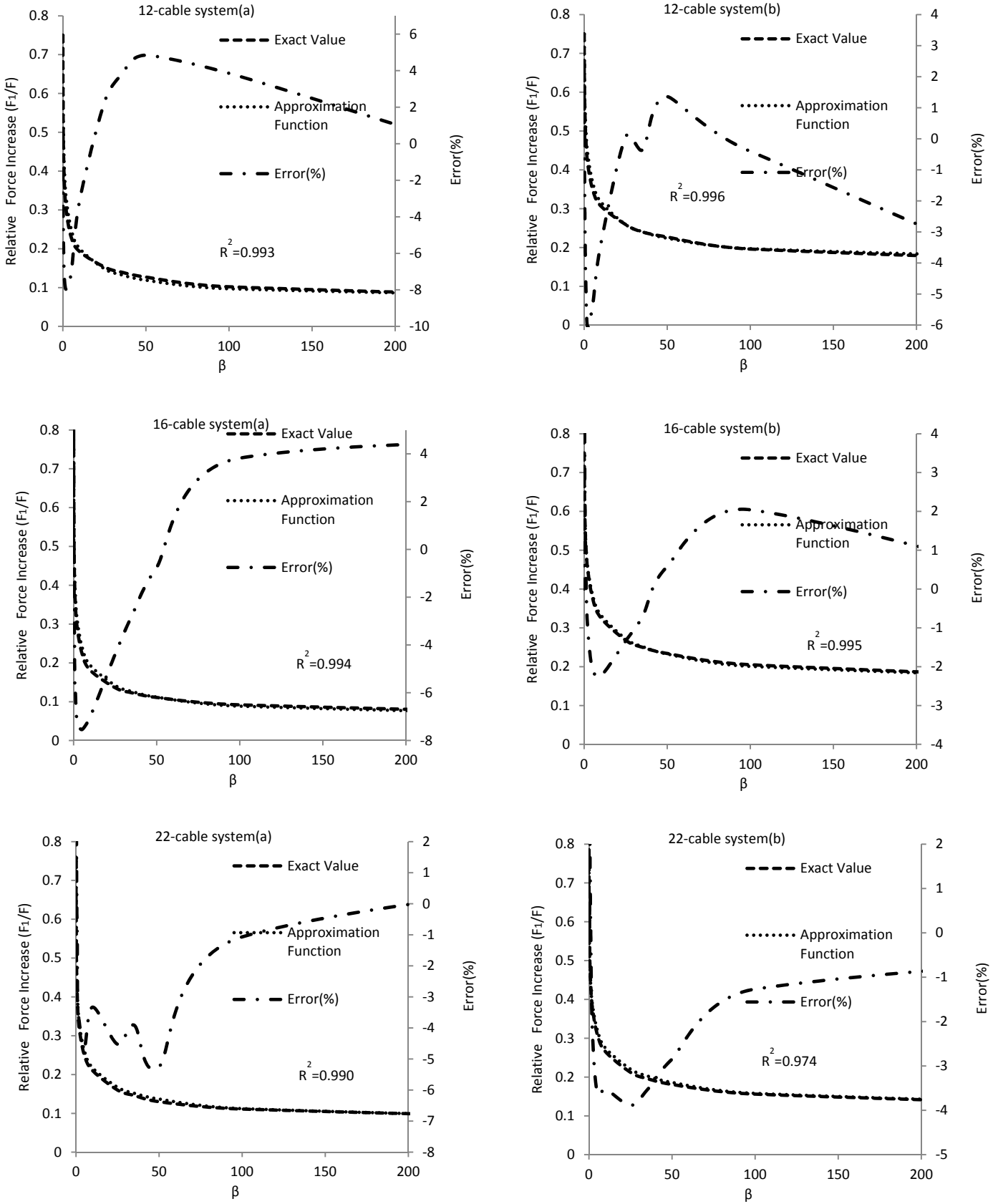


Fig. 3.21 Exact and approximate values of stress increase ratio in different systems

Chapter 4

Bending Moment Acting on the Girder of a Long-Span Cable Supported Bridge Suffering from Cable Failure

4.1 Introduction

In this chapter, the structural behavior of the girder of a long-span cable-supported bridge after the sudden rupture of one of its cables is of concern. Recently, the issue of cable failure in cable-supported bridges has been studied. These studies show that cable failure can cause the instability of the structural system and also produce large bending moments on the girder of the bridge.

Wolf and Starossek (2009 and 2010) studied the collapse behavior of a cable-stayed bridge in a cable-loss scenario. They showed that the initial failure of three adjacent short cables, which were responsible for the stabilization of the bridge girder in compression, caused the lack of bracing in the girder. The girder began to buckle in the vertical direction as a result of high normal forces, and finally, an instability type of collapse occurred in the girder.

A parametric study has also been conducted by Mozos and Aparicio (2010) on the dynamic response of cable-stayed bridges to the sudden failure of a cable. It was shown that the sudden failure of a cable can produce large bending moments on the deck and pylons.

The focus of this chapter is to find the increase of maximum bending moment on the girder due to cable failure. For this purpose, an analytical approach based on differential equations of the system will be used and an approximation function for the determination of the relative moment increase of the girder in a cable-loss scenario will be derived. The performed analytical approach is similar to the one in the previous chapter. The use of the LSM method is also applied to minimize the error of the approximation function. The proposed approximation function has been checked by numerical models to prove its accuracy.

To use the analytical approach, a conceptual model similar to the model in the last section of the previous chapter is considered (see Fig. 4.1). All of the structural specifications are explained in the previous chapter and are not repeated here. As shown in this chapter, the more realistic model of the bridge, which considers a unique axial stiffness in each cable, is employed.

The target is to find a general equation for the increase of the maximum bending moment of the girder due to cable failure.

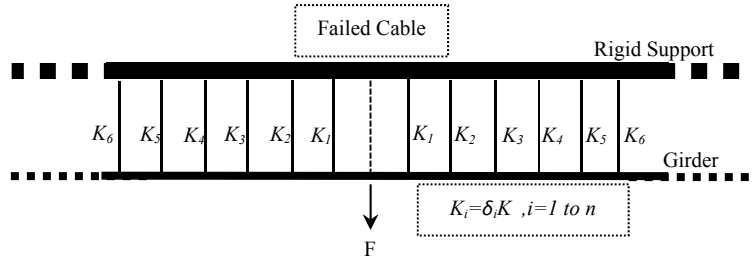


Fig. 4.1 The schematic view of the simplified model

4.2 An analytical approach for the determination of the increase of the maximum bending moment of the girder due to the cable loss

The performed analytical approach is similar to the one in the previous chapter. According to the mathematical calculations in the previous chapter, the final system of equations for the considered model can be derived as follows:

$$\left\{ \begin{array}{l}
 F_n + F_{n-1} + F_{n-2} + \dots + F_1 = \frac{F}{2} \\
 F_n \left(6 + \frac{6\beta}{\delta_n} \right) + F_{n-1} \left(1 - \frac{12\beta}{\delta_{n-1}} \right) + F_{n-2} \left(\frac{6\beta}{\delta_{n-2}} \right) = 0 \\
 F_n(12) + F_{n-1} \left(6 + \frac{6\beta}{\delta_{n-1}} \right) + F_{n-2} \left(1 - \frac{12\beta}{\delta_{n-2}} \right) + F_{n-3} \left(\frac{6\beta}{\delta_{n-3}} \right) = 0 \\
 F_n(18) + F_{n-1}(12) + F_{n-2} \left(6 + \frac{6\beta}{\delta_{n-2}} \right) + F_{n-3} \left(1 - \frac{12\beta}{\delta_{n-3}} \right) + F_{n-4} \left(\frac{6\beta}{\delta_{n-4}} \right) = 0 \\
 F_n(24) + F_{n-1}(18) + F_{n-2}(12) + F_{n-3} \left(6 + \frac{6\beta}{\delta_{n-3}} \right) + F_{n-4} \left(1 - \frac{12\beta}{\delta_{n-4}} \right) + F_{n-5} \left(\frac{6\beta}{\delta_{n-5}} \right) = 0 \quad (4.1) \\
 \vdots \\
 F_n(6n - 12) + F_{n-1}(6(n - 1) - 12) + \dots + F_3 \left(6 + \frac{6\beta}{\delta_3} \right) + F_2 \left(1 - \frac{12\beta}{\delta_2} \right) + F_1 \left(\frac{6\beta}{\delta_1} \right) = 0 \\
 F_n(9n - 7) + F_{n-1}(9(n - 1) - 7) + \dots + F_2 \left(11 + \frac{6\beta}{\delta_2} \right) + F_1 \left(3 - \frac{6\beta}{\delta_1} \right) = 0
 \end{array} \right.$$

In the previous chapter, only the axial force of the critical cable was determined. However, the calculation of the axial force in all cables is possible. By solving the aforementioned system of equations, the force in each cable and, consequently, the bending moment in each section of the girder can be calculated.

In Fig. 4.2, the results of the calculations of the relative moment increase of the girder for 10 and 20-cable systems are shown. The maximum bending moment due to cable failure occurs at the location of the failed cable (mid-span). It can be seen that as β -value increases, the maximum bending moment due to the cable loss increases.

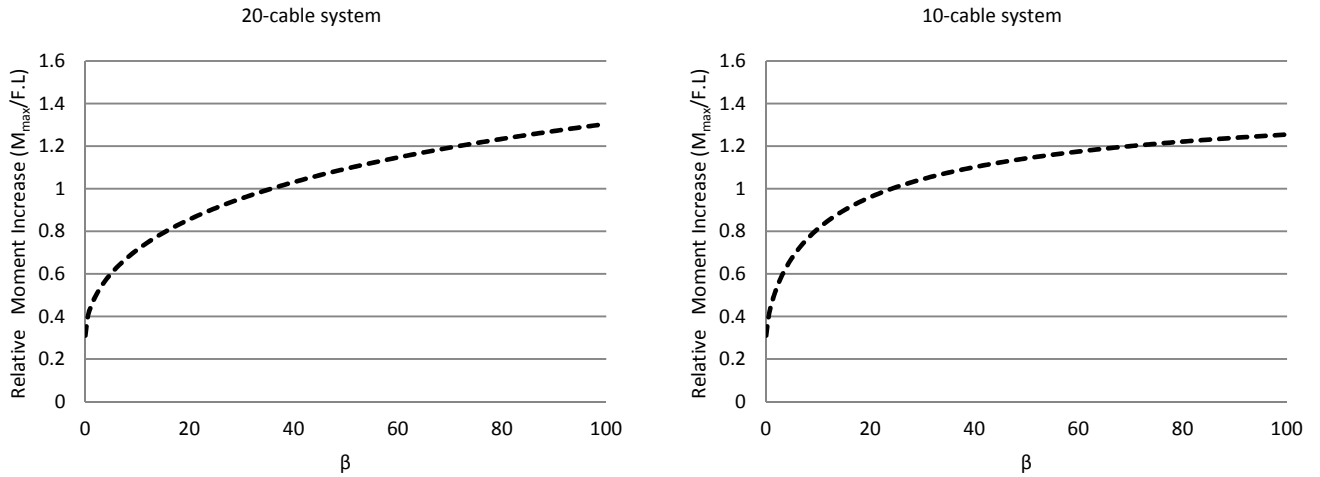


Fig. 4.2 Relative moment increase of the girder in 10 and 20-cable systems

For finding a general equation for the increase of the maximum bending moment on the girder, a step by step method is applied. In the first step, it is assumed that all cables have the same stiffness ($K_1 = K_2 = \dots = K_n$ or $\delta_1 = \delta_2 = \dots = \delta_n = 1$). Then, the system of linear equations is solved for different systems, and the relative moment increase ($M_{max}/F.L$) is calculated as a function of β .

For instance, the results of the calculations of the relative moment increase for four, six, and eight-cable systems are found below ($\delta_i = 1$):

Four-cable system:

$$\frac{M_{max}}{F.L} = \frac{5 + 18\beta}{16 + 24\beta} \quad (4.2)$$

Six-cable system:

$$\frac{M_{max}}{F.L} = \frac{19 + 294\beta + 216\beta^2}{62 + 744\beta + 216\beta^2} \quad (4.3)$$

Eight-cable system:

$$\frac{M_{max}}{F.L} = \frac{71 + 2094\beta + 8748\beta^2 + 2160\beta^3}{232 + 5976\beta + 18288\beta^2 + 1728\beta^3} \quad (4.4)$$

Similar to the previous case, the aforementioned results show that the general form of the maximum bending moment equation is as follows:

$$\frac{M_{max}}{F.L} = \frac{a' + b'\beta + c'\beta^2 + d'\beta^3 + \dots}{a'' + b''\beta + c''\beta^2 + d''\beta^3 + \dots} \quad (4.5)$$

Therefore, the previous form of the approximation function can be used once again. Equation 4.6 shows the general form of the approximation function for the calculation of the maximum bending moment on the girder due to cable failure.

$$\frac{M_{max}}{F.L} = a + \frac{b - a}{1 + \left(\frac{\beta}{c}\right)^d} \quad (4.6)$$

In other words, Equation 4.6 can express the maximum bending moment of the girder due to the cable loss if appropriate parameters (a , b , c , and d) can be found. By using this form of approximation function, the number of unknown coefficients has been reduced to four.

Although the general forms of Equation 4.6 and its corresponding equation in the previous chapter are the same, their representative graphs show two opposite trends. Fig. 4.2 reveals that the maximum bending moment due to the cable loss has an upward trend while the stress increase ratio of the critical cable has a downward trend. Hence, the definitions of parameters a and b are different from their definitions in the previous chapter. Here, parameter a stands for the maximum value of the function, which occurs when $\beta = \infty$. A β -value equal to infinity means that the girder is rigid and all cables have the same displacement. Therefore, for a system including $2n$ cables, parameter a is equal to $(n + 1)/4$. Parameter b stands for the minimum value of the function that occurs when $\beta = 0$. For finding parameter b different systems are investigated. After calculating the bending moment for several systems, the minimum value of the function is found to be close to 0.31 for all systems. For instance, parameter b equals 0.3059 and 0.3061 for six-cable and 30-cable systems, respectively. Therefore, the general form of the approximation function for the first step will be as follows ($\delta_i = 1$):

$$\frac{M_{max}}{F.L} = \left(\frac{n + 1}{4}\right) + \frac{0.31 - \left(\frac{n + 1}{4}\right)}{1 + \left(\frac{\beta}{c}\right)^d} \quad (4.7)$$

For finding the other two parameters, the LSM method is applied. The required information for the LSM method has been provided in the previous chapter. The procedure of calculations used for a data set consisting of x matching points (y_i and f_i) is presented in the following equations:

$$f_i = a + \frac{b - a}{1 + \left(\frac{\beta}{c}\right)^d} \quad (4.8)$$

$$\Delta_i = y_i - f_i = y_i - \left(a + \frac{b - a}{1 + \left(\frac{\beta}{c}\right)^d} \right) \quad (4.9)$$

$$\Delta_i^2 = (y_i - a)^2 + \frac{(b - a)^2}{1 + \left(\frac{\beta}{c}\right)^{2d} + 2\left(\frac{\beta}{c}\right)^d} - \frac{2(b - a)(y_i - a)}{1 + \left(\frac{\beta}{c}\right)^d} \quad (4.10)$$

$$\frac{\partial(\Delta_i^2)}{\partial d} = \frac{-(b - a)^2 \left(2\left(\frac{\beta}{c}\right)^{2d} \text{Ln}\left(\frac{\beta}{c}\right) + 2\left(\frac{\beta}{c}\right)^d \text{Ln}\left(\frac{\beta}{c}\right) \right)}{\left(1 + \left(\frac{\beta}{c}\right)^{2d} + 2\left(\frac{\beta}{c}\right)^d \right)^2} - \frac{-2(b - a)(y_i - a)\left(\frac{\beta}{c}\right)^d \text{Ln}\left(\frac{\beta}{c}\right)}{\left(1 + \left(\frac{\beta}{c}\right)^d \right)^2} \quad (4.11)$$

$$\frac{\partial(\Delta_i^2)}{\partial c} = \frac{(b - a)^2 (2d\beta^{2d}c^{-2d-1} + 2d\beta^d c^{-d-1})}{\left(1 + \left(\frac{\beta}{c}\right)^{2d} + 2\left(\frac{\beta}{c}\right)^d \right)^2} - \frac{2(b - a)(y_i - a)d\beta^d c^{-d-1}}{\left(1 + \left(\frac{\beta}{c}\right)^d \right)^2} \quad (4.12)$$

$$T = \sum_{i=1}^x \Delta_i^2 \quad (4.13)$$

$$\frac{\partial T}{\partial d} = 0 \quad (4.14)$$

$$\frac{\partial T}{\partial c} = 0 \quad (4.15)$$

where y_i and f_i are the exact and approximate maximum bending moment values for different β -values, respectively.

In the first step, Equation 4.14 is solved for different values of parameter c , and corresponding values of parameter d are calculated. In the next step, the calculated values of parameter d are used in Equation 4.15 and corresponding values of parameter c are calculated. There is only one pair of parameter c and parameter d that satisfy both equations.

In Fig. 4.3, the calculations of parameter c and parameter d for a 20-cable system is shown. In Fig. 4.4, parameters c and d for different systems are shown.

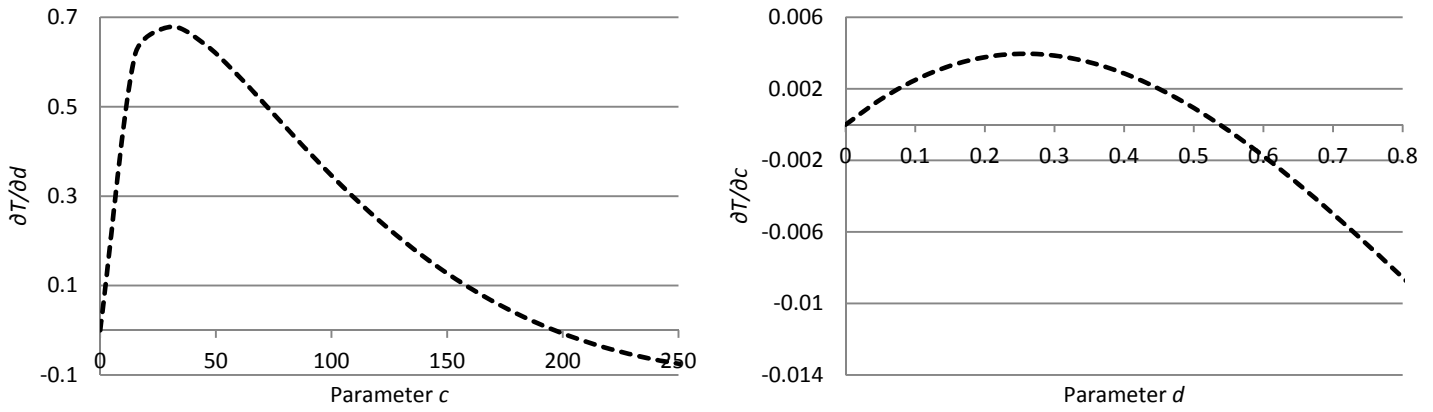


Fig. 4.3 Calculation of parameter c and parameter d for a 20-cable system

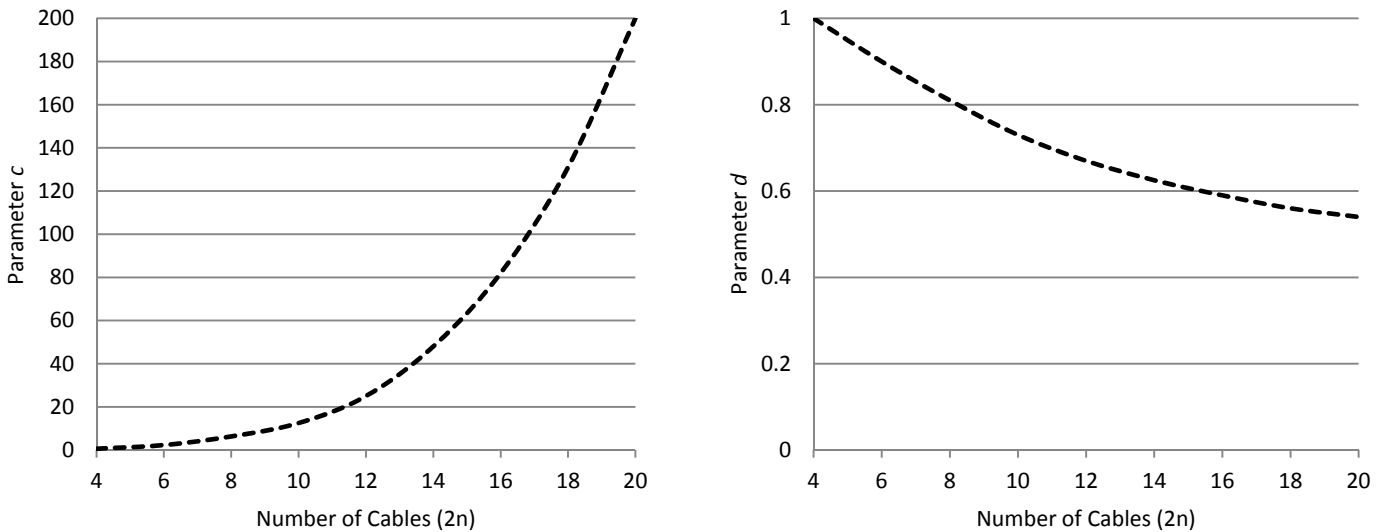


Fig. 4.4 Parameter c and parameter d for different systems

For finding an equation for parameter c and parameter d , the LSM method is used once again. In order to reduce the complexity of the equations and increase their accuracy for larger systems, only systems with more than 16 cables are considered.

As shown in Fig. 4.4, parameter c appears to have a power function trend. Therefore, the general form of parameter c is considered as gx^h , where x is the number of cables ($2n$), and g and h are unknown parameters that should be found using the LSM method. The procedure for the calculation of parameter c , for a data set consisting of x matching points (y_i and f_i), is presented in the following equations:

$$f_i = g(2n)^h \tag{4.16}$$

$$\Delta_i = y_i - f_i = y_i - g(2n)^h \tag{4.17}$$

$$\Delta_i^2 = y_i^2 + g^2(2n)^{2h} - 2y_i g(2n)^h \quad (4.18)$$

$$\frac{\partial(\Delta_i^2)}{\partial g} = 2g(2n)^{2h} - 2y_i(2n)^h \quad (4.19)$$

$$\frac{\partial(\Delta_i^2)}{\partial h} = 2g^2(2n)^{2h} \ln(2n) - 2y_i g(2n)^h \ln(2n) \quad (4.20)$$

$$T = \sum_{i=1}^x \Delta_i^2 \quad (4.21)$$

$$\frac{\partial T}{\partial g} = 0 \quad (4.22)$$

$$\frac{\partial T}{\partial h} = 0 \quad (4.23)$$

The results of the calculation of parameter g and parameter h are depicted in Fig. 4.5. Therefore, parameter c could be expressed as follows:

$$\text{Parameter } c = 0.00125(2n)^4 \quad 2n \geq 16 \quad (4.24)$$

The procedure for the calculation of an equation for parameter d is similar to Equation 4.8 through 4.15. Therefore, it is not mentioned again. Parameter d can be expressed by the following equation:

$$\text{Parameter } d = 0.30 + \frac{1.40}{1 + \left(\frac{2n}{4.70}\right)^{1.1}} \quad 2n \geq 16 \quad (4.25)$$

By calculating parameter c and parameter d , all unknown parameters of the approximation function in the first step are found. Considering the previously mentioned facts, the approximation function could be rewritten for a general system as follows:

$$\frac{M_{max}}{F.L} = \left(\frac{n+1}{4}\right) + \frac{0.31 - \left(\frac{n+1}{4}\right)}{1 + \left(\frac{\beta}{c}\right)^d} \quad , \delta_i = 1 \quad (i = 1 \text{ to } n) \quad (4.26)$$

where parameter c and parameter d should be calculated by Equation 4.24 and Equation 4.25, respectively.

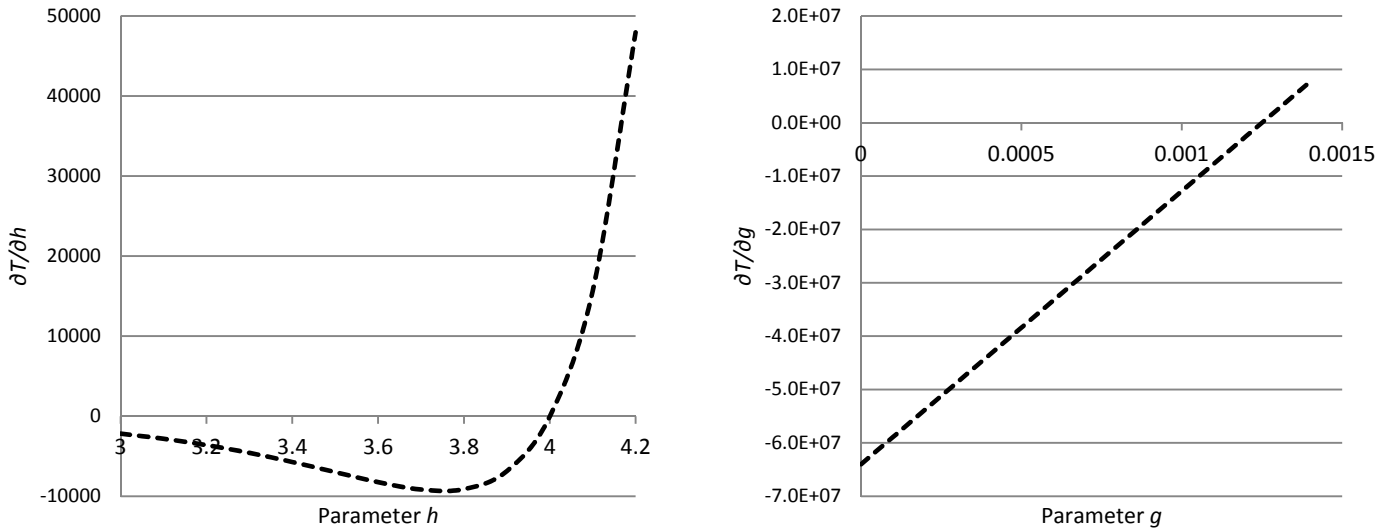


Fig. 4.5 The calculation of parameter g and parameter h

In Fig. 4.6, the exact and approximate values of the relative moment increase for different systems are shown. It is seen that the curves depicted from the approximation function express the exact values of the relative moment increase with good accuracy. Except for small β -values, the error of approximation is less than 5%. Similar to the previous chapter, parameter R-squared (R^2) is used to control the accuracy of the approximation function. In Table 4.1, a summary of the calculations of R-squared for different systems is presented.

Table 4.1 Calculation of R-squared for different systems

	R-squared (R^2)	$\sum_{i=1}^x y_i$	\bar{y}	SS_{tot}	SS_{res}
4-cable system	1	11.81	0.59	1.107	0.0005047
6-cable system	0.999	13.58	0.679	2.3878	0.001507
8-cable system	0.998	14.95	0.747	3.994	0.0074
10-cable system	0.997	16.089	0.804	5.76	0.0166
12-cable system	0.995	16.95	0.847	7.63	0.035
14-cable system	0.994	17.63	0.881	9.64	0.0583
16-cable system	0.994	18.228	0.911	11.707	0.064
18-cable system	0.991	18.75	0.937	13.78	0.126
20-cable system	0.989	19.2	0.96	15.82	0.171

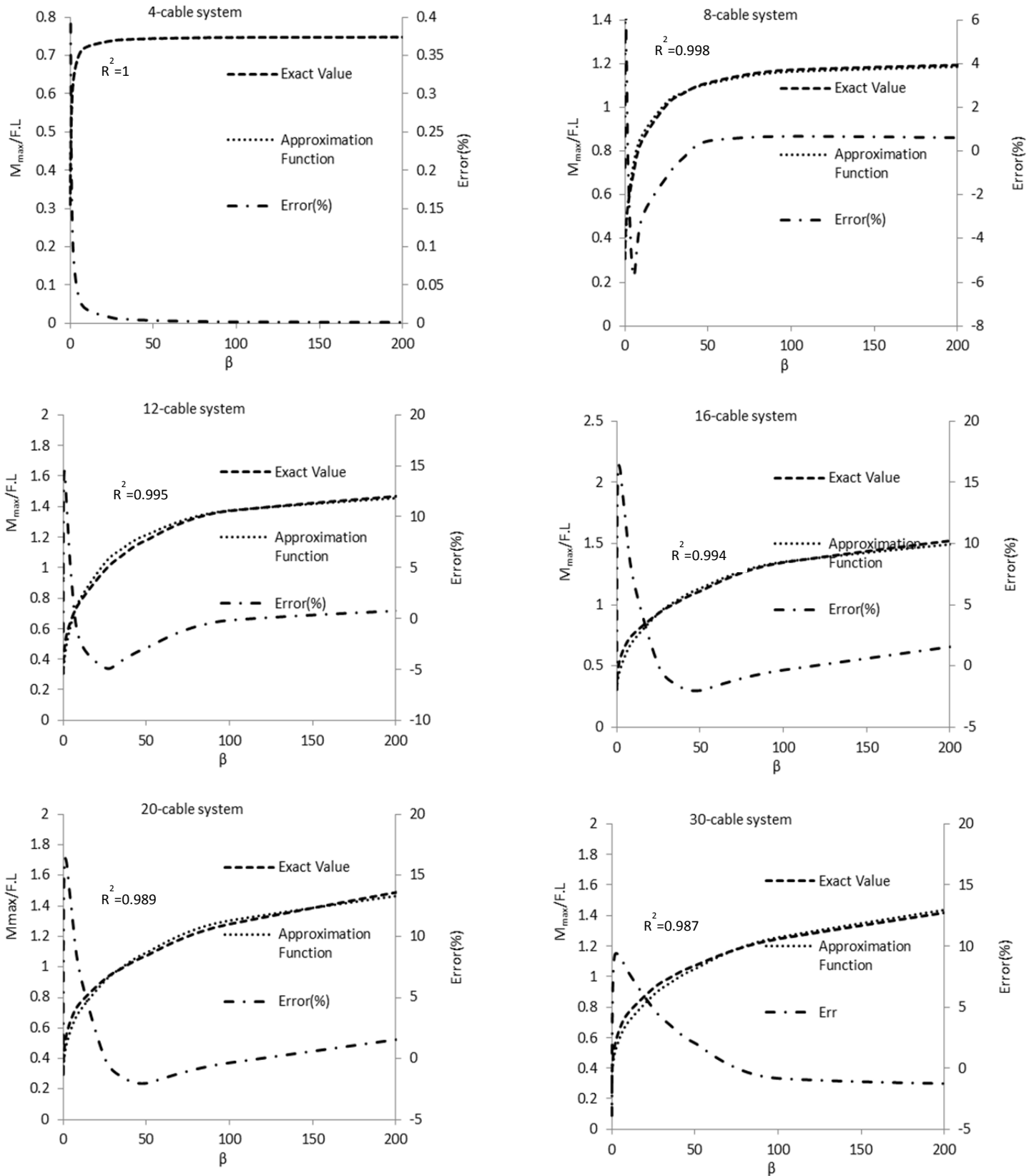


Fig. 4.6 The exact and approximate values of the relative moment increase for different systems

In the next step, the stiffness of all cables is altered. Therefore, in this step, each cable has a unique axial stiffness. As mentioned before, parameter a stands for the maximum value of the function, which occurs when $\beta = \infty$. Therefore, parameter a could be easily calculated as follows:

$$a = \frac{n\delta_n + (n-1)\delta_{n-1} + \dots + \delta_1}{2 \sum_{i=1}^n \delta_i}, \quad i = 1 \text{ to } n \quad (4.27)$$

Parameter b is the minimum value of the function, which occurs when β is equal to zero. Hence, δ has no effect on parameter b . For evaluating parameter c and parameter d for the current configuration, different systems are investigated. The results show that changing the stiffness of the cables has minimal effects on parameter d and, consequently, on the final results. In fact, parameter d is mainly influenced by the number of cables, as well as their stiffness. However, the effect of the cable stiffness is fairly insignificant. Furthermore, the main target of this study is to present a practical and simple approximation function. Hence, in order to keep the approximation function as simple as possible, the effect of the cable stiffness on parameter d is ignored.

In contrast to parameter d , changing the stiffness of the cables has a considerable effect on parameter c . In addition, the results show that parameter c is also influenced by the configuration of the cables. Therefore, a unique equation for parameter c in each configuration should be determined. However, it is impractical to consider the stiffness of all cables separately. Investigation of the different systems shows that considering the average of the stiffness of the cables in the approximation function leads to an acceptable accuracy. Therefore, In order to overcome this problem, the average of the stiffness of the cables is considered as the influential factor. Hence, the general form of parameter c is considered as $g\bar{\delta}x^h$, where $\bar{\delta}$ is the average of δ_1 to δ_n , x is the number of cables ($2n$), and g and h are unknown parameters that should be found using the LSM method. The procedure for the calculation of parameter c is similar to the previous step and the results for two different cable-configurations are ($2n \geq 16$):

$$\text{Parameter } c = 0.00125\bar{\delta}(2n)^4 \quad \delta_1 \leq \delta_2 \dots \leq \delta_n \quad \text{system (a)} \quad (4.28 a)$$

$$\text{Parameter } c = 0.001125\bar{\delta}(2n)^4 \quad \delta_1 > \delta_2 > \dots > \delta_n \quad \text{system (b)} \quad (4.28 b)$$

To summarize the previous steps, a general form of the approximation function considering a unique axial stiffness in each cable could be derived as follows:

$$\frac{M_{max}}{F.L} = a + \frac{0.31 - a}{1 + \left(\frac{\beta}{c}\right)^d} \quad (4.29)$$

where parameter a and parameter d should be calculated by Equation 4.27 and Equation 4.25, respectively. Parameter c should be calculated by Equation (4.28 a) or Equation (4.28 b), according to the configuration of the cables.

As the last step, to check the accuracy of the presented approximation function, three different systems, each with two different cable-configurations, are investigated (see Fig. 4.7). In Table 4.2, the structural specifications of each system are presented. Similar to the previous results, with an exception for small β -values, the error of approximation is less than 5%. The results also show that by increasing the ratio of the bending stiffness of the girder to the axial stiffness of the cables, the maximum bending moment due to the cable rupture increases.

The exact values of the relative moment increase for 12 and 16-cable systems are calculated by solving the corresponding system of linear equations, and for 22-cable systems, the exact values are calculated using the software package SAP2000. In doing so, the analytical approach that was used has been checked once again.

Table 4.2 Structural specifications of the investigated systems

Cable-Stiffness	12-cable system(a)	12-cable system(b)	16-cable system(a)	16-cable system(b)	22-cable system(a)	22-cable system(b)
K_1	K	3K	K	4.5K	K	2K
K_2	1.4K	2.6K	1.5K	4K	1.1K	1.9K
K_3	1.8K	2.2K	2K	3.5K	1.2K	1.8K
K_4	2.2K	1.8K	2.5K	3K	1.3K	1.7K
K_5	2.6K	1.4K	3K	2.5K	1.4k	1.6K
K_6	3K	K	3.5K	2K	1.5K	1.5k
K_7	-	-	4K	1.5K	1.6K	1.4K
K_8	-	-	4.5K	K	1.7k	1.3K
K_9	-	-	-	-	1.8K	1.2K
K_{10}	-	-	-	-	1.9K	1.1K
K_{11}	-	-	-	-	2K	K

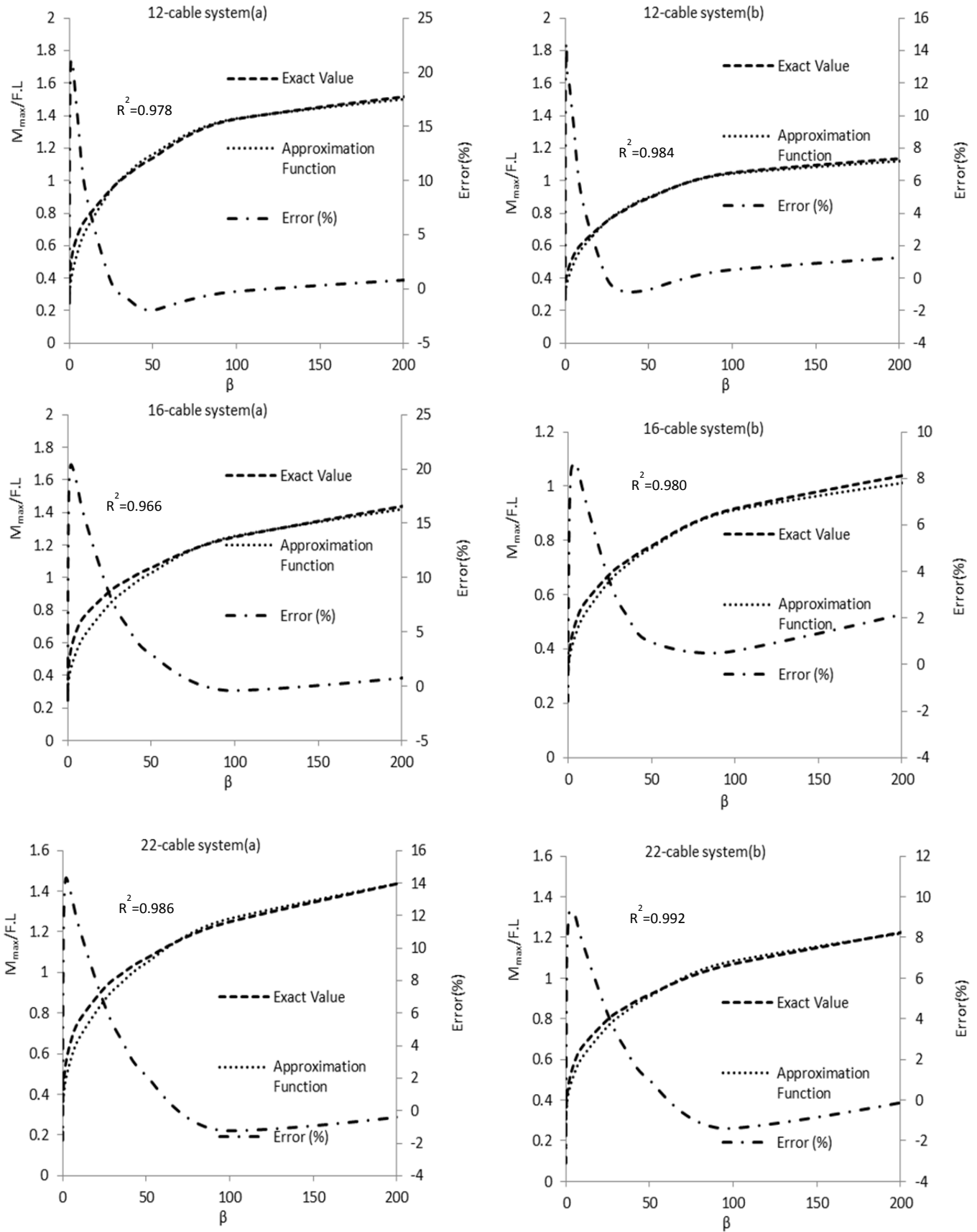


Fig. 4.7 The exact and approximate values of the relative moment increase for different systems

Chapter 5

Optimum Design of Long-Span Cable-Supported Bridges

Considering Cable-Loss Scenarios

5.1 Introduction

The target of this chapter is to use a practical method for the optimization of cable distance in long-span cable-supported bridges using the developed robustness index. The proposed optimization method minimizes the cost of bridge construction and guarantees a certain level of robustness. For this purpose, the reserve-based measure of robustness is employed to ensure that in possible cable-loss scenarios a zipper-type collapse does not occur. The reserve-based robustness index, developed in chapter three, considers the redistribution of forces after the failure of structural elements. For finding the optimum distance of cables, a simplified model similar to the previous chapters is considered. Different cable-loss scenarios are considered in the design process and the dynamic effect of cable failure is taken into account. The critical design load of the cables and the maximum bending moment acting on the girder after the cable rupture are calculated and incorporated into the structural design. The effect of other influential factors, such as the bending stiffness of the girder and the axial stiffness of the cables, on the optimum design of the system is also investigated.

Since a literature review regarding the optimum design of cable-supported bridges is not provided in chapter two, here, a brief review of the related studies is provided. In the family of bridge systems, the cable-supported bridges are distinguished by their ability to overcome large spans (Georgakis and Gimsing 2013). They are widely used because of their aesthetic typologies and their economic efficiency. As a result of constant improvements in design and construction technology, the number of cable-supported bridges and their span-length has increased rapidly over the past decades. Today, Akashi Kaikyo Bridge in Japan, with a main span of 1991 m, has the longest main span. However, the main span of Messina Strait Bridge in Italy is designed for 3300 m, which is 60% longer than the current longest bridge in the world. This shows the speed at which design and construction technology improves. Several studies have been conducted concerning the optimum design of cable-stayed and suspension bridges (Cid et al. 2018, Lonetti and Pascuzzo 2014, Cao et al. 2017, and Fabbrocino et al. 2017). However, most of the studies are related to the cable-stayed bridges and there is a lack of sufficient studies on the optimum design of suspension bridges.

Cid et al. (2018) proposed a strategy to optimize the cable system of multi-span cable-stayed bridges with crossing stay cables. Their approach minimizes the steel volume in the cables by optimizing the number of cables, their anchorage positions, and prestressing forces.

In another study, Cao et al. (2017) used a computationally efficient optimal design approach for suspension bridges. Their result showed that the parameters characterizing the size and geometry of the pylon and the main cable are very sensitive to the price ratio, and the most economical approach to strengthen the lateral stiffness of the pylon is to increase the stiffness of the cross beam.

Song et al. (2018) proposed an optimization method to determine the cable pre-tension forces in long-span cable-stayed bridges considering the counterweight. Their results showed that in an asymmetric bridge, considering the counterweight reduces the maximum bending moment of the girder and the tower, and consequently, reduces the construction cost.

Lonetti and Pascuzzo (2014) presented a design methodology for the optimum design of hybrid cable-stayed suspension (HCS) bridges.

Cable-supported bridges are usually statically indeterminate structures, and their structural behavior is greatly influenced by cable forces as well as the vibration of the girder. However, the accurate calculation of cable forces and girder behavior needs advanced analysis techniques and the use of modern computers. In the absence of the mentioned tools in the past, engineers tried to use as few cables as possible to make structural analysis easier. Therefore, the distance between cables was relatively long and the maximum span length was limited.

As computer technology became cheaper and more available, structural analysis became easier. Hence, there has been a trend to design longer bridges with shorter cable distances and, in the process, achieve a more economical design. In Fig. 5.1, the development of cable distance at the deck level in cable-stayed bridges during the time is shown.

The investigation of the development of cable distance during the past decades shows that structural engineers generally believe that using a shorter cable distance leads to a more economical design. Although using shorter cable distance usually leads to a more economical design, it also increases the vulnerability of the cables against abnormal events. Stay cables and hangers are easily accessible, and therefore, exposed to accident-related or malicious actions (see Fig. 5.2). Using a shorter cable distance reduces the cable cross-section and increases the risk of cable failure due to abnormal events. A smaller cable cross-section means that cable rupture can occur from a smaller car accident or weaker explosion. This increases the likelihood of cable failure during the lifetime of the bridge. In addition, in the case of the

occurrence of abnormal events, the number of affected cables increases, which in turn, increases the vulnerability of the whole structural system.

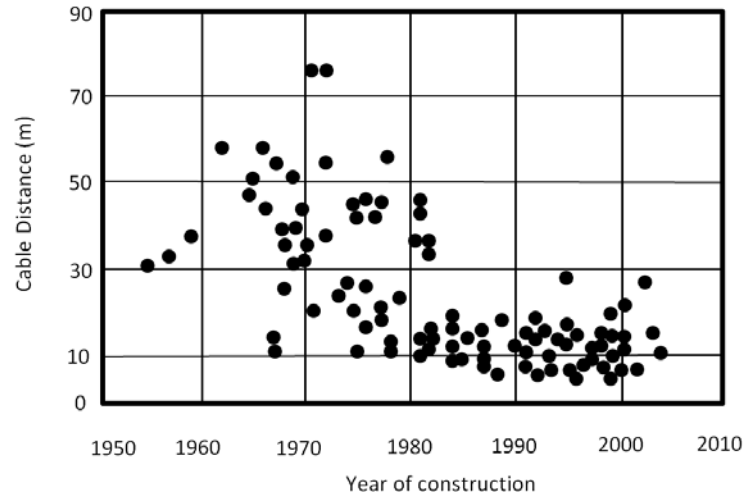


Fig. 5.1 The development of cable distance at the deck level in cable-stayed bridges during the time, based on Svensson (2012)

Current guidelines do not discuss the consideration of the failure of several cables. According to the PTI (2012), the sudden loss of any one cable must not lead to the rupture of the entire structure. As mentioned, in modern bridges, the distance between two adjacent cables is much shorter than in older bridges. Therefore, in the case of car accidents or explosions on new bridges, the rupture of more than one cable is more likely to happen. Accordingly, O'Donovan et al. (2003) considered the rupture of all cables within a 10 m range in a particular bridge project.



Fig.5.2 Accessibility to cables of cable-supported bridges-Starossek (2008)

Considering the mentioned facts, the assumed number of failed cables in a cable-loss scenario should be related to the cable distance. Hence, in this study, cable-loss scenarios are defined based on cable distances.

The target is to use a practical method for the optimization of cable distance in cable-supported bridges considering different cable-loss scenarios. For this purpose, a simplified bridge model is considered and the optimal cable distance is investigated.

Two cable-loss scenarios are considered. In the first one, the initial failure of all cables within a 5 m range is considered. In the second one, it is assumed that all cables within a 10 m range fail. All systems are designed in a way that they have a positive robustness index to ensure that they are safe against progressive collapse.

5.2 Structural specifications and loading conditions

In this study, the investigation of the optimum cable distance is performed based on 50 and 100-cable systems with three different cable lengths (30 m, 60 m, and 90 m). It is assumed that the width of the bridge is 12 m. The girder has a box cross-section and is made of structural steel S355. The elastic modulus and the ultimate tensile strength of the cables are $160 \frac{\text{kN}}{\text{mm}^2}$ and $1570 \frac{\text{N}}{\text{mm}^2}$, respectively.

For the primary design of the system, only vertical loads (dead loads and traffic loads) are considered. For the calculation of traffic loads, Eurocode EN 1991-2 (2006) is used. Accordingly, four different load models (*LM1* to *LM4*) are considered. For this purpose, the carriageway should be divided into notional lanes, generally three meters wide. In this study, the width of the bridge is assumed to be 12 m; hence there are four notional lanes. Load model *LM1* includes concentrated and uniformly distributed loads and reproduces traffic effects to be taken into account for global and local verifications. Characteristic values of the *LM1* are presented in Table 5.1.

Load model *LM2* consists of a single axle load of 400 kN, which should be applied on a rectangular tire area equal to 0.35×0.6 m, and is intended only for local verifications. Load models *LM3* and *LM4* are for special vehicles and crowd loading, respectively. They should be applied only when expressly required. In general, the use of load model *LM1* is safe-sided for road bridges with loaded lengths over 200 m (Chen and Duan 2014).

Table 5.1 Loading conditions corresponding to LMI

Position	Tandem system-Axle load (kN)	Uniformly distributed load(kN/m ²)
Notional lane N. 1	300	9
Notional lane N. 2	200	2.5
Notional lane N. 3	100	2.5
Other lanes	0	2.5
Remaining area	0	2.5

First, the intact structure is designed based on the normal loading conditions, as mentioned in Table 5.1. Then, the middle cable(s) is removed and the traffic load according to abnormal events is calculated. In the load case corresponding to cable-loss scenarios, the live load is reduced to 75% based on PTI recommendations.

The dead load includes the weights of the cables, the girder, the floor system, and the other parts of the bridge itself. The calculation of the weight of the cables and the girder is performed using an iterative process and the exact values have been taken into account. The floor system is assumed to be 0.20 m asphalt concrete. In addition, the weight of other parts of the bridge is considered as $6 \frac{\text{kN}}{\text{m}}$. The calculation of the applied load is mentioned below.

$$\text{Distributed load} = 3(9+2.5+2.5+2.5) = 49.5 \frac{\text{kN}}{\text{m}}$$

$$\text{Concentrated load (double axel)} = 300+200+100+0 = 600 \text{ kN}$$

$$\text{Floor system and other parts of the bridge} = 66 \frac{\text{kN}}{\text{m}}$$

As mentioned, the traffic load consists of distributed loads and concentrated loads. Concentrated loads must be applied on two axles with a distance of 1.2 m. Therefore, they must be applied at the most unfavorable location to account for the most critical situation. For this purpose, two situations are considered. First, two concentrated loads are applied with the same distance from the failed cable. In the next scenario, the first concentrated load is applied at the location of the failed cable and the second load is applied with a distance of 1.2 m. The comparison of these two situations gives us the critical location of the concentrated loads. When the initial failure of two cables is assumed, two extra situations must be considered. In the first situation, two loads are applied between failed cables and at the same distance from the center of the system. In the next situation, the first load should be applied at the center of the system and the second load should be applied at a distance of 1.2 m. The calculation of the

critical position of the concentrated loads for the systems with three failed cables follows the same rule.

The critical design load of the cables and the maximum bending moment acting on the girder after the cable failure are calculated and incorporated into the bridge design. A DAF of 2 is applied to account for the dynamic nature of cable failure.

In order to calculate the robustness index in the first step, the initial failure of all cables within a 5 m range is considered. It means that when the cable distance is larger than 5 m, only the initial failure of one cable is considered. When the cable distance is between 5 m and 2.5 m, the initial failure of two cables is considered, and for the system with a cable distance of 2.5 m, the initial failure of three cables is considered.

5.3 Estimation of the construction cost

The main target of the optimization process is to minimize the construction cost. Hence, an accurate estimation of the construction cost plays an essential role in this study. Although the considered bridge model is conceptual and some differences between an accurate bridge model and the simplified model are unavoidable, the efforts are made to estimate the construction cost as accurate as possible. For this purpose, the cost of the girder is calculated based on its exact weight plus the weight of other parts of the girder, such as connections and stiffeners. In order to estimate the weight of stiffeners, some actual cable-supported bridges are examined. The result showed that in girders with box cross-sections, the weight of stiffeners is almost 0.60% of the girder weight. Therefore, the calculated weight of the girder has been increased by a coefficient equal to 1.8 to account for the weight of stiffeners and other parts of the girder. In addition, the price of welding, coloring, and transportation must be estimated. After some discussion with experienced engineers, the price of 3500 Euro per ton is chosen for the estimation of the construction cost of the girder.

The estimation of the cable cost is more complex. In order to make a realistic estimation of the cable cost, a cost offer from a cabling factory is considered. A summary of the price for different cables is reported in Table 5.2. It should be noted that the mentioned price includes transportation costs.

As can be realized from Table 5.2, the price of cable depends on a variety of factors such as cable type, cable diameter and cable length. In fact, as the cable length and cable diameter increase, its cost per unit weight decreases. In addition, the installation cost of each cable should be taken into account. For this purpose, 4 percent of the cable price is considered as the installation cost for each cable. As the cable distance decreases, the number of cables, and consequently, the installation cost increases. Table 5.2 shows that there is no straightforward

relationship among the cable length, cable diameter and cable price. Therefore, the same cable lengths as offered in the price list of the cabling factory are used. By doing so, the effect of the cable length on the cable price is automatically considered, and the only influential factor on the final price is the cable diameter. In the following, the estimation of the cable prices based on cable cross-section for different cable lengths is derived.

$$\text{Cable price (€) for a 30 m cable} = 1059 + 2A$$

$$\text{Cable price (€) for a 60 m cable} = 1208 + 3.27A$$

$$\text{Cable price (€) for a 90 m cable} = 1308 + 4.55A$$

where A is the cross-sectional area of the cable (mm^2). A comparison of the exact and estimated cable cost is presented in Fig. 5.3.

5.4 Finding the optimum cable distance

In order to find the optimum cable distances, two cable systems with three cable lengths (h) are investigated. For this purpose, 50 and 100-cable systems with cable lengths of 30, 60, and 90 m are investigated. By doing so, the effect of the cable length and the stiffness ratio of the system (β) on the optimum cable distance can be evaluated. In the first part, the initial failure of all cables within a 5 m range is considered. The selected cable distances cover a range from 30 to 2.5 m. The number of failed cables in each system depends on the cable distance.

Table 5.2 The actual price of different cables

No.	Length (m)	Diameter (mm)	F_y (kN)	Total Price (€)	Price per Kg (€/Kg)	price per meter (€/m)
1	30	21	245	1875	23.00	62.50
2	60	21	245	2590	15.88	43.17
3	90	21	245	3285	13.43	36.50
4	30	31	555	2520	14.18	84.00
5	60	31	555	3545	9.98	59.08
6	90	31	555	4575	8.58	50.83
7	30	40	921	3465	11.71	115.50
8	60	40	921	4990	8.44	83.17
9	90	40	921	6515	7.34	72.39
10	30	60	2176	6790	10.20	226.33
11	60	60	2176	10560	7.93	176.00
12	90	60	2176	14340	7.18	159.33

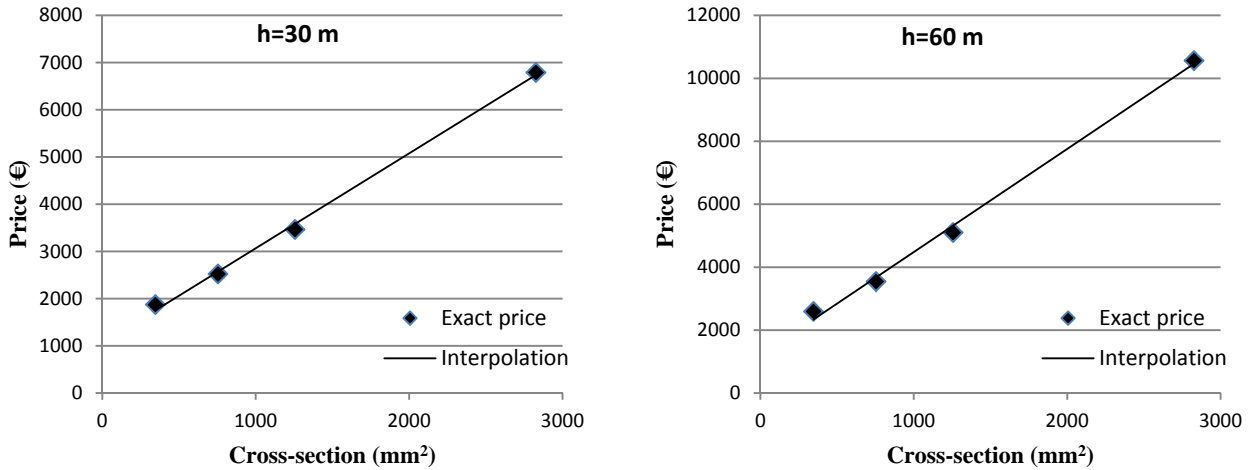


Fig. 5.3 The comparison of the exact cable price and the proposed approximate price

All systems are designed to survive the loads corresponding to cable-loss scenarios. Therefore, the robustness index of all designed systems is a positive value, which indicates the robustness of the system. Then, the construction costs of the designed systems are calculated based on the mentioned assumptions in the previous section. The prices of the girder and cables are calculated separately. Then, the total construction cost is calculated by summing these two values. All calculated costs are calibrated for a unit length of the bridge. In Fig. 5.4, the girder cost, the cable cost, and the total construction cost of a 50-cable system with a cable length of 30 m are demonstrated.

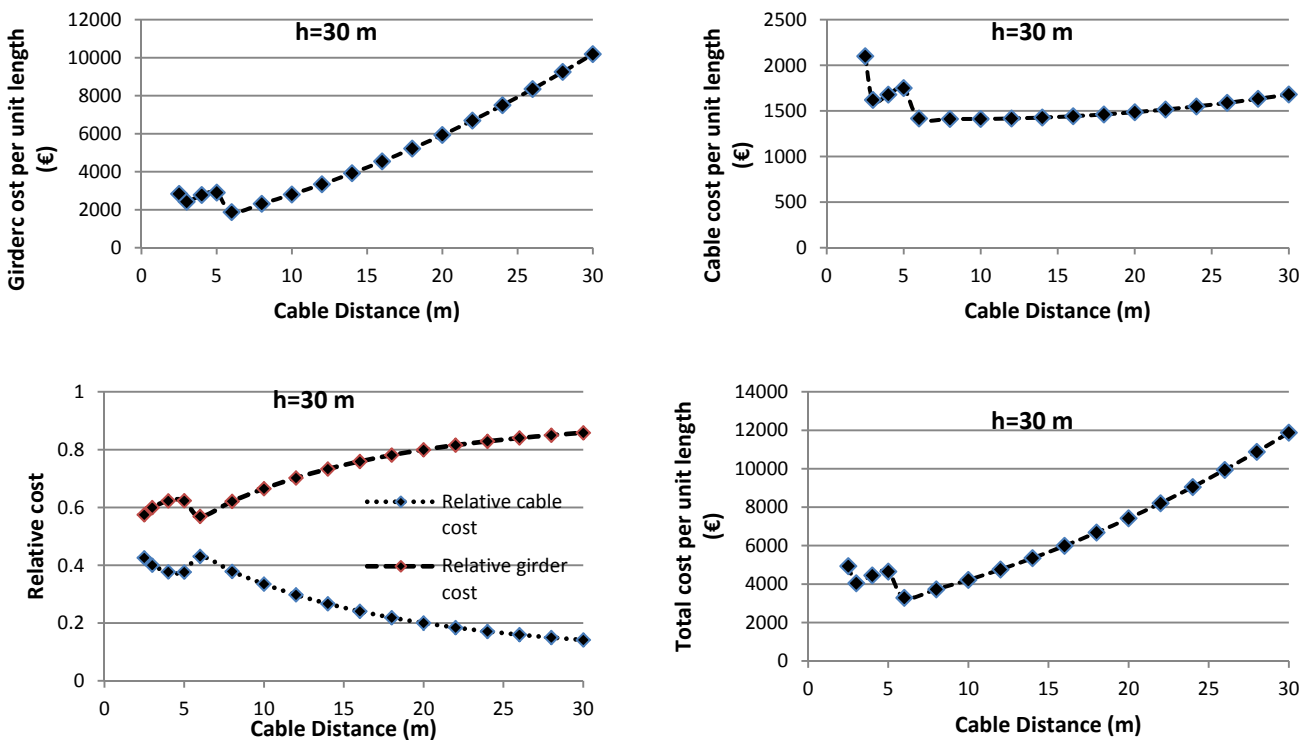


Fig. 5.4 Construction cost of a 50-cable system, h=30m

As can be seen, as the cable distance decreases, the total construction cost decreases. The decrease in the cost continues until the cable distance becomes shorter than 5 m. At this point, the initial failure of two cables is considered. Therefore, a sharp increase in the construction cost occurs. For systems with the cable distance of 5, 4, and 3 m, the initial failure of two cables is considered. Hence, the total cost of systems with cable distances of 4 and 3 m are slightly lower than that of the system with a cable distance of 5 m. When the cable distance is equal to 2.5 m, the initial failure of three adjacent cables must be considered. Therefore, a sharp increase in the construction cost occurs again at this point. The comparison of the girder cost and the total construction cost of the system shows that the total cost is mainly influenced by the girder cost rather than the cable cost. Investigation of the cable cost shows a very sharp increase after the consideration of the failure of two and three cables. As mentioned, in this study, it is assumed that all cables are the same. In fact, all cables are designed based on the critical load of the critical cable. Therefore, all cables can tolerate the redistributed load of the failed cable(s) in a cable loss scenario regardless of the location of the cable failure. When the cable distance is larger than 5 m, all cables just need to tolerate the additional load of one cable. However, when the cable distance is 2.5 m, all cables must be designed to tolerate the additional load of three failed cables. This is the reason for the very sharp increase in the cost of cables.

The results also show that as the cable distance decreases, the ratio of the cable cost to the total cost of the bridge increases. The ratio of the cable cost to the total cost increases from 15% to almost 44% when the cable distance decreases from 30 m to 2.5 m.

In Fig. 5.5 and Fig. 5.6, the girder cost, the cable cost, and the total construction cost of a 50-cable system with cable lengths of 60 and 90 m are demonstrated.

The trends of the cost alterations in the other two systems are basically the same as the previous system. The total cost has two sharp changes when the number of the assumed failed cables increases. As the cable length increases, the ratio of the cable cost to the total construction cost increases. For the system with a cable length of 60 m, the ratio of the cable cost to the total cost increases from 18% to almost 51% for cable distances of 30 and 2.5 m, respectively. This ratio for the system with a cable length of 90 m increases from 22% to almost 52%.

The other interesting point about the cost of cables is its relationship with the cable length. The comparison of the cable cost between systems with cable lengths of 60 m and 30 m shows that the cable cost of the longer system is, on average, 1.5 times more than the cable cost of the shorter system. A similar comparison between systems with cable lengths of 90 m and 30 m shows that the cable cost of the longer system is, on average, 2.15 times more than

that of the shorter system. It means that the increase in the cable cost is lower than our initial expectation. In fact, the cable length of the second system is two times that of the first system. Therefore, the cable cost of the second system might be expected to be around two times of the first system. The reason is that as the cable length increases, the stiffness ratio of the system, β , increases. As shown in chapter three, in systems with larger β values, the cable adjacent to the failed cable receives a smaller proportion of the redistributed load. It means that the critical cable can be designed for a smaller load. Consequently, the cable cross-section becomes smaller. In other words, the increase of the cable length leads to the decrease of the cable cross-section. Therefore, the relationship between the cable cost and cable length is not simply linear. It should be noted that the relationship between the cable length and β is not linear either. This is because changing the cable length changes the girder cross-section, which means that the axial stiffness of the cable and the bending stiffness of the girder are interdependent parameters. In fact, the comparison of two similar systems with different cable lengths shows that cable failure produces a larger bending moment in the system with longer cables. As shown in chapter four, in systems with larger β values, cable failure produces a larger bending moment on the girder.

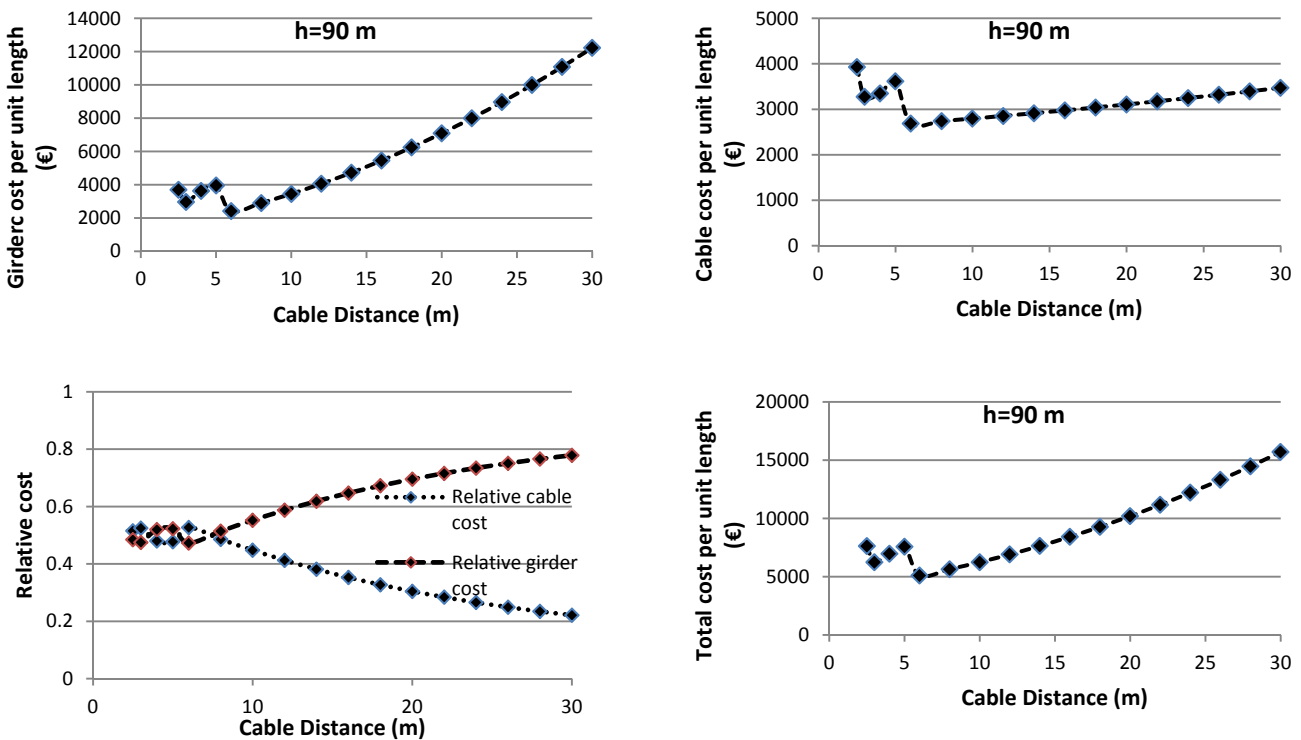


Fig. 5.5 Construction cost of a 50-cable system, $h=90\text{ m}$

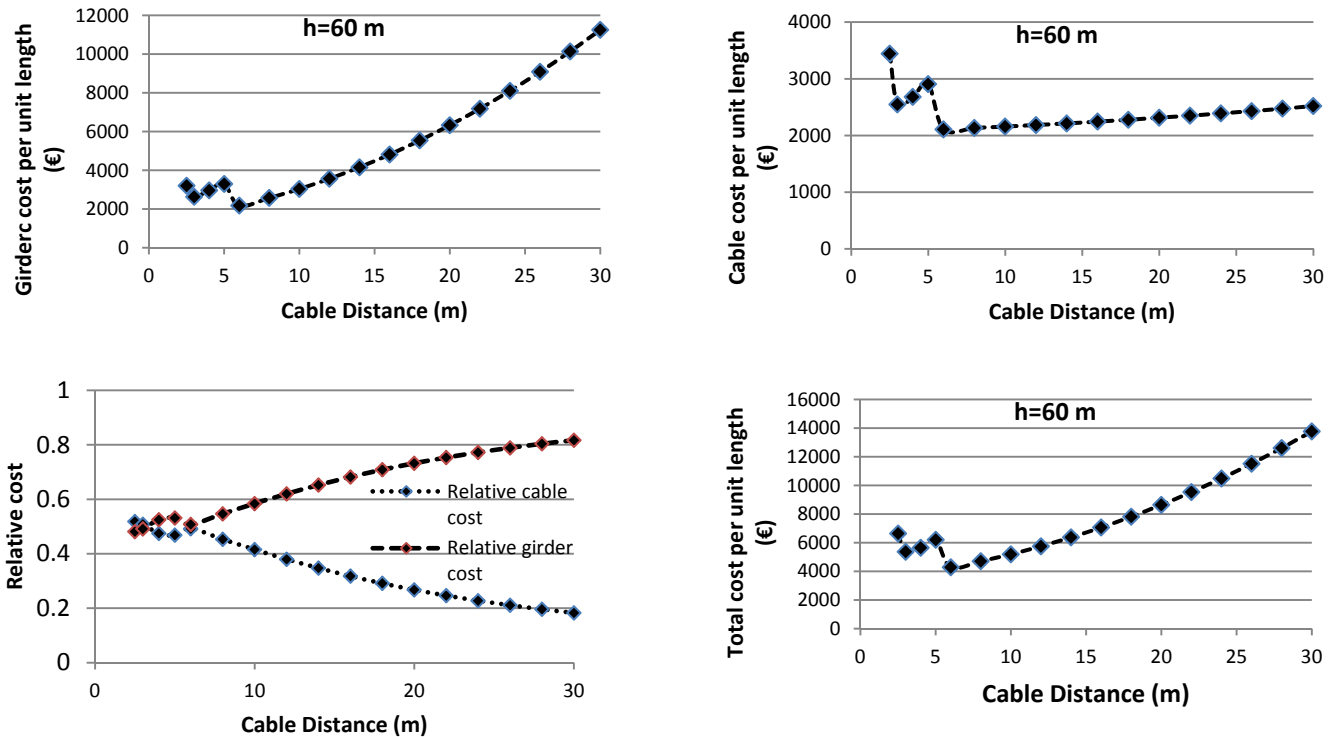


Fig. 5.6 Construction cost of a 50-cable system, $h=60$ m

In Fig. 5.7, the relationships between β and cable distance, as well as the relationship between β and the total cost for two systems, are demonstrated. It can be seen that as the cable distance decreases, β increases very fast. Larger β -value means that the girder is relatively rigid, and in the case of the cable failure, the load of the failed cable can be distributed more evenly among other cables, which could make the design of cables more economical. The relationship between β and the total cost also shows an obvious trend. As β increases, the total cost of the systems with the same number of failed cables decreases. However, this trend changes when the number of failed cables increases.

In this study, the optimum design of 50-cable and 100-cable systems is investigated. The comparison of the 50-cable and 100-cable systems shows identical results. Hence, only the results corresponding to the 50-cable system are mentioned. In fact, in order to minimize the effects of the assumed boundary conditions on the critical cable, both systems are selected to be large enough. In addition, the critical section of the girder and the failed cables are at the center of the system. Therefore, the differences between these two systems are extremely small. In the next section, the optimum design of a 50-cable system is investigated considering the initial failure of all cables within a range of 10 m, as suggested by O'Donovan et al. (2003). By doing so, the effect of these two assumptions on the optimum cable distance can be investigated.

In Fig. 5.8, the girder cost, the cable cost, and the total construction cost of a 50-cable system with a cable length of 60 m is demonstrated. As can be seen, the general trend of the cost variations is similar to the previous case. As the cable distance decreases, a reduction in the construction cost occurs. The cost reduction continues until the cable distance becomes shorter than 10 m. At this point, based on our first assumption, the initial failure of two cables should be considered. Therefore, a sharp increase in the cost of the girder and cables, and consequently, in the total cost appears. The increase of the construction cost, in this case, is sharper than that of in the previous case. An increase in the construction cost occurs again when the cable distance becomes shorter than 5 m because of the consideration of three failed cables.

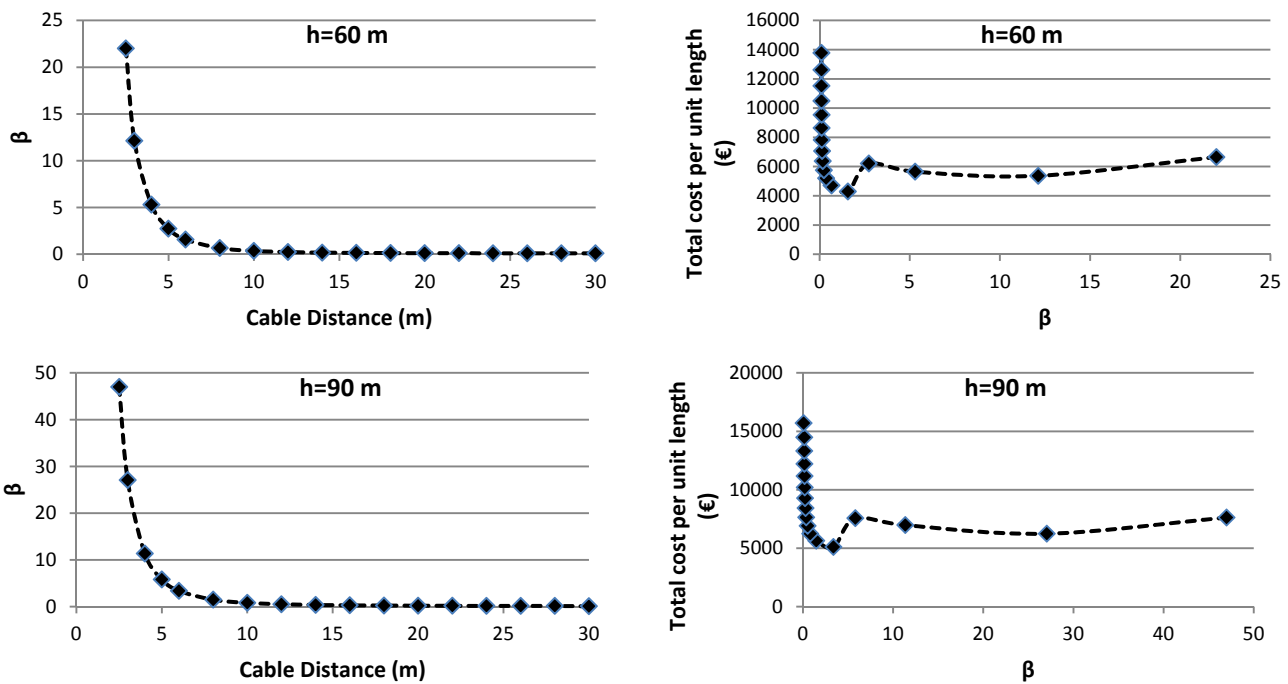


Fig. 5.7 The relationship between β and the cable distance as well as the relationship between β and the construction cost

Finding the optimum cable distance in the assumed cable-loss scenarios showed that the optimum cable distance fundamentally depends on the assumed number of failed cables. In other words, the optimum cable distance in each case is 5 m or 10 m, respectively.

5.5 Summary and discussion

With the availability of powerful structural analysis software and advanced construction technology, there is an increasing trend to build cable-supported bridges with longer spans and shorter cable distances. Although using a shorter cable distance usually leads to a more economical design, it also increases the vulnerability of the structural system in case of

accident-related or malicious actions. Stay cables and hangers are easily accessible and, therefore, exposed to accident-related or malicious actions. Using a shorter cable distance reduces the cable cross-section and increases the risk of cable failure. A smaller cable cross-section means that cable rupture can occur from a smaller car accident or weaker explosion. This increases the likelihood of cable failure during the lifetime of the bridge. In addition, in the case of abnormal events, the number of influenced cables increases. Current guidelines do not discuss the consideration of the failure of several cables. However, considering the mentioned facts, and as recently suggested in the literature, the assumed number of failed cables should be related to the cable distance. In this study, two cable-loss scenarios are defined. In the first one, the initial failure of all cables within a 5 m range is considered. In the second one, it is assumed that all cables within a 10 m range are failed. The results show that the optimum cable distance depends essentially on the assumed cable-loss scenario. As the cable distance decreases, the construction cost decreases. This cost reduction continues until the cable distance becomes shorter than 5 or 10 m corresponding to each case. At this point, a sharp increase in the construction cost occurs, provided the design takes into account the likelihood of multiple cable failure as suggested here. In other words, the optimum cable distances in the investigated cable-loss scenarios are 5 and 10 m, respectively. More generally, if we choose to consider the initial failure of all cables within a range of x meters, then, the optimum cable distance is equal to x . However, stipulating the range x needs more comprehensive studies based on statistical data and risk analysis. The determination of this range is not within the scope of this study. It should be determined by guidelines or in a project-based procedure.

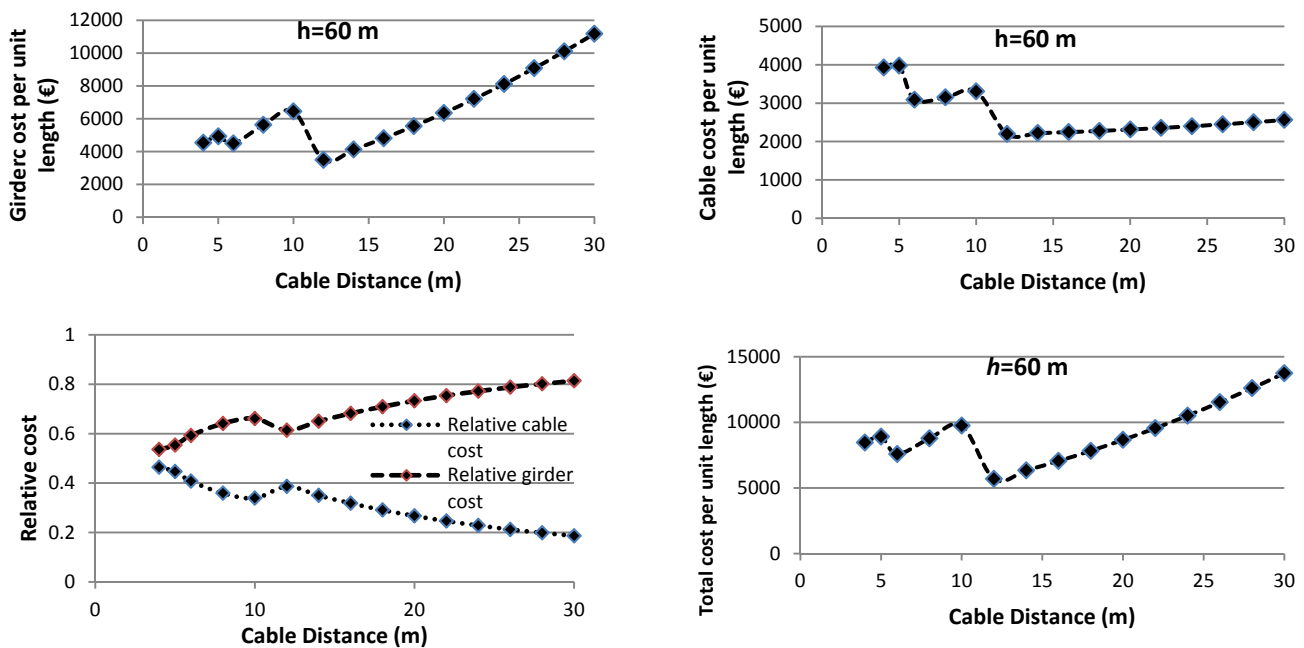


Fig. 5.8 Construction cost of a 50-cable system, $h=60$ m

Chapter 6

Conclusions and Recommendations

All types of structural systems may experience abnormal loads in their lifetime. Abnormal loads are loads other than ordinary design loads (dead, live, wind, seismic, etc.). In other words, abnormal loads can be defined as low-probability loads, which might cause high consequences. Such extreme loads can cause local damage. If a large part of the structure collapse because of local damage, the term progressive collapse comes in mind.

Progressive collapse can be defined as the spread of an initial local failure from element to element, eventually resulting in the collapse of an entire structure or a disproportionately large part of it (ASCE 2002). There are different types of progressive collapse with regard to the mechanism of collapse propagation. In other words, different kinds of structures respond differently to local damages and are susceptible to a different mechanism of collapse.

Parallel load-bearing systems are structural systems with load-bearing members that are similar in type and function and constitute alternative load paths. Cable-supported bridges are examples of such a structural system. Parallel load-bearing systems are susceptible to zipper-type collapse. In the case of the failure of one of the parallel load-bearing elements (cables), the load carried by the failed member must be redistributed to the remaining structure. In this situation, the member adjacent to the failed member receives most of the redistributed load and becomes the critical member. If this member cannot tolerate the redistributed load, the collapse will progress to the subsequent members and, possibly, the entire structure. Hence, because of the vital role of the critical member in the robustness of the structural system, the focus of this study is mostly on this member.

In this study, a parallel-load bearing system is considered as a conceptual model of long-span cable-supported bridges. A simplified model is intentionally selected to make the analytical approach easier. Hence, some differences between an accurate bridge model and the simplified model used here are unavoidable. If examining the simplified model shows a distinct phenomenon, a similar phenomenon in more sophisticated models can also be expected. One of the main targets of this study is to develop an analytical method that increases our understanding of the robustness of long-span cable-supported bridges in the case of the failure of several cables. The proposed method is expected to set the basis for further developments of practical methods for more complex structures. Immediate practical applications are not intended.

The main tasks of this study, as set-up in chapter one, are:

- Developing an analytical method for the investigation of cable failure in long-span cable-supported bridges.
- Developing an approximation function for the calculation of the “stress increase ratio” of the critical cable in a cable-loss scenario
- Modifying the developed approximation function for the consideration of the failure of several cables in a cable-loss scenario.
- Developing a reserve-based robustness index for parallel load-bearing systems.
- Investigation of the robustness of a structural system segmented by zipper-stoppers.
- Developing an approximation function for the calculation of the “maximum bending moment” on the girder due to cable failure.
- Investigation of the optimum design of long-span cable-supported bridges considering different cable-loss scenarios.

An overview of the proposed conceptual models in the literature for the analysis of suspension bridges is presented in chapter two. In chapter three, a parallel load-bearing system, representative of a long-span cable-supported bridge, is considered, and the “stress increase ratio” of the critical cable in a cable-loss scenario is investigated. The structural characteristics of the system, including the bending stiffness of the girder and a unique axial stiffness in each cable, are taken into account. The failure of several cables has also been considered. An analytical approach based on differential equations of the system has been used, and an approximation function for the calculation of the stress increase ratio of the critical cable in a cable-loss scenario has been derived. The use of the least squares method has been applied to minimize the error of the approximation function. The acceptable accuracy of the presented approximation function has been proved by the comparison of the exact stress increase ratio values, and the one calculated from the proposed approximation function. Except for small β -values (stiffness ratio of the system), the error of the proposed approximation function is less than 5% in the investigated systems. The results show that by increasing the β -value, the stress increase ratio of the critical cable decreases. It has been shown that the design load of a cable is influenced by β . This means that for systems with larger β -values, smaller design loads are required. Therefore, in the case of long-span cable-supported bridges, the bridge could be divided into different zones corresponding to different β -values. Then, the minimum design load of each zone can be calculated. Thus, using the proposed method can make the design of cables in a cable-loss scenario more economical. In addition, the structural robustness of a system segmented by zipper-stoppers has been investigated, and the stress increase ratio of the zipper-stopper in a cable-loss scenario has been examined. The results show that by increasing the β -value, the stress increase ratio of the

zipper-stopper decreases. Finally, the developed approximation function has been employed to derive a reserve-based robustness index. The reserve-based robustness index reflects the capability of the structure in load redistribution and providing alternative load paths and can be expressive for structures that are susceptible to zipper-type collapse. The reserve-based robustness index is simple, calculable and objective. However, it reflects only the possibility of failure progression.

The focus of chapter four is to find the increase of the maximum bending moment on the girder due to cable failure. A similar analytical approach has been performed and an approximation function for the calculation of the relative moment increase has been derived. The accuracy of the proposed approximation function has been checked by numerical models and it has been shown that except for small β -values, the error of the proposed approximation function is less than 5% in the investigated systems. The results also show that by increasing the β -value, cable failure produces a larger bending moment on the girder. This means that for systems with smaller β -values, bending moments are smaller.

The target of chapter five is to develop a practical method for the optimization of cable distance in cable-supported bridges using the robustness index. The applied method minimizes the cost of bridge construction and guarantees a certain level of robustness. For this purpose, the developed reserve-based measure of robustness has been used to ensure that in possible cable-loss scenarios a zipper-type collapse does not occur.

Two cable-loss scenarios are considered. In the first one, the initial failure of all cables within a 5 m range is considered. In the second one, it is assumed that all cables within a 10 m range are failed. The results show that the optimum cable distance fundamentally depends on the assumed number of failed cables. As the cable distance decreases, the construction cost decreases. This cost reduction continues until the cable distance becomes shorter than 5 or 10 m corresponding to each case. At this point, a sharp increase in the construction cost occurs, provided the design takes into account the likelihood of multiple cable failure as suggested here. In other words, the optimum cable distance in each case is 5 and 10 m, respectively. More generally, if we choose to consider the initial failure of all cables within a range of x meters, then, the optimum cable distance is equal to x . However, stipulating the range x needs more comprehensive studies based on statistical data and risk analysis. The determination of this range is not within the scope of this study. It should be determined by guidelines or in a project-based procedure.

It should be emphasized that, in this study, a conceptual bridge model is applied. Hence, some differences between an accurate bridge model and the simplified model used here are unavoidable. For instance, assuming rigid upper cable supports does not exactly correspond to

the actual structures. Besides, the nonlinear behavior of the structural system is not considered here. Plastic deformations are, especially in the case of the failure of several cables, very important. Hence, the inadequacy of the analytical model in this respect should be mentioned. Therefore, the main recommendations for future studies are to develop a more realistic bridge model and to consider the nonlinear behavior of the structural system. In addition, modeling the deck as a beam fails to capture the two degrees of freedom of the deck, namely, longitudinal and torsional degrees of freedom. Therefore, using a three-dimensional model of the deck for the investigation of the torsional behavior of the bridge in a cable-loss scenario is suggested.

References

- Adam, J., Parisi, F., Sagaseta, J., and Lu, X. (2018). "Research and practice on progressive collapse and robustness of building structures in the 21st century." *Engineering Structures*, 173, 122-149.
- Agarwal, J., Blockley, D., and Woodman, N. (2003). "Vulnerability of structural systems." *Structural Safety*, 25(3), 263-286.
- Agarwal, J., and England, J. (2008). "Recent developments in robustness and relation with risk." *Proceedings of the Institution of Civil Engineers - Structures and Buildings*, 161(4), 183-188.
- Allen, D.E., and Schriever, W.R. (1979). "Progressive collapse, abnormal loads and building codes." Division of Building Research Council, Québec.
- Ammann, O. (1941). "The failure of the Tacoma Narrows Bridge." Board of Engineers, Pasadena.
- Ammann, O., von Karman, T. and Woodruff, G.B. (1941), "The failure of the Tacoma Narrows Bridge." Federal Works Agency, Washington, D. C.
- Andrew, C. (1952). "Final report on Tacoma Narrows Bridge." University of Washington, Tacoma.
- Aoki, Y. (2014). "Analysis of the performance of cable-stayed bridges under extreme events." Doctoral dissertation, University of Technology Sydney, Sydney, Australia.
- Arioli, G., and Gazzola, F., (2013). "Old and new explanations of the Tacoma Narrows Bridge collapse." *Atti XXI Congresso AIMETA*, Sapienza University of Rome, Italy.
- Arioli, G., and Gazzola, F. (2015). "A new mathematical explanation of what triggered the catastrophic torsional mode of the Tacoma Narrows Bridge." *Applied Mathematical Modelling*, 39(2), 901-912.
- ASCE, American Society of Civil Engineers. (2002). "Minimum design loads for buildings and other structures." ASCE 7-02, Reston, Va.
- Baker, J., Schubert, M., and Faber, M. (2008). "On the assessment of robustness." *Structural Safety*, 30(3), 253-267.
- Benci, V., Fortunato, D., and Gazzola, F. (2017). "Existence of torsional solitons in a beam model of suspension bridge." *Archive for Rational Mechanics and Analysis*, 226(2), 559-585.

References

Beverly, P. (2013). "Fib model code for concrete structures 2010." International Federation for Structural Concrete (fib), Lausanne, Switzerland.

Bi, K., Ren, W., Cheng, P. and Hao, H. (2015). "Domino-type progressive collapse analysis of a multi-span simply-supported bridge: A case study." *Engineering Structures*, 90, pp.172-182.

Biondini, F., Frangopol, D.M., and Restell, S. (2008). "On structural robustness, redundancy and static indeterminacy." *Proc., the ASCE-SEI Structures Congress*, American Society of Civil Engineers, Reston, U.S.

Bleich, F. (1950). "The mathematical theory of vibration in suspension bridges." Dept. of Commerce, Bureau of Public Roads, Washington.

Bontempi, F., Giuliani, L., and Gkoumas, K. (2007). "Handling the exceptions: robustness assessment of a complex structural system." *Structural Engineering, Mechanics and Computation (SEMC)* 3, 1747-1752.

Canisius, T., Sorensen, J.D., and Baker, J. (2007). "Robustness of structural systems – a new focus for the Joint Committee on Structural Safety (JCSS)." *Proc., 10th international conference on applications of statistics and probability in civil engineering (ICASP10)*, Taylor & Francis Group, Abingdon, U.K.

Cao, H., Qian, X., Chen, Z., and Zhu, H. (2017). "Layout and size optimization of suspension bridges based on coupled modelling approach and enhanced particle swarm optimization." *Engineering Structures*, 146, 170-183.

Castigliano, A. (1879). "The theory of equilibrium of elastic systems and its applications." Negro, Torino.

Cavaco, E., Casas, J., Neves, L., and Huespe, A. (2010). "Robustness of corroded reinforced concrete structures – a structural performance approach." *Structure and Infrastructure Engineering*, 1-17.

Chen, W., and Duan, L. (2014). "Bridge engineering handbook." Taylor & Francis Ltd, London.

Chopra, A. (2001). "Dynamics of structures. In: theory and applications to earthquake engineering." Prentice-Hall, New Jersey.

Christianson, J., Cruz, M., and Nolan, K. (2011). "Hyatt Regency Hotel walkways collapse." Seattle University, Seattle.

References

- Cid, C., Baldomir, A., and Hernández, S. (2018). "Optimum crossing cable system in multi-span cable-stayed bridges." *Engineering Structures*, 160, 342-355.
- Como, M., Ferraro, S., and Grimaldi, A. (2005). "A parametric analysis of the flutter instability for long span suspension bridges." *Wind and Structures*, 8(1), 1-12.
- Das, R., Pandey, A., Soumya, Mahesh, M., Saini, P. and Anvesh, S. (2016). "Effect of dynamic unloading of cables in collapse progression through a cable stayed bridge." *Asian Journal of Civil Engineering*, 17(4), 397-416.
- Delatte, N. (2009). "Beyond failure." ASCE Press, Reston, VA.
- Doole, S., and Hogan, S. (2000). "Non-linear dynamics of the extended Lazer-McKenna bridge oscillation model." *Dynamics and Stability of Systems*, 15(1), 43-58.
- Ellingwood, B. (2006). "Mitigating risk from abnormal loads and progressive collapse." *Journal of Performance of Constructed Facilities*, 20(4), 315-323.
- European Committee for Standardization. (2006). "Eurocode 1-actions on structures." EN 1991-1-7, CEN, Brussels.
- Fabbrocino, F., Modano, M., Farina, I., Carpentieri, G., and Fraternali, F. (2017). "Optimal prestress design of composite cable-stayed bridges." *Composite Structures*, 169, 167-172.
- Fatollahzadeh, A., Naghipour, M., and Abdollahzadeh, G. (2016). "Analysis of progressive collapse in cable-stayed bridges due to cable failure during earthquake." *International Journal of Bridge Engineering (IJBE)*, 4(2), 63-72.
- Fonda, A., Schneider, Z., and Zanolin, F. (1994). "Periodic oscillations for a nonlinear suspension bridge model." *Journal of Computational and Applied Mathematics*, 52(1-3), 113-140.
- Frangopol, D., and Curley, J. (1987). "Effects of damage and redundancy on structural reliability." *Journal of Structural Engineering*, 113(7), 1533-1549.
- Gazzola, F. (2015). "Mathematical models for suspension bridges." Springer, New York.
- Gazzola, F., Jleli, M., and Samet, B. (2014). "On the Melan equation for suspension bridges." *Journal of Fixed Point Theory and Applications*, 16(1-2), 159-188.
- Gazzola, F., and Sperone, G. (2018). "Thresholds for hanger slackening and cable shortening in the Melan equation for suspension bridges." *Nonlinear Analysis: Real World Applications*, 39, 520-536

References

- Georgakis, C., and Gimsing, N. (2013). "Cable supported bridges." Wiley, Hoboken, N.J.
- Green, D., and Unruh, W. (2006). "The failure of the Tacoma Bridge: A physical model." *American Journal of Physics*, 74(8), 706-716.
- Gross, J., and McGuire, W. (1983). "Progressive collapse resistant design." *Journal of Structural Engineering*, 109(1), 1-15.
- GSA (General Services Administration). (2003). "Progressive collapse analysis and design guidelines for new federal office buildings and major modernization projects." GSA, Office of Chief Architect, Washington, DC.
- Haberland, M. (2007). "Progressiver Kollaps und Robustheit." Diploma thesis, Hamburg University of Technology, Hamburg, Germany.
- Haberland, M. (2012). "Unverhältnismäßiger Kollaps und Robustheit von Tragwerken." Doctoral dissertation, Hamburg University of Technology, Hamburg, Germany.
- Haberland, M., Haß, S., and Starossek, U. (2012). "Robustness assessment of suspension bridges." Proc., 6th International Conference on Bridge Maintenance, Safety and Management (IABMAS), Taylor & Francis Group, Abingdon, U.K.
- Hoang, V., Kiyomiya, O., and An, T. (2015). "Experimental study on impact force factor during sudden cable loss in cable-stayed bridges." *IABSE Symposium Report*, 103(2), 252-259.
- Hashemi, S., Bradford, M., and Valipour, H. (2016). "Dynamic response of cable-stayed bridge under blast load." *Engineering Structures*, 127, 719-736.
- Hauck, G. (1983). "Hyatt-Regency walkway collapse: design alternates." *Journal of Structural Engineering*, 109(5), 1226-1234.
- Hilton, W. (1977). "Tacoma Narrows Bridge collapse, a demonstration." *The Physics Teacher*, 15(3), 189-189.
- Husain, M., and Tsopelas, P. (2004). "Measures of structural redundancy in reinforced concrete buildings. I: Redundancy Indices." *Journal of Structural Engineering*, 130(11), 1651-1658.
- Hyttinen, E., Välimäki, J., and Järevenpää, E. (1994). "Effect of breaking of a cable. In: cable-stayed and suspension bridges." Proc., AFPC Conference, AFPC, Paris, France.

References

- Irwin, P., Stoyanoff, S., Xie, J., and Hunter, M. (2005). "Tacoma Narrows 50 years later—wind engineering investigations for parallel bridges." *Bridge Structures*, 1(1), 3-17.
- Jadhav, A. (2019). "Progressive Collapse of Cable Stayed Bridge under Blast Loading." *International Journal for Research in Applied Science and Engineering Technology*, 7(10), 801-809.
- JCSS (Joint Committee on Structural Safety). (2008). "Risk assessment in engineering principles, system representation & risk criteria." JCSS, Zurich, Switzerland.
- Kanno, Y., and Ben-Haim, Y. (2011). "Redundancy and robustness, or when is redundancy redundant? ." *Journal of Structural Engineering*, 137(9), 935-945.
- Karman, T., and Edson, L. (1967). "The wind and beyond." Little and Brown, Boston.
- Kawada, T. (2000). "The fall of the Tacoma Narrows Bridge." *Wind Engineers, JAWE*, 2000(83), 25-32.
- Kawada, T., Scott, R., and Ohashi, H. (2014). "History of the modern suspension bridge." American Society of Civil Engineers, Reston, Va.
- Kempski, J. (2016). "Steifigkeits- und Flexibilitätsmatrix eines unendlichen Systems." Project for master degree, Hamburg University of Technology, Hamburg, Germany.
- Khuyen, H., and Iwasaki, E. (2016). "An approximate method of dynamic amplification factor for alternate load path in redundancy and progressive collapse linear static analysis for steel truss bridges." *Case Studies in Structural Engineering*, 6, 53-62.
- Kokot, S., Solomos, G. (2012). "Progressive collapse risk analysis: literature survey, relevant construction standards and guidelines." Joint Research Centre, European Commission, Ispra, Italy.
- Krauthammer, T. (2008). "Modern protective structures." CRC Press, Boca Raton, Florida.
- Larsen, A. (2000). "Aerodynamics of the Tacoma Narrows Bridge - 60 years later." *Structural Engineering International*, 10(4), 243-248.
- Lazer, A., and McKenna, P. (1990). "Large-amplitude periodic oscillations in suspension bridges: some new connections with nonlinear analysis." *SIAM Review*, 32(4), 537-578.
- Lind, N. (1995). "A measure of vulnerability and damage tolerance." *Reliability Engineering & System Safety*, 48(1), 1-6.

References

- Lonetti, P., and Pascuzzo, A. (2014). "Vulnerability and failure analysis of hybrid cable-stayed suspension bridges subjected to damage mechanisms." *Engineering Failure Analysis*, 45, 470-495.
- Luth, G. (2000). "Chronology and context of the Hyatt-Regency collapse." *Journal of Performance of Constructed Facilities*, 14(2), 51-61.
- Maes, M., Fritzsos, K., and Glowienka, S. (2006). "Structural robustness in the light of risk and consequence analysis." *Structural Engineering International*, 16(2), 101-107.
- Malik, J. (2013). "Sudden lateral asymmetry and torsional oscillations in the original Tacoma suspension bridge." *Journal of Sound and Vibration*, 332(15), 3772-3789.
- Marshall, R. (1982). "Investigation of the Kansas City Hyatt Regency walkways collapse." U.S. Dept. of Commerce, National Bureau of Standards, Washington, D.C.
- Matsumoto, M. (2003). "Mystery of and lessons from Tacoma Narrows Bridge failure." *Wind Engineers, JAWE*, 2003(96), 3-5.
- McKenna, P. (1999). "Large torsional oscillations in suspension bridges revisited: fixing an old approximation." *The American Mathematical Monthly*, 106(1), 1.
- McKenna, P., and Walter, W. (1987). "Nonlinear oscillations in a suspension bridge." *Archive for Rational Mechanics and Analysis*, 98(2), 167-177.
- Melan, J., and Steinman, D. (1913). "Theory of arches and suspension bridges." M.C. Clark Pub., Chicago.
- Miao, F. and Ghosn, M. (2016). "Reliability-based progressive collapse analysis of highway bridges." *Structural Safety*, 63, pp.33-46.
- Middleton, W. (2003). "In the wake of Tacoma: suspension bridges and the quest for aerodynamic stability (review)." *Technology and Culture*, 44(3), 618-620.
- Moncarz, P., and Taylor, R. (2000). "Engineering process failure. Hyatt-Walkway collapse." *Journal of Performance of Constructed Facilities*, 14(2), 46-50.
- Morin, C., and Fischer, C. (2006). "Kansas City Hyatt Hotel skyway collapse." *Journal of Failure Analysis and Prevention*, 6(2), 5-11.
- Mozos, C., and Aparicio, A. (2006). "Cable-stayed bridges. Failure of a stay: Dynamic and pseudo-dynamic analysis of structural behavior." *Proc., 3th International Conference on Bridge Maintenance, Safety and Management (IABMAS)*, Porto, Portugal.

References

Mozos, C., and Aparicio, A. (2009). "Static strain energy and dynamic amplification factor on multiple degree of freedom systems." *Engineering Structures*, 31(11), 2756-2765.

Mozos, C., and Aparicio, A. (2010a). "Parametric study on the dynamic response of cable stayed bridges to the sudden failure of a stay, part I: Bending moment acting on the deck." *Engineering Structures*, 32(10), 3288-3300.

Mozos, C., and Aparicio, A. (2010b). "Parametric study on the dynamic response of cable stayed bridges to the sudden failure of a stay, part II: Bending moment acting on the pylons and stress on the stays." *Engineering Structures*, 32(10), 3301-3312.

Mozos, C., and Aparicio, A. (2011). "Numerical and experimental study on the interaction cable structure during the failure of a stay in a cable stayed bridge." *Engineering Structures*, 33(8), 2330-2341.

National Institute of Standards and Technology(NISTIR). (2007)."Best practices for reducing the potential for progressive collapse in buildings. " NISTIR 7396, Gaithersburg, Montgomery.

Neves Carneiro, G. and Conceição António, C. (2019a). "Global optimal reliability index of implicit composite laminate structures by evolutionary algorithms." *Structural Safety*, 79, pp.54-65.

Neves Carneiro, G. and Conceição António, C. (2019b). "Reliability-based robust design optimization with the reliability index approach applied to composite laminate structures." *Composite Structures*, 209, pp.844-855.

Nguyen Trong Nghia, and Vanja Samec. (2016). "Cable-stay bridges-investigation of cable rupture." *Journal of Traffic and Transportation Engineering*, 4(5).

O'Donovan, J., Wilson, K., and Dempsey, T. (2003). "The design and construction of Taney Bridge." Tom McCormack Memorial Lecture, The institution of Structural Engineering, Republic of Ireland Branch, Dublin.

Olson, D., Hook, J., Doescher, R., and Wolf, S. (2015). "The Tacoma Narrows Bridge collapse on film and video." *The Physics Teacher*, 53(8), 461-465.

Olson, D., Wolf, S., and Hook, J. (2015). "The Tacoma Narrows Bridge collapse." *Physics Today*, 68(11), 64-65.

Parisi, F., and Augenti, N. (2012). "Influence of seismic design criteria on blast resistance of RC framed buildings: A case study." *Engineering Structures*, 44, 78-93.

References

- Park, Y., Starossek, U., Koh, H., Choo, J., Kim, H., and Lee, S. (2007). "Effect of cable loss in cable stayed bridges – focus on dynamic amplification." Proc., IABSE Symposium Weimar (Improving Infrastructure Worldwide), Taylor & Francis Group, Abingdon, U.K.
- Pfatteicher, S. (2000). "The Hyatt horror: failure and responsibility in american engineering." *Journal of Performance of Constructed Facilities*, 14(2), 62-66.
- Plaut, R. (2008). "Snap loads and torsional oscillations of the original Tacoma Narrows Bridge." *Journal of Sound and Vibration*, 309(3-5), 613-636.
- PTI (Post-Tensioning Institute). (2012). "Recommendations for stay-cable design, testing and installation." Cable-stayed bridges committee, Phoenix, USA.
- Qiu, W., Jiang, M., and Huang, C. (2014). "Parametric study on responses of a self-anchored suspension bridge to sudden breakage of a hanger." *The Scientific World Journal*, 2014, 1-10.
- Robinson, A. (1967). "A re-examination of the theory of suspension bridges." Doctoral Dissertation, University of Illinois at Urbana-Champaign, Illinois, USA.
- Rocard, Y. (1957). "Dynamic instability. Automobiles, aircraft, suspension bridges." Crosby Lockwood, London.
- Ruiz-Teran, A., and Aparicio, A. (2007). "Dynamic amplification factors in cable-stayed structures." *Journal of Sound and Vibration*, 300(1-2), 197-216.
- Ruiz-Teran, A., and Aparicio, A. (2009). "Response of under-deck cable-stayed bridges to the accidental breakage of stay cables." *Engineering Structures*, 31(7), 1425-1434.
- Shulman, A. (2017). "Hyatt regency hotel in Kansas city collapse – a case study." Proc., Project Management Symposium, Maryland, USA.
- Slogoff, H., and Berner, B. (2000). "A simulation of the Tacoma narrows bridge oscillations." *The Physics Teacher*, 38(7), 442-443.
- Smith, J. (2006). "Structural robustness analysis and the fast fracture analogy." *Structural Engineering International*, 16(2), 118-123.
- Smith, F., and Vincent, G. (1950). "Aerodynamic stability of suspension bridges." University of Washington Engineering Experiment Station, Washington.
- Song, C., Xiao, R., and Sun, B. (2018). "Optimization of cable pre-tension forces in long-span cable-stayed bridges considering the counterweight." *Engineering Structures*, 172, 919-928.

References

- Starossek, U. (1999). "Progressive collapse study of a multi-span bridge." *Structural Engineering International*, 9(2), 121-125.
- Starossek, U. (2006). "Progressive collapse of bridges – aspects of analysis and design." *Proc., International Symposium on Sea-Crossing Long-Span Bridges*, Mokpo, Korea.
- Starossek, U. (2007). "Typology of progressive collapse." *Engineering Structures*, 29(9), 2302-2307.
- Starossek, U. (2008). "Collapse resistance and robustness of bridges." *Proc., 4th International Conference on Bridge Maintenance, Safety, and Management (IABMAS'08)*, Seoul, Korea.
- Starossek, U. (2009). "Avoiding disproportionate collapse of Major Bridges." *Structural Engineering International*, 19(3), 289-297.
- Starossek, U. (2018). "Progressive collapse of structures." ICE Publishing, London.
- Starossek, U., and Haberland, M. (2010). "Disproportionate collapse: terminology and procedures." *Journal of Performance of Constructed Facilities*, 24(6), 519-528.
- Starossek, U., and Haberland, M. (2011). "Approaches to measures of structural robustness." *Structure and Infrastructure Engineering*, 7(7-8), 625-631.
- Steinman, D., and Watson, S. (1958). "Bridges and their builders." *Journal of the Franklin Institute*, 265(4), 355.
- Svensson, H. (2012). "Cable-stayed bridges: 40 years of experience worldwide." Ernst & Sohn, Berlin.
- Teipelke, R. (2010). "Hyatt Regency walkway collapse 1981." Grin Verlag, Munich .
- Tsai, M. (2010). "An analytical methodology for the dynamic amplification factor in progressive collapse evaluation of building structures." *Mechanics Research Communications*, 37(1), 61-66.
- Tsai, M., and You, Z. (2012). "Experimental evaluation of inelastic dynamic amplification factors for progressive collapse analysis under sudden support loss." *Mechanics Research Communications*, 40, 56-62.
- Turmo, J., and Luco, J. (2010). "Effect of hanger flexibility on dynamic response of suspension bridges." *Journal of Engineering Mechanics*, 136(12), 1444-1459.
- U. S. Department of Defense. (2013). "Design of buildings to resist progressive collapse." UFC 4-023-03, DoD, Washington, D.C.

References

- Val, D., and Val, E. (2006). "Robustness of frame structures." *Structural Engineering International*, 16(2), 108-112.
- Vrouwenvelder, T. (2008). "Treatment of risk and reliability in the Eurocodes." *Proceedings of the Institution of Civil Engineers - Structures and Buildings*, 161(4), 209-214.
- Wang, P., Zhang, J., Zhai, H., and Qiu, J. (2017). "A new structural reliability index based on uncertainty theory." *Chinese Journal of Aeronautics*, 30(4), pp.1451-1458.
- Wilkinson, C. (1983). "Aftermath of a disaster: the collapse of the Hyatt Regency Hotel skywalks." *American Journal of Psychiatry*, 140(9), 1134-1139.
- Wisniewski, D., Casas, J., and Ghosn, M. (2006). "Load capacity evaluation of existing railway bridges based on robustness quantification." *Structural Engineering International*, 16(2), 161-166.
- Wolf, M., and Starossek, U. (2008). "Robustness assessment of a cable-stayed bridge." *Proc., 4th International Conference on Bridge Maintenance, Safety and Management (IABMAS)*, Seoul, Korea.
- Wolf, M., and Starossek, U. (2009). "Cable loss and progressive collapse in cable-stayed bridges." *Bridge Structures*, 5(1), 17-28.
- Wolf, M., and Starossek, U. (2010). "Cable-loss analyses and collapse behavior of cable-stayed bridges." *Proc. of 5th International Conf. on Bridge Maintenance, Safety and Management (IABMAS)*, Taylor & Francis Group, Abingdon, U.K.
- Wu, G., and Qiu, W. (2018). "Dynamic analysis of self-anchored suspension bridge to sudden hanger-breakage event." *Proc., The 2018 Structures Congress, ASCE, Reston, Va.*
- Wyatt, T. (1992). "Bridge aerodynamics 50 years after Tacoma Narrows - part I: the Tacoma Narrows failure and after." *Journal of Wind Engineering and Industrial Aerodynamics*, 40(3), 317-326.
- Xiang, Y., Chen, Z., Yang, Y., Lin, H., and Zhu, S. (2018). "Dynamic response analysis for submerged floating tunnel with anchor-cables subjected to sudden cable breakage." *Marine Structures*, 59, 179-191.
- Zhai, H. and Zhang, J. (2019). "Equilibrium reliability measure for structural design under twofold uncertainty." *Information Sciences*, 477, pp.466-489.
- Zhou, Y., and Chen, S. (2014). "Time-progressive dynamic assessment of abrupt cable-breakage events on cable-stayed bridges." *Journal of Bridge Engineering*, 19(2), 159-171.

References

Zoli, T., and Woodward, R. (2005). "Design of long span bridges for cable loss." Proc., IABSE Symposium (Structures and Extreme Events), Taylor & Francis Group, Abingdon, U.K.

Lebenslauf

Name Shoghijavan
Vorname Mohammad
Staatsangehörigkeit iranisch
Geburtsdatum 18.09.1985
Geburtsort, -land Mashhad, Iran

Ausbildung

09.1999 - 09.2003 Gymnasium in Mashhad

09.2003 - 09.2007 Studium Bauingenieurwesen
an der Zanzanuniversität in Zanzan
Abschluss: Bachelor

09.2008 - 01.2011 Studium Bauingenieurwesen
(Erdbebeningenieurwesen)
an der Semnanuniversität in Semnan
Abschluss: Master

Seit 07.2013 Stipendiat DAAD
Technische Universität Hamburg
Institut für Baustatik

Berufserfahrung

10.2007 - 08.2008 Tragwerksplaner bei Afarinehtoos

02.2011 - 05.2013 Tragwerksplaner bei Ariaye Shargh Toos